



November 13, 2023

CPSC^{1,2} Staff Statement on: Release Potential for Carbon Nanotubes Used in Children’s Backpacks for Ballistic Protection

1. Background

The 2016 report titled, “Release Potential for Carbon Nanotubes Used in Children’s Backpacks for Ballistic Protection” describes studies performed by the US Army Engineer Research and Development Center (ERDC) of the Department of Army in collaboration with the National Institute of Standards and Technology (NIST). The studies were supported by interagency agreements CPSC-I-13-0015, CPSC-I-14-0008 and CPSC-I-14-0011 between the Consumer Product Safety Commission (CPSC) and ERDC and NIST.

ERDC is the research and development center for the U.S. Army Corps of Engineers. They conduct research to discover, develop, and deliver innovative solutions to the challenges in military engineering, installations and operational environments, civil works, geospatial research and engineering, and engineered resilient systems.

2. Introduction

Carbon nanotubes (CNT) are used in children’s backpacks that are marketed as offering personal protection from small firearms. Nanoparticles, including CNT, could pose health risks to consumer product users, especially via inhalational exposure.

Nanoparticles are of concern because their nanoscale size enables the particles to penetrate to the lung deeply when inhaled, to potentially move across lung cell walls, and to become systemically distributed. Published literature from *in vivo* studies has shown that CNTs and carbon nanofibers (CNFs) can cause persistent pulmonary inflammation, granulomatosis, and fibrosis. In addition, immunosuppression, neuroinflammation, and cardiovascular effects, such as endothelial dysfunction, may occur from systemic inflammation in laboratory animals following inhalation exposure to CNTs. While these health effects have been observed in animal studies, epidemiological studies in CNT/CNF workplaces have not shown consistent patterns in the health effects assessed.

¹ This statement was prepared by the CPSC staff, and the attached report was prepared by ERDC for CPSC staff. The statement and reports have not been reviewed or approved by, and do not necessarily represent the views of, the Commission.

² The CPSC nanotechnology program is working to publicly post technical reports produced from interagency agreements and contracts.

In this report, ERDC states from reviewing literature that it is controversial whether nanomaterials incorporated into consumer products pose exposure-related health risks to consumers. ERDC also highlights, at the time of these studies, a lack of testing protocols to evaluate the exposure of consumers to nanoparticles used in consumer products. Furthermore, the absence of nanotechnology-specific guidance on testing is a significant challenge for evaluating nanomaterials incorporated into consumer products. Accurate quantification of nanomaterial release from nanotechnology-incorporated products is necessary for reliable exposure analysis and characterization of human health risks during the intended use.

3. Objectives

The study's purpose was to perform a health risk evaluation of a ballistic insert used in clothing, vests, and school backpacks. The insert material is composed of a polymer matrix with multi-walled carbon nanotubes (MWCNTs). The objectives of this ERDC work were to (1) capture product use scenarios, (2) develop a framework about testing considerations to estimate exposure, (3) develop analytical methods to quantify the release of particles, including CNTs, and (4) achieve quantitative exposure data of CNTs released from the backpack insert.

4. Experimental Design and Methods

CPSC staff identified plausible use scenarios including dragging, pulling, rubbing, and compressing backpacks as well as liquid spillage, weathering, washing/drying, and mouthing of the backpacks.

ERDC with CPSC and NIST collaboratively developed a comprehensive testing plan to detect and quantify nanoparticles released from the backpack inserts during the various use scenarios. To maximize the potential release of CNTs as a worst-case scenario, ERDC removed the insert's external vinyl casing thereby referring to the modified insert as "compromised." A two-tiered testing approach was developed to evaluate CNT release from the compromised insert. The first-tier testing assessed compromised inserts that did not undergo any advanced material aging. For the second-tier testing, ERDC evaluated compromised samples aged by UV exposure, washing, heating or other physical challenges to imitate various lifecycle uses of the backpacks.

To test for CNT release from liquid exposures, compromised samples were exposed to eight solutions, such as phosphoric acid to mimic cola, citric acid for orange juice, a saline solution for ocean water, sodium dodecyl sulfate (SDS) and sodium borate (Borax) as detergent components, as well as powder detergent reference solutions European Colourfastness Establishment (ECE)-(A) No.2 (phosphate-free, without optical brightener) and International Electrotechnical Commission (IEC)-(A) No.3 (phosphate-free, with optical brightener). Deionized (DI) water was used as a control.

To simulate CNT release from mechanical wash-induced wear, samples were incubated with the different detergent solutions (i.e., SDS, Borax, ECE-(A), or IEC-(A)) and glass beads (15 mm diameter) at room temperature for 30 minutes on a rotating platform.

After the insert samples were exposed to the test liquids, both filtered and unfiltered solutions were used for optical image analysis of CNTs.

The potential release of CNTs from UV-aged samples was evaluated with an adhesion test, where an adhesive coated copper tape was placed onto the surface of the aged samples, followed by image analysis of the tape.

For quantitative analyses of released CNTs, various analytical technologies were used, such as Fourier transform infrared (FTIR) spectroscopy, scanning electron microscopy (SEM), Raman spectroscopy, thermogravimetric analysis (TGA), inductively coupled plasma mass spectroscopy (ICP-MS), UV-VIS spectroscopy and digital image intensity analysis.

5. Results

a. Non-aged compromised samples

ERDC determined that the ballistic insert consisted of a high density polypropylene cushion foam (thickness ~ 2.75 mm) sandwiched between multiple ballistic panel layers that are coated with a MWCNT polymer.

SEM analysis identified single and agglomerated CNTs surrounded by thin layers of polymer coating, which was confirmed via Raman spectroscopy. TGA detected sample mass loss as the testing temperature increased up to more than 1,000°C with similar patterns in mass loss between inert (i.e., nitrogen gas) and oxidizing (i.e., air) conditions. These similar patterns in mass loss between the two experimental conditions support the presence of CNTs that increased the thermal stability of polymer composites.

According to the SEM analysis, ERDC stated that no or few CNTs were released from exposure to DI water, ocean water, as well as the citric and phosphoric acid solutions. In contrast, detergent exposures (e.g., Borax) released CNTs that were either standalone polymer/CNT particles or polymer/CNT particles attached to polymer sheets. Exposure to the ECE-(A) and IEC-(A) reference solutions resulted in greater release of materials, including polymer matrix containing protruding CNTs, polymer sheets and membranes.

ERDC was not able to detect via Raman spectroscopy analysis CNTs released into DI water, ocean water, citric acid and phosphoric acid solutions, while they were able to in the detergent solutions. Micron-sized particles with protruding CNTs (MWCNTs) were observed in the detergent solutions. ERDC believed the scarcity of released material and the technical difficulty in locating CNTs under 100x optical magnification were the reasons for lack of Raman spectra in the non-detergent liquids.

ERDC used UV-VIS spectroscopy and digital image intensity analysis to derive quantitative estimates of CNTs released in the different liquids. The DI water, ocean water, citric acid, phosphoric acid, SDS, and Borax solutions contained less than 1.25 µg/ml or minimal levels of CNTs. For the reference ECE-(A) and ICE-(A) detergent solutions, UV-VIS spectroscopy alone could not reliably estimate the amount of released CNTs due to optical disturbance (i.e., high background) by a large amount of detergent in the solutions. ERDC determined from the digital image analysis with a standard curve of CNT that ECE-(A) and IEC-(A) solutions released the highest amount of CNTs.

b. Compromised UV-aged Samples

ERDC observed FTIR spectral changes in the UV-aged samples indicating UV-induced material changes. SEM analysis provided detail of the UV-induced changes, with surface cracking with exposed CNTs as well as accumulation of CNTs on the polymer surface. ERDC noted that cracking of the polymer surface renders the matrix more prone to particle release and disintegration by pieces breaking off during abrasion. Therefore, larger CNT release would be expected from the UV-aged samples.

SEM analysis of UV-aged samples collected with the adhesion test presented visible CNTs protruding from the sample surfaces as well as some particles without notable CNTs.

Optical microscopy after liquid exposure/washing simulation identified that UV-aged samples exhibited more colorations (e.g., brown color) compared to non-aged samples.

Similar to the results from the non-aged samples, SEM analysis could not conclusively identify that the released particles were CNTs from the UV-aged samples exposed to DI water, ocean water, citric acid and phosphoric acid solutions. In contrast, SEM analysis could determine particles were CNTs from SDS, Borax, ECE-(A), and IEC-(A) solutions of the UV-aged samples.

Raman spectroscopy identified the presence of released CNTs from all detergent solutions (SDS, Borax, ECE-(a), and IEC-(A)) and DI water, but not from ocean water, citric acid and phosphoric acid solutions.

UV-VIS spectroscopy and digital image intensity analysis were conducted for quantitative estimation of released particles from the UV-aged samples. Based on the UV-VIS spectroscopy, ERDC determined the DI water, ocean water, citric acid, and phosphoric acid solutions contained MWCNTs up to 1.25 µg/ml while SDS and Borax solutions contained up to 8.75 and 3.75 µg/ml, respectively. UV-VIS spectroscopy could not reliably evaluate ECE-(A) and IEC-(A) solutions because of abundant detergent particles remaining in the collected samples. According to the digital image intensity analysis, detergent solutions released the highest amount of CNTs.

6. Summary

The observed results suggest that CNTs can be released from the use of the ballistic backpack insert. However, ERDC stated that the release is likely to occur only under the most extreme conditions, including removal of the outer casing and exposing the insert to UV light or mechanical abrasion and detergent washing.

ERDC states that SEM and Raman spectroscopy are efficient technologies to detect CNTs from the compromised and UV-aged samples but are not efficient for quantitative analysis in complex media.

Exposure of samples to simulated food and environmental liquids leads to a modest release of CNTs, whereas washing with detergents leads to the release of micron-sized particles and polymer matrix containing protruding CNT particles.

UV-aging increased exposed CNT levels on the surface of the samples. Furthermore, because of matrix surface degradation, UV-aged samples were likely to release CNTs at a higher rate than non-aged samples during the washing simulations.

ERDC stated a challenge with this study was that CNTs were already embedded into the polymer so that quantitative analysis was not possible. Applied CNT analysis technologies had limitations

for both low and high release of particles after treatment with various simulant food, environmental and detergent solutions. For low release scenarios (e.g., DI water, ocean water), it was difficult to identify the presence of CNTs because of the extremely low number of CNTs among the released materials. For higher release scenarios with the reference detergents (e.g., ECE-(A) and IEC-(A)), it was also a challenge to identify and quantify the presence of CNTs because of excess and variable detergent remaining in the collected samples. To understand the risks associated with this type of consumer product, ERDC explained that the exposure study results should be interpreted in the context of use, receptors, and toxicity information.

Release Potential for Carbon Nanotubes Used in Children's Backpacks for Ballistic Protection

Prepared for:

Treye Thomas, Ph.D.
U.S. Consumer Product Safety Commission
Directorate for Hazard Identification and Reduction
4330 East West Highway
Bethesda, MD 20814

Prepared by:

Department of the Army
US Army Engineer Research and Development Center
Environmental Laboratory
Geotechnical and Structures Laboratory
3909 Halls Ferry Rd, EP-R
Vicksburg, MS 39180

1 July 2016

EXECUTIVE SUMMARY

Liquid exposure, with and without washing-induced wear simulation, has been carried out on coupons coated with a polymer containing engineered nanomaterials (ENMs) in order to investigate the release potential of the embedded nanomaterials, namely carbon nanotubes (CNTs). It has been determined that for pristine coupons the release products include micron and submicron size polymer clusters with protruding carbon nanotubes, whereas for UV-aged coupons, photo-degradation of the polymer matrix leads to the release of individual CNTs, in addition to the larger clusters. We have used a variety of characterization techniques to determine whether release occurs, identify the release products and attempt to quantify release. Major challenges include quantification of CNT release, which is an ongoing struggle for the entire scientific community, as well as analysis in the presence of complex solutions. Our release estimates indicate UV-aged compromised coupons washed in powder detergents, such as ECE-(A) and IEC-(A), have the highest potential for release. The highest release, from all solutions, was that of the UV-aged coupon washed in the IEC-(A) solution: the average release calculated from three runs is ~ 61 mg/m². In our analysis, we assumed worst case scenario where the entirety of the release products are CNTs.

TABLE OF CONTENTS

TABLE OF CONTENTS	3
Introduction and Background.....	6
1. Exposure Scenarios	7
1.1. Development and Prioritization of Potential Release and Exposure Scenarios.....	8
1.2. Age of Concern	8
1.3. Foreseeable Use	9
2. Evaluation Strategy/Work Plan Development.....	14
3. Analytical approaches quantifying the release and form of particles from the consumer product	15
3.1. Materials And Methods.....	15
3.1.1. Ballistics Report	15
3.1.2. Compromised Material Preparation.....	15
3.1.3. Solution Preparation.....	15
3.1.4. Accelerated UV Aging	16
3.1.5. Liquid Exposure, With OR Without Washing-Induced Wear Simulation	16
3.1.6. Release From UV-aged Compromised Material Based on Adhesion Test	17
3.1.7. Optical Imaging.....	17
3.1.8. Fourier Transform Infrared (FT-IR) Spectroscopy.....	17
3.1.9. Scanning Electron Microscopy (SEM)	18
3.1.10. Raman Spectroscopy	18
3.1.11. Thermogravimetric Analysis (TGA)	19
3.1.12. Total Metals Analysis	20
3.1.13. UV-VIS Spectroscopy and Digital Image Intensity Analysis For Quantitative Estimation of Release Products.....	21
4. Results from the study.....	21
4.1. Results	21
4.1.1. Preliminary Assessment of Ballistic Backpack Insert	21
4.1.2. Compromised Pristine Material.....	22
4.1.2.1. Analysis of Compromised Pristine Material Prior to Liquid Exposure/Washing Simulation.....	22
Optical Microscopy	22
FT-IR Analysis	23
SEM Analysis	25
Raman Spectroscopy	26
Thermogravimetric Analysis	27
4.1.2.1. Analysis of Release Products From Compromised Pristine Material After Liquid Exposure/Washing Simulations	29
Optical Microscopy	29

SEM Analysis	30
4.1.2.1.1. DI Water	30
4.1.2.1.2. Ocean Water	30
4.1.2.1.3. Citric Acid Solution	30
4.1.2.1.4. Phosphoric Acid Solution	30
4.1.2.1.5. SDS Solution	30
4.1.2.1.6. Borax Solution	31
4.1.2.1.7. ECE-(A) Solution	31
4.1.2.1.8. IEC-(A) Solution	31
Raman Spectroscopy	41
Total Metals Analysis	42
UV-VIS Spectroscopy and Digital Image Intensity Analysis for Quantitative Estimation of Release Products	45
4.1.3. Compromised UV-aged Material	50
4.1.3.1. Analysis of Compromised UV-aged Material Prior to Liquid Exposure/Washing Simulation	50
SEM analysis	50
4.1.3.2. Evaluation of Release From UV-aged Material Based on Adhesion Test	54
SEM analysis	54
4.1.3.3. Analysis of Release Products From Compromised UV-aged Material After Liquid Exposure/Washing Simulation	55
Optical Microscopy	55
SEM ANALYSIS	56
4.1.3.3.1. DI Water	56
4.1.3.3.2. Ocean Water	56
4.1.3.3.3. Citric Acid Solution	56
4.1.3.3.4. Phosphoric Acid Solution	56
4.1.3.3.5. SDS Solution	56
4.1.3.3.6. Borax Solution	57
4.1.3.3.7. ECE-(A) Solution	57
4.1.3.3.8. IEC-(A) Solution	57
Raman Spectroscopy	69
UV-VIS Spectroscopy and Digital Image Intensity Analysis for Quantitative Estimation of Release Products	71
4.2. Issues, Summary and Conclusions	73
4.2.1. Issues	73
4.2.2. Summary and Conclusions	73
5. Methodology or protocol for release testing that can be used for evaluating the presence and release of nanoparticles from other products	74
References	79
6. Appendices	80

6.1. FT-IR Spectroscopy	80
6.2. Reference Detergent composition.....	81
6.3. Optical Images of Unfiltered/Filtered Solutions	82
6.4. Raman Results	83
6.4.1. Compromised Pristine material: ECE-(A)	83
6.4.2. Compromised Pristine Material IEC-(A)	84
6.5. Thermogravimetric Analysis of Coating	86
6.6. UV-VIS Comparison with OH-MWCNT Solutions	89
6.6.1. UV-VIS Comparison Pristine Coupons – Run 1.....	89
6.6.2. UV-VIS Comparison Pristine Coupons – Run 2.....	90
6.6.3. UV-VIS Comparison UV-aged Coupons – Run 1	91
6.7. Standard Operating Procedure.....	93
6.8. Laboratory Data Sheets (See separate DVD)	103
6.8.1. SEM Micrographs – DVD.....	103
6.8.2. RAMAN and TGA Results – DVD	103
6.9. Term Definitions	103

INTRODUCTION AND BACKGROUND

Despite hundreds of published studies on the potential effects of engineered nanomaterials on health and the environment, most Environmental Health and Safety (EHS) data is representative of only the parent nanomaterial. Little progress has been made evaluating technologies or products that contain nanomaterials. There is little agreement about whether nanomaterials pose unique risks to consumers once they are incorporated into products. In addition, the lack of testing protocols aimed at nanotechnology-based consumer products relative to “raw nanomaterial” has made most determinations on relevant safety based on “raw material” testing while analysis of particles in the technology itself remains elusive.

Risk managers and regulatory agencies are required to make decisions regarding the safety of nanotechnologies but currently do not have reliable, accurate, standardized test methods to develop reliable exposure data for specific nanotechnologies or products containing nanomaterials. By default, EHS risk calculations are being based on the worst case or extreme scenarios for parent materials found in the scientific literature, and may not necessarily be relevant to current applications of nanomaterials, namely nanotechnology-based consumer products. Accurate characterization and quantification of nanomaterial release is needed. This requires the development of methods to support scenario-based testing to account for how nanoparticles are potentially released through the life cycle of the technology and, more specifically, during the intended use of the product. A significant repository of formal testing protocols for materials properties, release schemes, environmental fate, exposure scenarios, and risk determination guidance exists from ASTM, ISO, and OECD. Their application toward nano-specific products remains limited due to the unique methods required for analysis and uncertainty in the methods used to assess exposure and hazard. Many of these testing guidance documents focus on the nanomaterial itself rather than the product that incorporates the nanomaterial. This narrowed view fails to consider the potential release mechanisms from nanomaterials from the product during use, overall characteristics of the particles once embedded into a material, and, in some cases, perhaps inhibit the transitioning of a nanotechnology due to erroneous interpretations of potential environmental risk. The absence of nanotechnology-specific guidance currently creates significant capacity gaps in terms of fielding or testing new technology containing nanomaterials.

This study focuses on a model test product, namely a ballistic backpack insert, to use as an example for the development of protocols to evaluate the release of carbon nanotubes (CNTs) from a polymer-based composite. This material is used for personal armor against small firearms and is intended to be used as an insert for clothing, vests and backpacks. The material is composed of a polymer matrix with multi-walled carbon nanotubes (MWCNTs) intended to provide ballistics protection. For the purpose of this study, we will develop potential exposure scenarios based on the use of the panels in backpacks. These backpacks are currently marketed to the parents of school-aged children. Thus, these nanomaterials are in a children’s product, and special precautions may be required to manage risk in this sensitive subpopulation.

The objectives for this project are:

1. Demonstrate the use of a risk-based approach that captures product use scenarios. These scenarios ultimately form a conceptual model that guide the selection of approaches used to evaluate the potential release of particles from a consumer product;
2. Develop a process or framework that can be used to guide decisions regarding the testing considerations and mechanisms that can be used to estimate exposure;
3. Develop analytical protocols, release testing, and methods to quantify the release and form of particles from the consumer product, in this case a composite material containing carbon nanotubes; and that can be used for other products
4. Use the approach and methods described above to obtain quantitative exposure data for a consumer product, a ballistic insert for backpacks containing carbon nanotubes, which can be used to assess the risk of this product by its intended consumer.

1. EXPOSURE SCENARIOS

Exposure scenarios are used to focus material testing and analysis on the most relevant release pathways. Relevant environmental conditions and processes have been identified that children's backpacks may experience during typical use (Figure 1). This figure illustrates potential physical and chemical challenges encountered by a child's backpack and includes mechanical stressors, weathering, chemical exposure and cleaning. In partnership with the CPSC, scenarios representing the challenges below have been selected for the development of testing protocols. The bounding of the case scenarios has been provided by input from the CPSC using background data pools representing typical exposure measurements and assumptions.



Figure 1. Typical environmental conditions and processes expected during backpack “use” as related to use by children.

1.1. DEVELOPMENT AND PRIORITIZATION OF POTENTIAL RELEASE AND EXPOSURE SCENARIOS

The CPSC Human Factors Team developed a description of scenarios where release and exposure may occur. Currently, published literature on backpack use is extremely limited, mostly covering the topic of the weight of the backpack and contents relative to the weight and size of the user. Usage scenarios are not covered. Input from the CPSC Human Factors team guided the approach for determining reasonably foreseeable use scenarios based on the design of the product and likely users of the backpacks.

1.2. AGE OF CONCERN

While consumers of all ages can use ballistic backpacks, children from 9 through 12 years (starting in 4th grade) were selected to be the age range of greatest concern. This age range was selected because of the following reasons: 1) they are likely to be tall and strong enough to use regular adult-sized backpacks (for ages 10 and up this is the largest regular backpack size at LLBean.com), 2) this age is recognized as susceptible to toxicants as they are still developing, 3) they have a greater appreciation for products that resemble adult versions (Age Determination Guidelines 2002, p. 99), 4) they receive longer reading assignments and therefore heavier books, 5) they carry books from class to class across campus in a middle school setting (age 11 or 6th grade), especially in schools that do not have lockers and 6) they are more likely than adults to spill liquid food items in their backpacks. For all of these reasons, children ages 9-12 are a sensitive sub population and likely to exert the most extreme environmental conditions and processes on backpacks and result in CNT release.

1.3. FORESEEABLE USE

Ballistic backpacks can be purchased from several retailers, including the backpack shown in Figure 2 and Figure 3. Backpacks can be purchased with the ballistic insert or the consumer can purchase a ballistic insert that can be placed into the computer sleeve of a backpack. CPSC staff evaluated the backpack purchased directly from the retailer for approximately \$300. Backpacks arrived with the ballistic insert sewn into a fabric pouch.

The higher cost of backpack will likely influence the behavior of those purchasing and using the backpacks; CPSC staff believe this will lead to longer use period than a less expensive backpack. Due to the investment of the backpack purchase, the consumer will be more likely to wash the backpack when exposed to liquid or other elements to ensure the product's longevity. Instructions from the manufacturer for the care of the insert are 1) wipe with damp cloth, 2) not machine wash and dry and 3) not to bleach, dry clean, or iron (Figure 4 and Figure 5). However, the care instructions informing consumers to not machine wash and dry, bleach, dry clean, and iron are located behind a sewn-in panel which is not accessible unless removing the stitching (Figure 6).

CPSC staff recommended a test wash cycle to determine durability and deformation of backpack. Additional considerations included exposure to UV sunlight (outdoor exposure) and the potential for liquid mediated exposure from accidental spillage (contact with liquids). A possible scenario resulting in the most CNT release was a combination scenario described as a wash and dry cycle, and then liquid mediated exposure. CPSC staff suggested a reasonable order to the exposure scenarios 1) Liquid mediated, 2) Force, 3) Wash/dry, then 4) Liquid mediated, 5) Force.



Figure 2. Ballistic backpack.

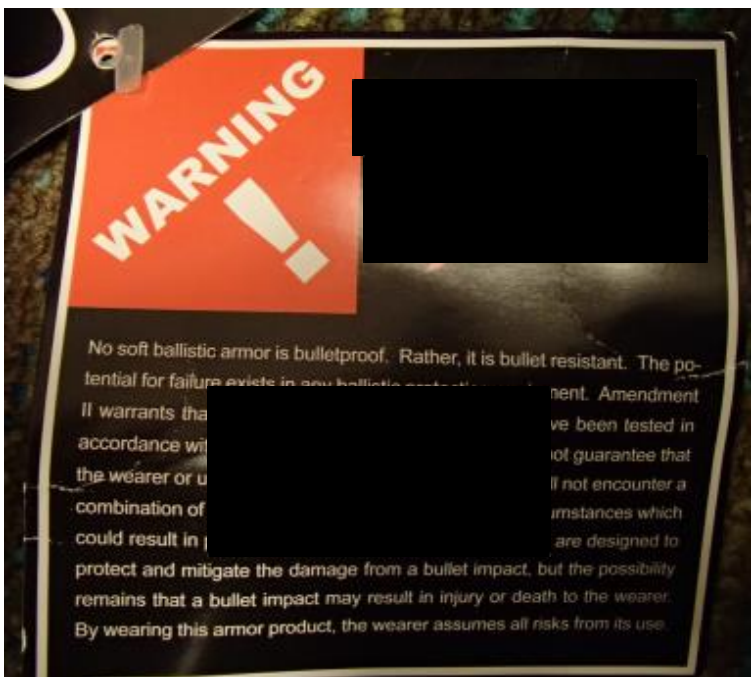
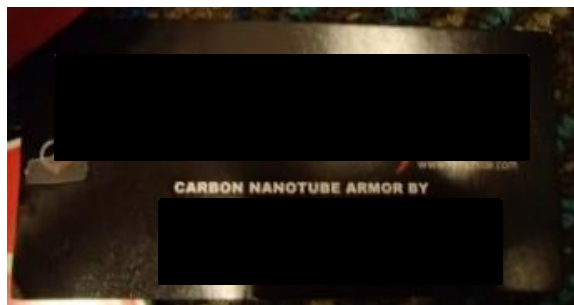


Figure 3. Information tags located on the backpack.

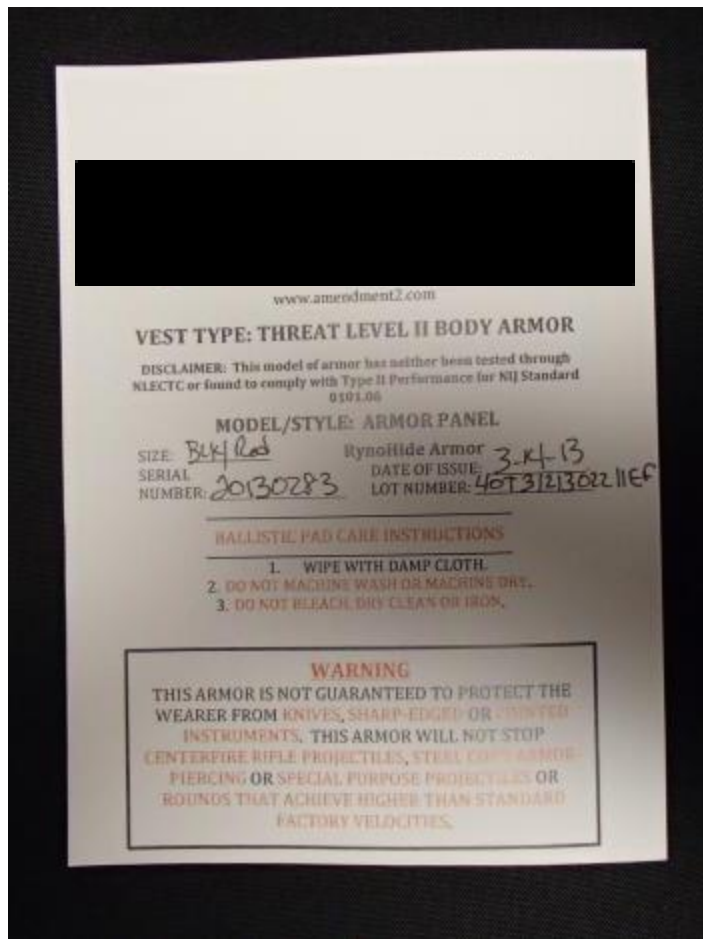


Figure 4. Information presented on ballistic insert (sewn into backpack and not visible to consumers).



Figure 5. Ballistic insert care instructions.



Figure 6. Consumer view when opening main section of backpack. Stitching has been removed in order to access ballistic panel.

2. EVALUATION STRATEGY/TESTING PLAN DEVELOPMENT

A comprehensive testing plan was developed with input from CPSC staff, NIST staff and ERDC staff to address the release scenario and exposure scenario. It was decided that release from this “uncompromised form” would be the least likely route to exposure. To maximize the potential for release measurement we decided to remove this outer casing thus “compromising” the pristine insert for initial experiments. This “compromised” form was determined to be a worst case scenario as the outer casing would need to be torn and removed prior to measurements. In addition, the removal of the outer casing allowed for the insert to be subdivided into 50.8 mm × 50.8 mm squares to facilitate multiple test cases. These squares were cut with a band-saw and resulted in partially frayed edges. Upon visual inspection, the edges of the cut material resembled the original edges of the insert.

A two tiered testing approach was developed to evaluate CNT release from the ballistic panel. The first tier focused on the pristine material. Pristine was used to describe the test squares that were not subjected to any advanced aging techniques. The second tier focused on an aged sample that encompassed UV exposure, washing, heat or physical abuse. In addition, the testing in tier 2 included analysis of liquid mediated release from dry release testing. Testing within the study described here focuses only on the liquid mediated testing. Liquids used for the release testing include wash solutions (detergents/surfactants), sweat (saline solutions) and beverages (Coke, Milk, Orange Juice). Dry exposure scenarios will not be discussed in this report. A graphical illustration of the work plan is shown in Figure 7.

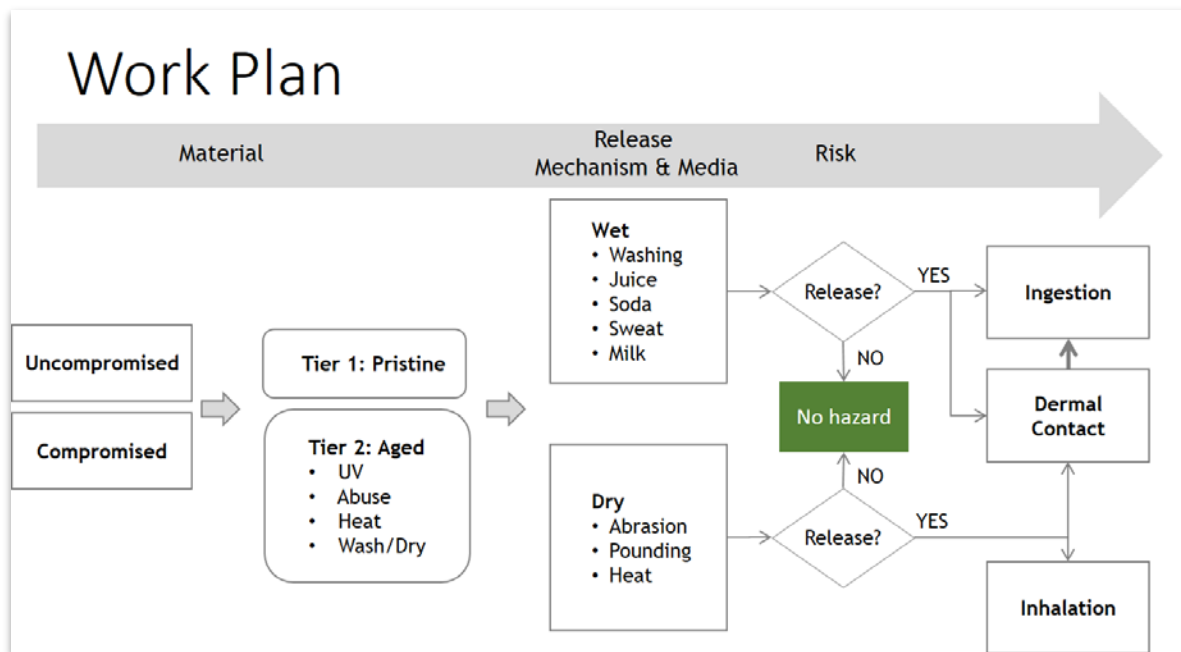


Figure 7. Graphical illustration of the testing plan.

3. MATERIALS AND METHODS USED TO QUANTIFY THE RELEASE AND FORM OF PARTICLES FROM THE CONSUMER PRODUCT

3.1 MATERIALS AND METHODS

3.1.1. BALLISTICS REPORT

The ballistic performance of the ballistic panel insert is reported in Appendix 6.7.

A video is shown in <https://www.youtube.com/watch?v=ZYm9y3iKnDQ>

3.1.2. COMPROMISED PRISTINE MATERIAL PREPARATION

As previously described in Section 2, coupons from the compromised pristine panels were pre-prepared as follows: 50.8 mm × 50.8 mm squares were cut with a band saw, resulting in coupons with partially frayed edges. Kevlar shears were used to trim excess Kevlar fibers protruding from the edges of the coupons. Upon visual inspection, the edges of the cut material resembled the original edges of the insert. Throughout this report, these coupons are referred to as “compromised pristine samples.”

3.1.3. SOLUTION PREPARATION

The wet release exposure scenario testing was carried out by exposing the compromised pristine coupons to eight solutions, each of which was either a common liquid or a substitute of common liquids/detergents. In particular, phosphoric acid and citric acid solutions were used to mimic cola and orange juice; a saline solution was representative of ocean water. Two detergent component solutions, sodium dodecyl sulfate (SDS) and sodium borate (Borax), and two reference powder detergent solutions containing European Colourfastness Establishment (ECE) -(A) reference detergent No. 2 (phosphate-free, without optical brightener) and International Electrotechnical Commission (IEC) -(A) reference detergent No. 3 (phosphate-free, with optical brightener) were also tested. Deionized water (DI, 18 MΩ·cm, ultrapure water) was used as a control. We also carried out milk exposure using store brand vitamin D milk, but no analysis was carried out due to the difficulty associated with analysis of such a complex liquid medium (curdling/large fat accumulation on filter). No other standardized milk substitutes were available.

The phosphoric acid solution was prepared at a concentration similar to that found in Coca-Cola ([What is in Coca-Cola? A briefing on our ingredients](#)) (43 mg phosphorus from phosphoric acid in 250 mL of soda, suggesting a concentration of phosphoric acid of 0.0056 M). A 0.0056 M solution of phosphoric acid was prepared by diluting concentrated (85%) H₃PO₄ in DI water. Orange juice typically contains about 0.25 g citric acid per fluid ounce according to a wide survey of juice manufacturers' nutritional information. A 0.044 M solution of citric acid was prepared by dissolving 0.845 g powdered citric acid in 100 ml of DI water. The substitute ocean water was prepared from two stock solutions, according to a standard ASTM method (ASTM D1141-98 2013). Briefly, the first stock solution consists of magnesium chloride hexahydrate, anhydrous calcium chloride, and strontium chloride hexahydrate while the

second contains potassium chloride, sodium bicarbonate, potassium bromide, boric acid, and sodium fluoride. These stocks are combined in a 2:1 ratio of the first and second solutions in a sodium chloride/sodium sulfate solution. The resulting solution contains the inorganic salts in proportions and concentrations typical of those found in average ocean water. Finally, the SDS, Borax, ECE-(A) and IEC-(A) solutions were prepared at a concentration of 4 grams/L in ultrapure water according to ISO-105-C06.

3.1.4. ACCELERATED ULTRAVIOLET LIGHT AGING

Accelerated ultraviolet (UV) light aging was carried out with a Suntest XLS+ Solar Simulator (Atlas Material Testing Solutions) using test coupons according to the weathering standard ISO-4892-2:2013. The intensity of the Xenon lamp was 60 mW/cm² between 300 and 400 nm, and the coupons were irradiated for 60 hours, corresponding to 30 days of UV aging under sun exposure. During the test, the temperature at the Black Standard Temperature, or BST, was maintained at 65 °C. The exposure period was chosen to be continuously dry. Mass loss due to UV-aging was estimated by weighing 5 coupons before (pristine) and after (UV-aged) aging with a calibrated scale (Adventurer Pro AV114 by Ohaus) with 0.1 mg readability and 0.1 mg standard deviation.

3.1.5. LIQUID EXPOSURE, WITH OR WITHOUT WASHING-INDUCED WEAR SIMULATION

Liquid exposure was carried out based on a modified version of the ISO-105-C06 test A1S in order to accommodate our experimental washing apparatus and expedite subsequent solution analysis. In more detail, compromised pristine coupons were placed in 50 mL Luer-lock syringes containing 25 mL of a test solution. For the washing scenario (SDS, Borax, ECE-(A) and IEC-(A) solutions), 5 glass beads (15 mm diameter) were also added in order to simulate wash-induced wear. Stainless steel beads were initially used but they were replaced with glass beads due to concerns regarding corrosion and metal leaching. Each filled syringe was placed on a rotating arm assembly operating at a speed of ~40 RPM (measured at 39.2 RPM with an ES 332 tachometer) for 30 minutes. All of the tests were carried out at room temperature (~25 °C). The UV-aged coupons were placed inside the syringe such that the UV exposed side faced the center of the syringe.

At the end of the liquid exposure the coupons were immediately removed, dried in a bake module (Brewer Science 200CBX) maintained at 95 °C, and stored for further analysis. Five mL of the (unfiltered) solution was collected and the remaining solution (20 mL) was filtered through an in-line stainless steel filter holder assembly containing a 0.4 µm pore size, gold coated polycarbonate track etch (PCTE) membrane filter at a rate of 0.2 mL/minute (KDS 220 or KDS 101 syringe pumps). The PCTE membrane filter was previously sputter coated with a thin layer of gold in order to facilitate subsequent scanning electron microscopy (SEM) observations. The filtered solutions were collected in glass vials. We used two different methods to minimize the amount of solution remaining inside the filter assembly during the filtering process. For transparent unfiltered solutions, which were not likely to deposit a significant amount of material onto the membrane filters, when the syringe plunger reached the end of its travel, the filter assembly was disconnected from the syringe and connected to a compressed air gas line. The amount of the filtered solution was periodically monitored and compared to that of a known standard (for example, 20 mL of DI water in a vial of the same volume and size). Filtration was deemed complete

when the volume of the extracted solution became visually equal to that of the reference. By blowing air into the filter assembly, filtration of the remaining solution was accomplished within 10 minutes. For opaque solutions, which deposit a significant amount of material onto the membrane filter, a gentler approach was used. The syringe plunger was set back to accommodate a total volume of ~45 mL (20 mL solution + 25 mL air) and filtration was carried out at a rate of 0.2 mL/minute.

3.1.6. RELEASE FROM UV-AGED COMPROMISED MATERIAL BASED ON ADHESION TEST

The release potential from UV-aged coupons was evaluated by carrying out an adhesion test which involved pressing and peeling away a 5.0 × 5.0 mm adhesive coated copper tape onto the surface of a UV-aged coupon. The test was carried out twice on two separate UV-aged coupons and SEM images from the surface of the copper tape which came in direct contact with the coupon surface were obtained. This method was similar to traditional tape testing for adhesion testing of coatings such as referenced in ASTM D3359. The method was altered to include copper tape vs scotch tape and not cross hatching was performed.

3.1.7. OPTICAL IMAGING

Optical images of the filtered and unfiltered solutions and filters were taken with a Zeiss stereo microscope Discovery.V20 and a Canon EOS Rebel T1i digital camera equipped with an EF-S 18-55 mm 1:3.5-5.6 IS zoom lens respectively. All other photos were taken with an 8 megapixel camera (Blackberry Z10).

3.1.8. FOURIER TRANSFORM INFRARED (FTIR) SPECTROSCOPY

Attenuated total reflectance (ATR) FTIR absorbance spectra, between 500 and 4500 cm^{-1} , were acquired with a Nicolet 6700 FTIR spectrophotometer equipped with an ATR crystal. FTIR spectra were collected from various components of the ballistic insert, including the pristine and UV-aged coupons. The spectra were acquired by placing either the full coupon in contact with the ATR crystal or by forming a compacted pellet from the CNT containing matrix which was removed from a coupon after soaking in chloroform for 5-10 minutes.

FTIR spectroscopy is a technique based on the selective absorption of infrared radiation through a sample. Infrared (IR) spectra are sensitive to changes in the dipole moment of materials (vibrational modes) and can be used to monitor hetero-nuclear functional group vibrations and polar bonds such as O-H stretching in water. Depending on the molecular structure of a material, some of the infrared radiation will be absorbed and some will be transmitted, and the resulting spectrum can uniquely identify the material. Therefore, IR spectroscopy can be used to identify unknown materials, determine the quality or consistency of a sample, as well as determine the amount of components in a mixture. Fourier Transform Infrared (FTIR) spectroscopy overcomes limitations of dispersive instruments (e. g. single point collection, slow scanning process) by measuring all of the infrared frequencies simultaneously, rather than individually. FTIR employs a broadband infrared illumination source coupled to a scanning interferometer. The scanning interferometer consists of a beam splitter which splits the incoming beam into two beam

paths, one of which has a fixed length and the other can be scanned resulting into interference of the two beams. The resulting signal is an interferogram which can be transformed (by Fourier transformation) to a broadband absorption spectrum.

3.1.9. SCANNING ELECTRON MICROSCOPY (SEM)

High-resolution SEM images are obtained by scanning an electron beam in a rectangular raster pattern across a defined area on the sample surface allowing for magnifications much higher than those achieved with optical microscopy. The position of the electron beam is controlled by electromagnetic lenses in the column of the microscope. As the electron beam interacts with the sample, its position is spatially correlated with signal received by various types of detectors. Secondary electron (SE) detectors are designed to detect low-energy secondary electron ionization products emitted from atoms when impacted by the incident electron beam. SE detectors are generally better for imaging surface topography. Backscattered electron (BSE) detectors are designed to detect high-energy electrons emitted from the sample as a result of scattering events as the incident beam scans across the surface. Since scattering of electrons is dependent on the relative density of a given phase (i.e., low density phases absorb more electrons than high density phases), the amount of BSE signal detected is proportional to the density of the phase. As a result, brightness can be used as an indicator of relative density (e.g., dense metallic particles will be brighter than a low-density organic matrix).

SEM measurements were performed using a FEI Nova NanoSEM 630 Field Emission scanning electron microscope under high vacuum. Accelerating voltages of 5 kV to 10 kV and spot sizes of 2.0 to 5.0 nm were used for imaging. Samples were attached to stubs with double-sided conductive carbon tape. In order to assess the surface of the coupons prior to liquid exposure or washing experiments, samples from the pristine and UV-aged coupons were also imaged. Rectangular samples were cut out from coupons with Kevlar shears and SEM imaging was carried out on the surface of the polymer matrix impregnated with the MWCNTs. For filters with a significant amount of accumulated material, SEM imaging was limited by surface charging, irregular topography and compaction of the collected material. Therefore, in order to facilitate SEM observations, additional washing experiments were carried out with ECE-(A) and IEC-(A) solutions with a smaller amount of detergent present in the washing solution than the one recommended by the ISO 105-C06 standard (4 grams/L). Alternatively, aliquots from collected unfiltered solutions were drop-cast on gold-coated silicon wafer pieces. Finally, in order to minimize surface charging and allow high resolution imaging of non-conductive particles, gold was sputtered onto the samples/filters. The film thickness of the gold film was estimated to be between 20 and 60 Angstroms.

3.1.10. RAMAN SPECTROSCOPY

Raman spectroscopy is a technique based on the inelastic scattering of photons (light) due to the interaction of incident photons with the vibrational energy levels of a material. Raman spectra are unique fingerprints enabling chemical identification of compounds under investigation.

Raman spectra are obtained by focusing laser light onto the surface of a sample and detecting inelastically scattered light with a spectrometer and a charge coupled device (CCD) detector. Raman spectroscopy is an invaluable tool for the identification of CNTs because they exhibit strong Raman signatures. Quantification of carbon nanotube release is generally very difficult with this technique. The Raman peaks associated with CNTs are the D band, the G band, the D' band which appears as a shoulder of the G band, and the second-order harmonic of the G band, the G' (or 2D or D*) band. The D (defect) band originates from the first order scattering of sp^2 carbons in the defects such as in-plane substitutional hetero-atoms, vacancies and grain boundaries which lower the crystalline symmetry of the carbon nanotube's quasi-infinite lattice (McNally *et al.* 2011). The G band is attributed to tangential modes of the carbon nanotube lattice whereas the D' band arises due to the symmetry breaking from sp^2 crystallites (Soin *et al.* 2011). The location of the bands depends on a number of parameters such as carbon nanotube diameter, defects, excitation wavelength, temperature, etc. For MWCNTs under visible excitation (514 nm) the D band is located at $\sim 1350\text{ cm}^{-1}$, the G band is located at $\sim 1580\text{ cm}^{-1}$ and the G' band is at $\sim 2700\text{ cm}^{-1}$ (Bokobza *et al.* 2012). Under infrared excitation, the D and G' bands show a significant shift to lower wavenumbers (Bokobza *et al.* 2013). With Raman spectroscopy, MWCNTs can be distinguished from single walled CNTs due to the lack of the low wavenumber, radial breathing modes (RBMs) (Soin *et al.* 2011).

Raman spectra were collected using a confocal Raman microscope (Horiba XploRA). As reference, carbon nanotube spectra were collected from a thin layer of the polymer matrix extracted from a pristine coupon. The coating was removed from the pristine coupon after soaking the entire coupon in chloroform for 5-10 minutes, and then smearing it onto the surface of a polydimethylsiloxane (PDMS) stamp. Areas of interest were identified under 10 \times and 100 \times optical magnifications. Under 532 nm and 785 nm laser excitation, backscattered Raman spectra were collected with the 100 \times objective (Olympus, 0.9 NA) and resolved with a 1200 lines/mm or a 600 lines/mm grating. The 1200 lines/mm grating provides higher resolution spectra whereas the 600 lines/mm grating has lower resolution but higher optical power throughput to the detector. The bandwidth of the laser line filter allows collection of meaningful data for wavenumbers higher than approximately 150 cm^{-1} . Prior to collecting Raman spectra, the instrument was calibrated using the first order peak Raman peak of a silicon wafer (520.6 cm^{-1}). We were not able to obtain Raman spectra from particles collected on the filters because, even at the lowest power settings, the membrane filter melted. Alternatively, aliquots from each unfiltered solution were drop-cast on gold-coated silicon wafer pieces and examined under the Raman microscope. Depending on the strength of the observed Raman signal, the integration time was varied between 2.5 and 60 seconds. The maximum laser power incident on the samples was $3.5\text{ }\mu\text{W}$ under 532 nm excitation and $30\text{ }\mu\text{W}$ for 785 nm excitation. In order to aid visualization of the Raman data, the spectra were plotted after removal of a broad fluorescence background (background subtraction), intensity scaling and vertical translation.

3.1.11. THERMOGRAVIMETRIC ANALYSIS (TGA)

TGA is an analytical technique in which changes in physical and chemical properties of materials are measured as a function of increasing temperature (with constant heating rate), or as a function of time (with constant temperature and/or constant mass loss). TGA is typically used to determine a material's thermal stability and its fraction of volatile components by monitoring the changes in mass that occurs as a specimen is heated. TGA is carried out in air or in an inert atmosphere, with sample mass recorded as a function of increasing temperature.

TGA measurements were carried out with a Netzsch TG 449 F1 Jupiter combined TGA/DSC in nitrogen and in air. Alumina crucibles were filled with the coupon coating (previously extracted from pristine coupons with chloroform). The extracted material was kept in a dry box prior to the TGA measurements in order to reduce the amount of moisture in the samples. We carried out three TGA experiments with two replicates (Replicate 1 and Replicate 2). Under inert atmosphere, the temperature was initially increased continuously from 30 to 1200 °C at a rate of 10 °C/min, whereas subsequently the temperature was increased in the form of a custom ramp, which included constant temperature intervals. In air, the temperature was continuously increased from 30 to 1100 °C at a rate of 10 °C/min.

3.1.12. TOTAL METALS ANALYSIS

Total metals analysis was performed on the filtered and unfiltered solutions, obtained from pristine coupons, using inductively coupled plasma mass spectroscopy (ICP-MS). In this technique, samples are introduced to a plasma (partially ionized gas consisting of highly energetic species) which operates at sufficient power to break down and ionize the elemental components of the samples. A quadrupole mass spectrometer filters the ions based on their mass to charge ratio so that only ions with a specific mass to charge ratio reach the electron multiplier detection system. The signal intensity for a given ion is proportional to its concentration in the solution presented to the instrument.

Detection of CNTs in complex media using ICP-MS has been previously demonstrated (Reed *et al.* 2013). This technique is based on the detection of metal nanoparticle catalysts embedded in the CNT structure, and it has been successfully used to detect release of CNTs from a polymer matrix with increased loading. Quantification of CNT release is based on a calibration curve of the ICP-MS signal, for the given catalyst, as function of CNT concentration. 5 mL and 0.5 mL of the filtered and unfiltered solutions, respectively, were prepared by hot block digestion of a ~0.5 g portion of raw material in concentrated HNO₃. The digested samples were diluted to a total volume of 50 mL in 1% HNO₃. A 0.5 mL aliquot of this volume was diluted to 10 mL in 1% HNO₃. This final volume was analyzed using a Perkin Elmer Optima 5300 DV ICP-AES, utilizing check standards at the beginning and end of each run. Similarly, undigested samples from filtered and unfiltered solutions were also tested. Calibration curves yielded the relevant metals' absolute concentrations. These concentrations were transformed to weight percentages by stoichiometric calculations. The catalysts present in the CNTs embedded in the polymer matrix were determined to be nickel and zinc. Therefore, the nickel signal was monitored for ⁶⁰Ni isotope and the zinc signal was monitored for the ⁶⁶Zn isotope.

3.1.13. UV-VIS SPECTROSCOPY AND DIGITAL IMAGE INTENSITY ANALYSIS FOR QUANTITATIVE ESTIMATION OF RELEASE PRODUCTS

The presence of release products in the solutions was investigated by UV-VIS spectroscopy. In a double-beam spectrophotometer, light splits into two beams before reaching the sample. One beam is used as a reference whereas the other beam passes through the sample. The intensity of the reference beam is taken as 100% Transmission (or 0 Absorbance), and the measurement displayed is the ratio of the two beam intensities. Absorption spectra, from 190-900 nm, were measured with a Thermo-Scientific Evolution 600 UV-VIS spectrophotometer double beam spectrophotometer, with solutions placed in a quartz cuvette. The absorption spectra were calibrated (100% Transmission) with respect to DI water. Further, the absorption spectra of DI-water standard solutions containing OH-functionalized MWCNTs (Cheaptubes) were obtained for reference to the MWCNT concentration. According to the manufacturer specifications, the OH-functionalized MWCNTs had an outer diameter of 10-20 nm and length between 10-30 μm . The MWCNTs were dispersed in DI water with the aid of an ultrasonic cell disruptor and UV-VIS spectra were collected. Calibration plots of MWCNT concentration versus absorbance were obtained for 250 nm, 500 nm, 700 nm and 800 nm; all of which exhibited a linear concentration dependence, as dictated by the Beer-Lambert law, up to 0.05 mg/mL (see Figure 29 (b)).

In addition to the UV-VIS measurements, digital image intensity analysis was employed as a means for estimating the amount of CNTs in the unfiltered solutions. In more detail, for each solution (unfiltered pristine, unfiltered UV-aged and neat solution) we collected a digital image of cuvettes with a known amount of OH-MWCNTs in suspension and that of the solution of interest. In order to ensure uniform background illumination, the cuvettes were placed in front of a laptop screen showing a blank (white) slide. Using ImageJ, each photo was converted to an 8 bit grayscale image. Next, a rectangular section (150 x 150 pixels), from each of the liquid filled cuvettes, was selected using the rectangular selection tool and its mean grayscale intensity and standard deviation were obtained under the "Analyze: Measure" option of the software (Schneider *et al.* 2012). Therefore, for each image a calibration curve of grayscale intensity versus CNT concentration was constructed. Solutions for which the corresponding neat solution was darker than the DI water, were adjusted to DI water baseline by subtracting the contribution of the neat solution. Here we assume that all of the release products are CNTs; therefore once again we overestimate the amount of CNTs present in the solutions. In addition, since the digital images are converted to grayscale intensity, any solution colors will contribute to the grayscale intensity regardless of whether the original solution color is gray or black.

4. RESULTS AND INTERPRETATION

4.1. RESULTS

4.1.1. PRELIMINARY ASSESSMENT OF BALLISTIC BACKPACK INSERT

Figure 8 shows a representative ballistic backpack insert after removal from its case. The ballistic insert consists of a high density polypropylene cushion foam (thickness ~ 2.75 mm) sandwiched between multiple ballistic panel layers (sheets). In particular, four panels are layered on the front

and three on the back of the polypropylene cushion. Each of the ballistic panels consists of a woven fiber mat which is coated on both sides with a polymer containing MWCNTs.



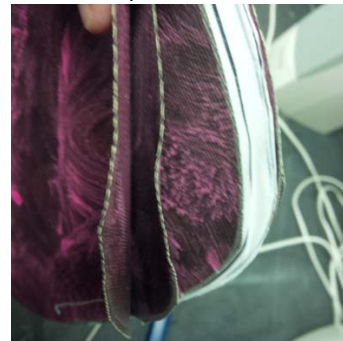
(a) Optical image of a ballistic backpack insert removed from a backpack.



(b) Front: 4 panels



(c) Middle:
High density polypropylene



(d) Back: 3 panels

Figure 8. Optical images of the ballistic backpack insert: (a) after removal from the backpack, (b) front portion consisting of four ballistic panel layers, (c) middle portion consisting of a high density polypropylene cushion, and (d) back layer consisting of three ballistic panel layers.

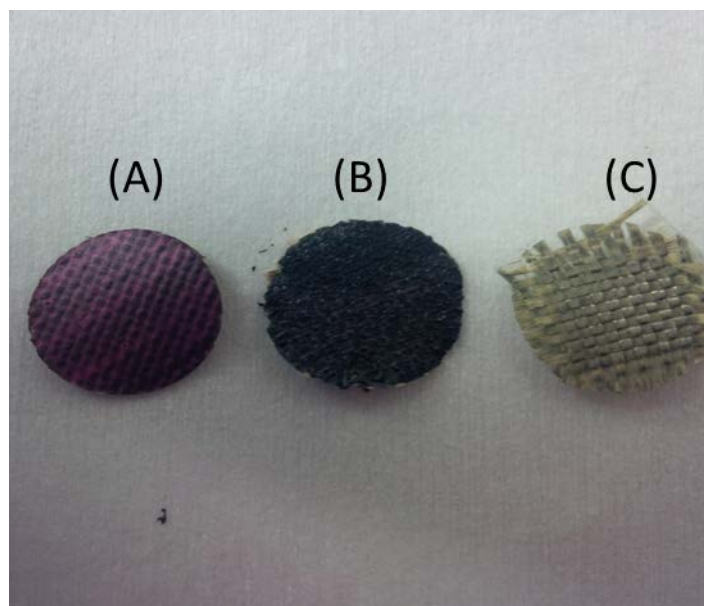
4.1.2. COMPROMISED PRISTINE MATERIAL

4.1.2.1. ANALYSIS OF COMPROMISED PRISTINE MATERIAL PRIOR TO LIQUID EXPOSURE/WASHING SIMULATION

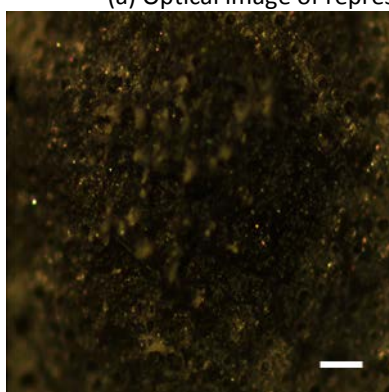
OPTICAL MICROSCOPY

Optical images of 1-inch circular cut-outs obtained from the ballistic panels are shown in Figure 9. The cutouts correspond to: (A) as received panel material, (B) post chloroform swelling material and (C) panel with coating removed following chloroform swelling, revealing the underlying

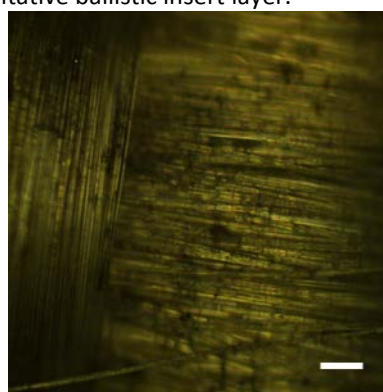
fiber woven mat geometry in more detail. Higher optical magnification images of the (B) and (C) surfaces are shown in Figure 9(b) and Figure 9(c).



(a) Optical image of representative ballistic insert layer.



(b) Optical image of "(B)"



(c) Optical image of "(C)"

Figure 9. Optical images of the material used for the front and back layers of the ballistic insert panel. (a) "(A)" as received layer material, "(B)" post chloroform swelling and "(C)" coating removed after swelling, (b) and (c) higher magnification optical images of "(B)" and "(C)". Scale bars correspond to 10 μm .

FTIR ANALYSIS

Preliminary identification of the materials used in the ballistic insert was carried out with FTIR spectroscopy. The FTIR absorbance spectra collected from the yellow fiber (woven mat material) and the coating are shown in Figure 10. The coating was removed from a pristine coupon after soaking the entire coupon in chloroform for 5-10 minutes. Based on FTIR peak indexing, the yellow fiber has been identified as Kevlar (see Appendix 6.1), whereas the polymer from the coating material reasonably matched the FTIR signatures of polychloroprene (81.6% match).

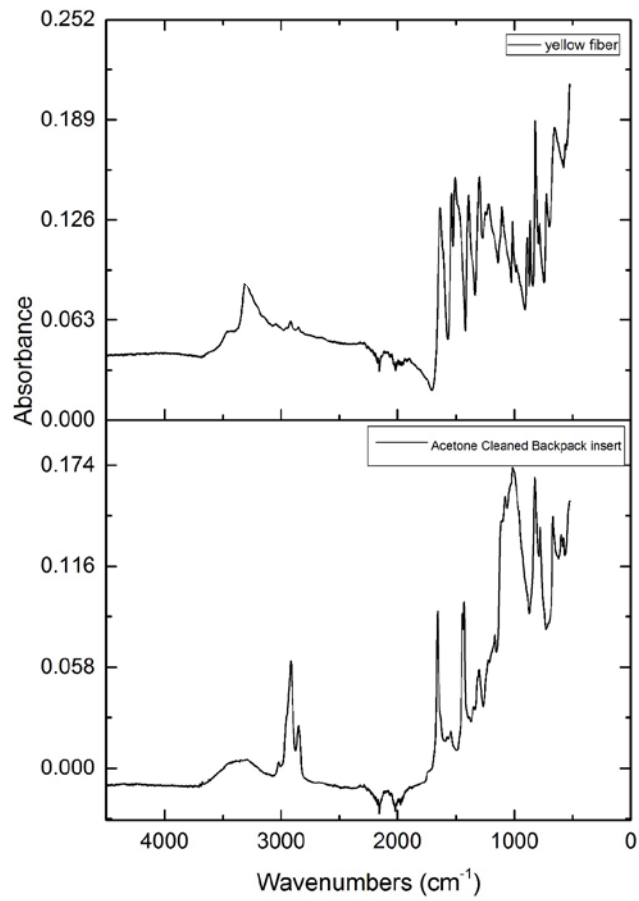


Figure 10. FTIR absorbance spectra obtained from the fibers and coating (black material). The fibers have been identified as Kevlar whereas the coating material has been matched to polychloroprene (81.6% match).

SEM ANALYSIS

SEM micrographs of the compromised pristine coupons are shown in Figure 11. Additional micrographs are provided in Appendix 6.9.1. Figure 11(a) is a low magnification SEM micrograph representative of the typical morphology encountered in the compromised material comprising of wrinkles, dimples and a few protruding fibrous strands which are likely Kevlar fibers. Figure 11(b) is a high magnification micrograph of an individual carbon nanotube protruding from the surface of the coupon. The carbon nanotube (inner lighter portion) is surrounded by a thin layer of material which is likely a polymer coating. As shown in Figure 11(c), another type of surface defect was observed. The defect is a cluster with pronounced surface roughness and protruding nanoparticles consistent with the morphology of CNTs. These defects are typically the result of inhomogeneous mixing of CNTs within the polymer blend typically due to carbon nanotube agglomeration (Huang *et al.* 2008).

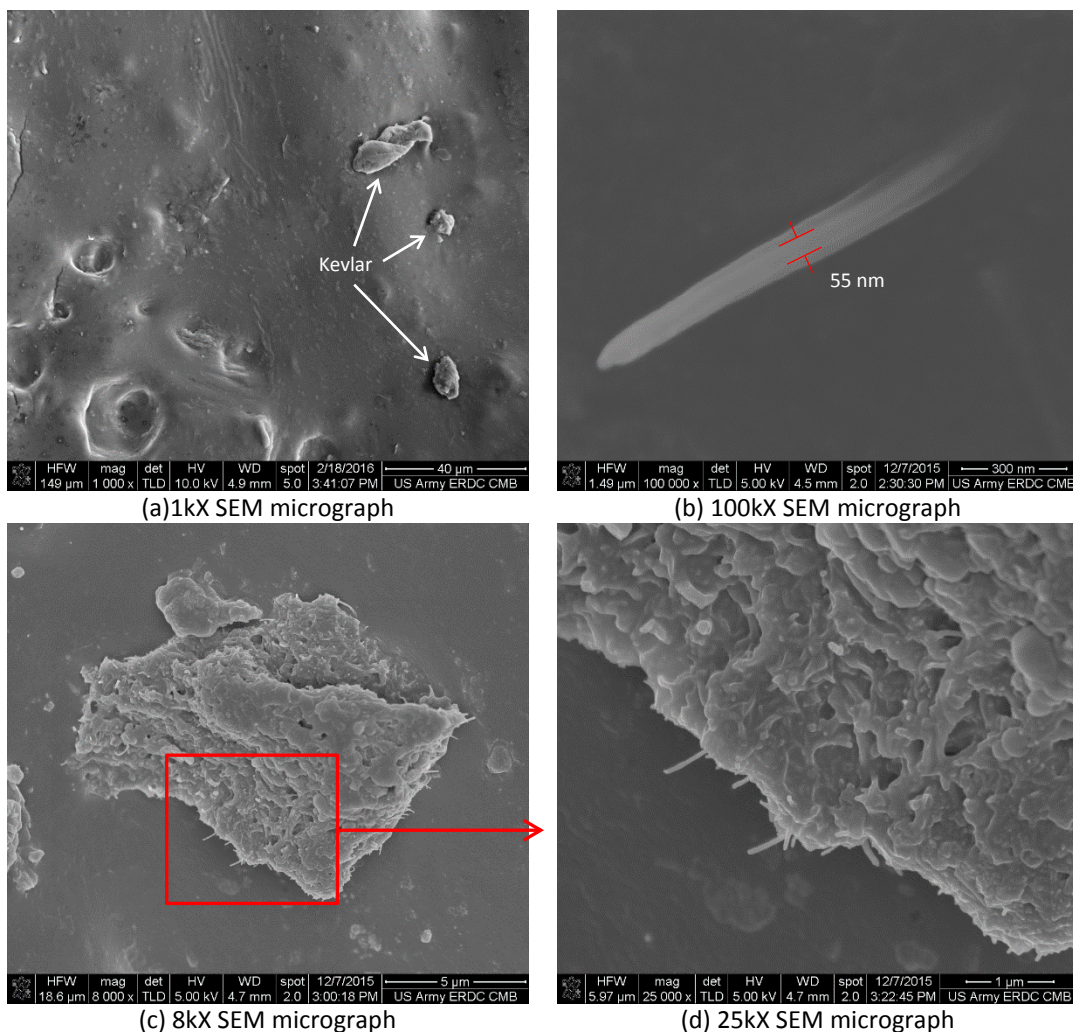


Figure 11. SEM micrographs of the compromised pristine coupon obtained from a Kevlar® woven mat with MWCNT-reinforced polymer coating. (a) Representative surface morphology under low SEM magnification, (b) high magnification SEM image of protruding carbon nanotube, (c) surface defect due to inhomogeneous mixing of MWCNTs, and (d) higher magnification SEM of (c).

RAMAN SPECTROSCOPY

Raman spectra from the coupon coating were obtained under 532 nm and 785 nm laser excitation are shown in Figure 12. The coating was removed from a pristine coupon after soaking the entire coupon in chloroform for 5-10 minutes. The spectra are background subtracted in order to remove fluorescence contributions (broad background) and facilitate identification and comparison of the relevant Raman peaks. The spectra are indicative of the presence of CNTs. In particular, the D, G, D' and G' peaks associated with CNTs are identified. The spectral location of the peaks and their dependence on wavelength is in good agreement with previous studies (Bokobza *et al.* 2013). The observation of a strong D peak is indicative of CNTs with defects, i. e. low quality CNTs, whereas the lack of radial breathing modes (RBM) between 150-300 cm^{-1} are indicative of MWCNTs. For 532 nm and measurements at six different locations, the ratio of the D peak intensity (amplitude not area) I_D over the intensity of the G peak I_G was calculated to be $I_D/I_G = 1.15 \pm 0.13$. According to Doudrick *et al.*, such a ratio is indicative of thermally "weak" CNTs with oxidation temperatures for 50% mass loss expected to be between 700 and 750 $^{\circ}\text{C}$.

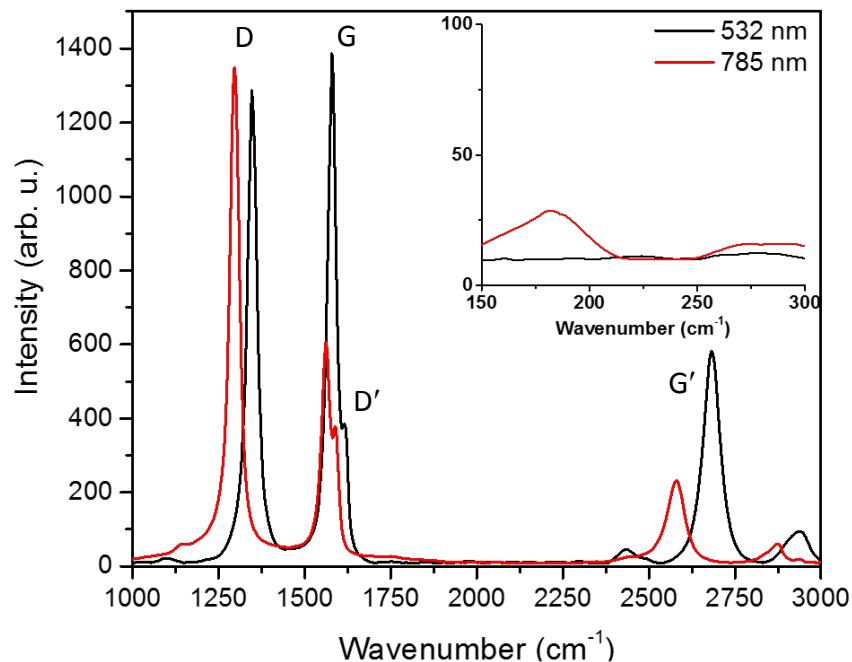
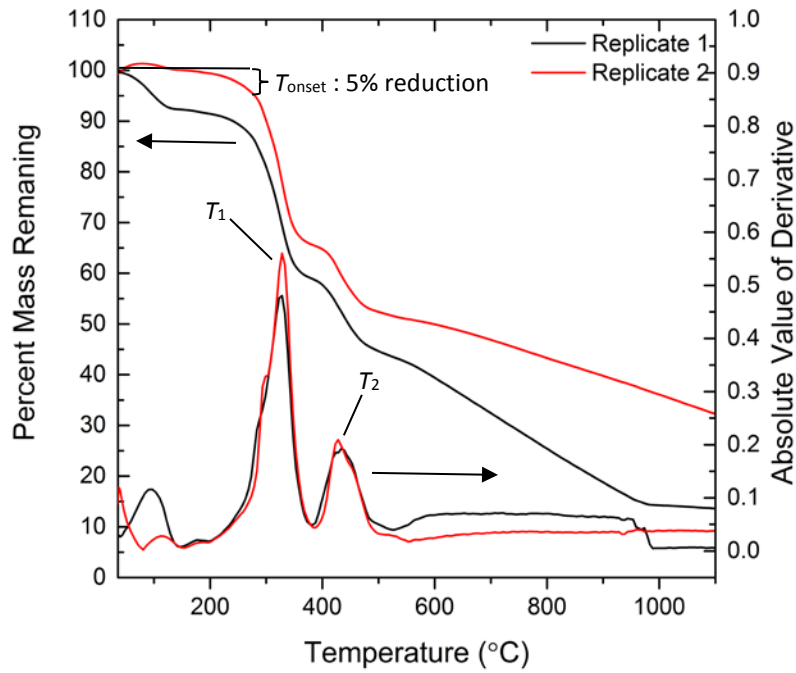


Figure 12. Raman spectra verifying the presence of CNTs in the coating, obtained from a pristine coupon, under 532 nm and 785 nm laser excitation. The inset shows the 150-300 cm^{-1} spectral region where no RBMs are observed indicating that the CNTs are MWCNTs. The coating was removed from the Kevlar mat after soaking the entire coupon in chloroform for 5-10 minutes.

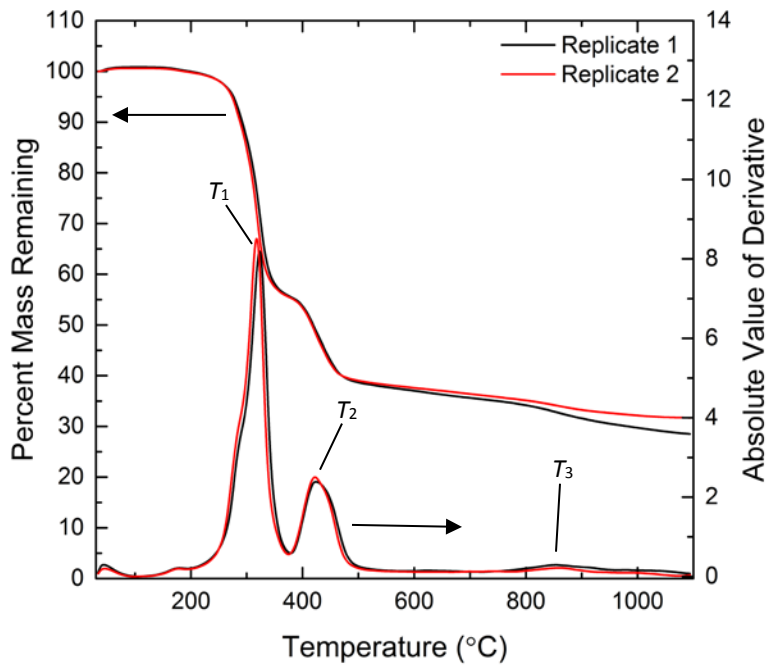
THERMOGRAVIMETRIC ANALYSIS

Mass loss curves of the coating (polymer with CNTs) were obtained using TGA in an inert (nitrogen) environment and in air, and they are shown in Figure 13. The coating was removed from a pristine coupon after soaking the entire coupon in chloroform for 5-10 minutes. The increase in the mass observed at the lower temperatures is an artifact attributed to variations in initial moisture content in the material. Regardless of the environment, all mass loss curves exhibit multi-step decomposition of the material. In both environments, we have identified three stages of material degradation below 500°C. The first stage (onset stage) occurs at <300 °C and typically involves the degradation of organic additives which are incorporated during or post polymerization of the monomer (Subramaniam *et al.* 2012). In our experiments, the onset temperature (T_{onset}) of this stage is defined as the temperature corresponding to 5% degradation of the mass present between 150 and 250 °C. The temperature range and the corresponding mass were chosen in order to avoid artifacts related to moisture present in the samples. The average T_{onset} was determined to be ~ 273 °C in nitrogen and ~ 271.5 °C in air. The negligible difference between T_{onset} in nitrogen and in air can be attributed to the increased thermal stability of the composite material due to the presence of CNTs (Subramaniam *et al.* 2012). According to Subramaniam *et al.*, polymer degradation occurs in the next two stages, with hydrogen chloride, in addition to other degradation products, forming during both the second and third stage. By taking the derivative of the mass loss curve we can determine the temperatures at which the mass loss are maximum. These temperatures are denoted as T_1 and T_2 , and they describe the second and third stage of polymer degradation, respectively. The average T_1 and T_2 were determined to be ~ 324 °C and ~ 428 °C in nitrogen and ~ 321 °C and ~ 428 °C in air, respectively. As previously discussed, the proximity of T_1 and T_2 under inert and oxidizing conditions is indicative of CNT-induced increase in the thermal stability in the composite. The increased thermal stability of the composite is further verified by the large amount of residual mass (34.7%) present at 800 °C under oxidizing conditions.

Based on Doudrick *et al.*, the CNTs embedded into the polymer matrix are expected to be thermally weak with significant mass loss between 700 and 750 °C under oxidizing conditions. With TGA, a small mass loss, under oxidizing conditions only, is observed at a somewhat higher temperature of $T_3 \sim 853.5$ °C. This mass loss could be attributed to CNT combustion because no other mass loss is expected at such high temperatures from polychloroprene (Subramaniam *et al.* 2012). Unfortunately, quantitative estimation of the actual amount of CNTs present in the composite was not possible with TGA. Weight loss events were observed to be dependent on material starting mass. This indicates that there was variability within the polymer matrix. With no prior knowledge of additional additives their ratio relative to the polymer it is difficult to quantify the amount of CNTs present in the polymer film. This method would need further development and standardization before definitive values could be reported.



(a) TGA of coating in nitrogen under continuous heating, constant ramp



(b) TGA of coating in air under continuous heating, constant ramp

Figure 13. TGA mass loss curves of coating (polymer with CNTs) in (a) inert (nitrogen) and (b) oxidizing (air) conditions. T_{onset} corresponds to the temperature at which 5% of the plateau mass is reduced by 5% whereas T_1 , T_2 and T_3 are the local maxima of the absolute values of the derivative of the mass loss. Each temperature is descriptive of a specific thermal decomposition stage of the composite material. T_{onset} corresponds to decomposition of additives; T_1 and T_2 correspond to decomposition mechanisms of polychloroprene and T_3 is attributed to CNT combustion.

4.1.2.1. ANALYSIS OF RELEASE PRODUCTS FROM COMPROMISED PRISTINE MATERIAL AFTER LIQUID EXPOSURE/WASHING SIMULATIONS

OPTICAL MICROSCOPY

Optical images of the dried filters from all solutions are shown in Figure 14. The filters for DI water, citric acid and phosphoric acid are highly reflective, indicating limited or no material release from the coupons. The ocean water substitute, SDS and Borax filters exhibit opaque areas indicative of material deposition onto the filters. More detailed imaging with SEM is required in order to determine whether the deposited material is CNT containing release product from the coupon or it was filtered from the solution itself (for example, salt crystals from the ocean water). The ECE-(A) and IEC-(A) filters show a large amount of detergent accumulation. Figure 15 shows the unfiltered solutions, which overall visually have a clear appearance. The ECE-(A) and IEC-(A) solutions exhibit high turbidity due to the presence of undissolved detergent.

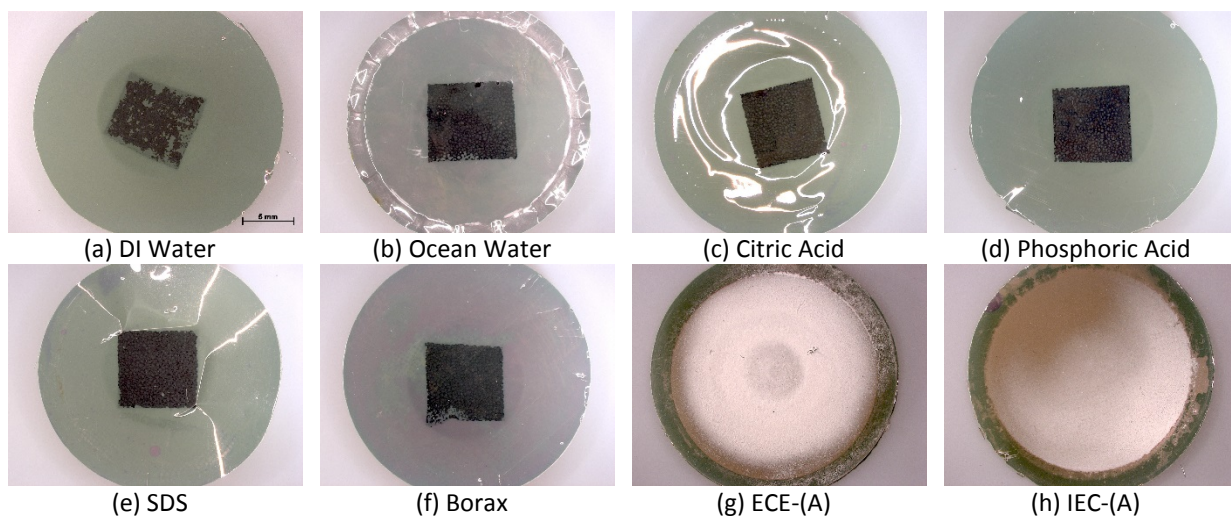


Figure 14. Optical images of the membrane filters obtained after filtering 20 mL of the solutions used for liquid exposure/ washing simulations of compromised pristine coupons. The dark rectangle in the center of the filters in (a)-(f) is carbon tape used to mount the filters prior to SEM imaging.

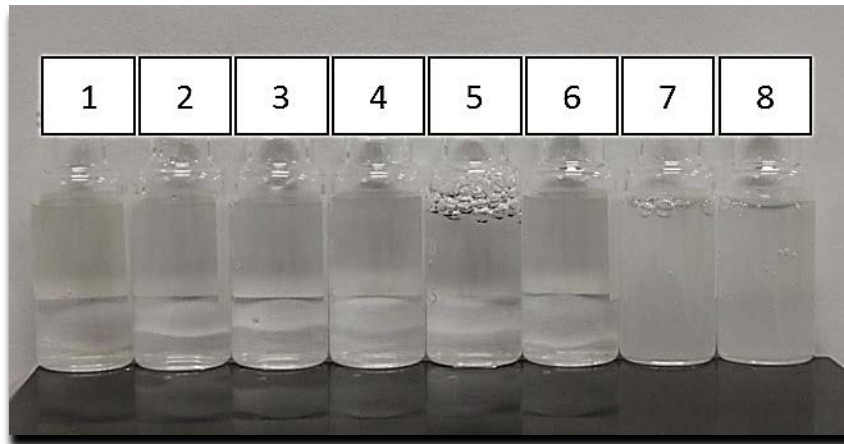


Figure 15. Optical image of unfiltered solutions obtained from the liquid exposure/washing simulation of compromised pristine coupons. From left to right: 1-DI water, 2-ocean water substitute, 3-citric acid solution, 4-phosphoric acid solution, 5-SDS solution, 6-Borax solution, 7-ECE-(A) solution and 8-IEC-(A) solutions. The cloudiness of the ECE-(A) and IEC-(A) is due to the presence of undissolved detergent in the solutions.

SEM ANALYSIS

4.1.2.1.1. DI WATER

An SEM micrograph of a release product found on the surface of the DI water filter is shown in Figure 16. Additional micrographs are provided in Appendix 6.9.1. Observation of any release products on the DI water filter was limited.

4.1.2.1.2. OCEAN WATER

A representative SEM micrograph obtained from the ocean water filter, showing salt crystals, is shown in Figure 17. Additional micrographs are provided in Appendix 6.9.1. Release products from the coupon were not observed on the filter.

4.1.2.1.3. CITRIC ACID SOLUTION

An SEM micrograph obtained from the citric acid solution filter is shown in Figure 18. The morphology of the observed particle is consistent with that of agglomerated CNTs. Additional micrographs are provided in Appendix 6.9.1. Based on SEM, release products, including CNTs, were Occasionally observed on the filter. After 30 minutes of SEM examination only 8 released particles were observed.

4.1.2.1.4. PHOSPHORIC ACID SOLUTION

Figure 19 shows an SEM micrograph obtained from the phosphoric acid solution filter. Additional micrographs are provided in Appendix 6.9.1. Based on SEM, a small amount of release products, were Occasionally observed on the filter.

4.1.2.1.5. SDS SOLUTION

SEM micrographs of the release products on the SDS filter are shown in Figure 20. Additional micrographs are provided in Appendix 6.9.1. Overall, more release products were observed on the SDS filter when compared to the DI water, ocean water, citric acid and phosphoric acid filters. The particle in the center of the micrograph has features protruding from the surface consistent with CNTs. Based on our observations ($n = 52$ particles), the release products can be either standalone polymer/carbon nanotube particles, such as the one shown in Figure 20, or polymer/carbon nanotube particles partially attached to polymer sheets such as the one shown in Figure 21. For the SDS solution, the majority of the observed release particles are of the first type. We have obtained a particle area distribution curve where the area of the particles was calculated from standalone particles with CNTs or only from the portion of the particle which contains protruding CNTs (for example, the upper left portion of the particle in Figure 21). The area of each particle was calculated as follows: the corresponding SEM image was imported to ImageJ and the pixel to micron calibration was obtained from the length of the scale bar. Next, the outline of the particle was selected using the selection brush tool, and the area of the enclosed section was calculated using the measurement tool. Automatic implementation of the particle area calculation based on the intensity threshold method was not possible due to the complex morphology of the particles exhibiting both high and low intensities as well as their lack of contrast with the background.

4.1.2.1.6. BORAX SOLUTION

SEM micrographs of the release products on the Borax filter are shown in Figure 22. Additional micrographs are provided in Appendix 6.9.1. Similar to the SDS filter, more release products were observed on the Borax filter when compared to the DI water, ocean water, citric acid and phosphoric acid filters. The highlighted particles exhibit CNTs protruding from their surface. The majority of release products are standalone polymer/carbon nanotube particles. Figure 22 (c) shows the particle area distribution curve obtained from sampling $n = 55$ particles. We used the same methodology as the one used to obtain the particle area distribution curve from the SDS solution.

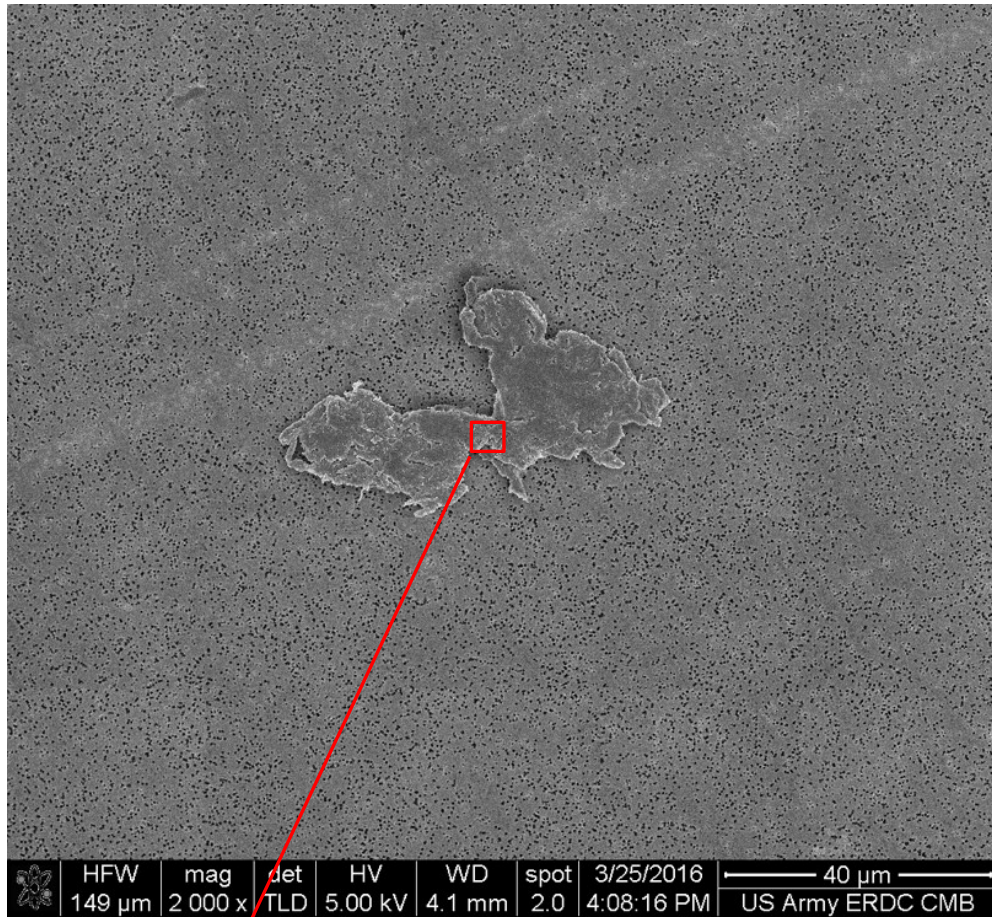
4.1.2.1.7. ECE-(A) SOLUTION

Representative SEM micrographs of the release products on the ECE-(A) filter are shown in Figure 23. Additional micrographs are provided in Appendix 6.9.1. The surface of the filter exhibits a dense network of filtered material consisting of the polymer matrix, which includes particles with protruding CNTs, polymer sheets and membranes as well as undissolved detergent. Due to the complexity of this network, it is challenging to determine whether the particles with CNTs are part of a larger cluster or unattached. Based on our SEM observations, when compared to the SDS and Borax filters, the ECE-(A) solution exhibits more release products. Figure 23(c) shows the particle area distribution curve obtained from sampling $n = 45$ particles. We used the same methodology as the one used to obtain the particle area distribution curve from the SDS solution.

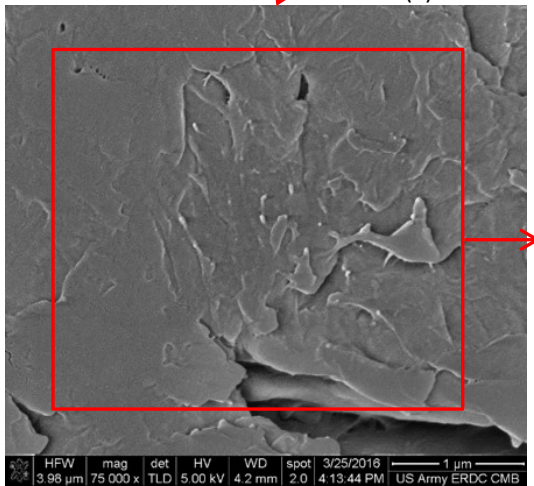
4.1.2.1.8. IEC-(A) SOLUTION

Representative SEM micrographs of the release products on the IEC-(A) filter are shown in Figure 24. Additional micrographs are provided in Appendix 6.9.1. Similar to the ECE-(A) filter, the surface of the IEC-(A) filter also exhibits a dense network of filtered material and a density of release products similar to those of the ECE-(A) filter. The particle area distribution curve was obtained

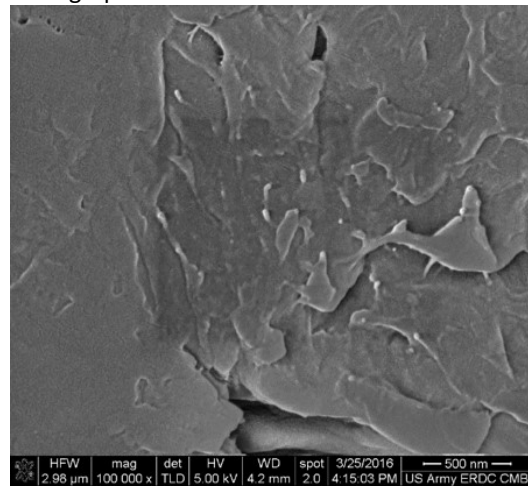
from sampling $n = 56$ particles. We used the same methodology as the one used to obtain the particle are distribution curve from the SDS solution.



(a) 10kX SEM micrograph



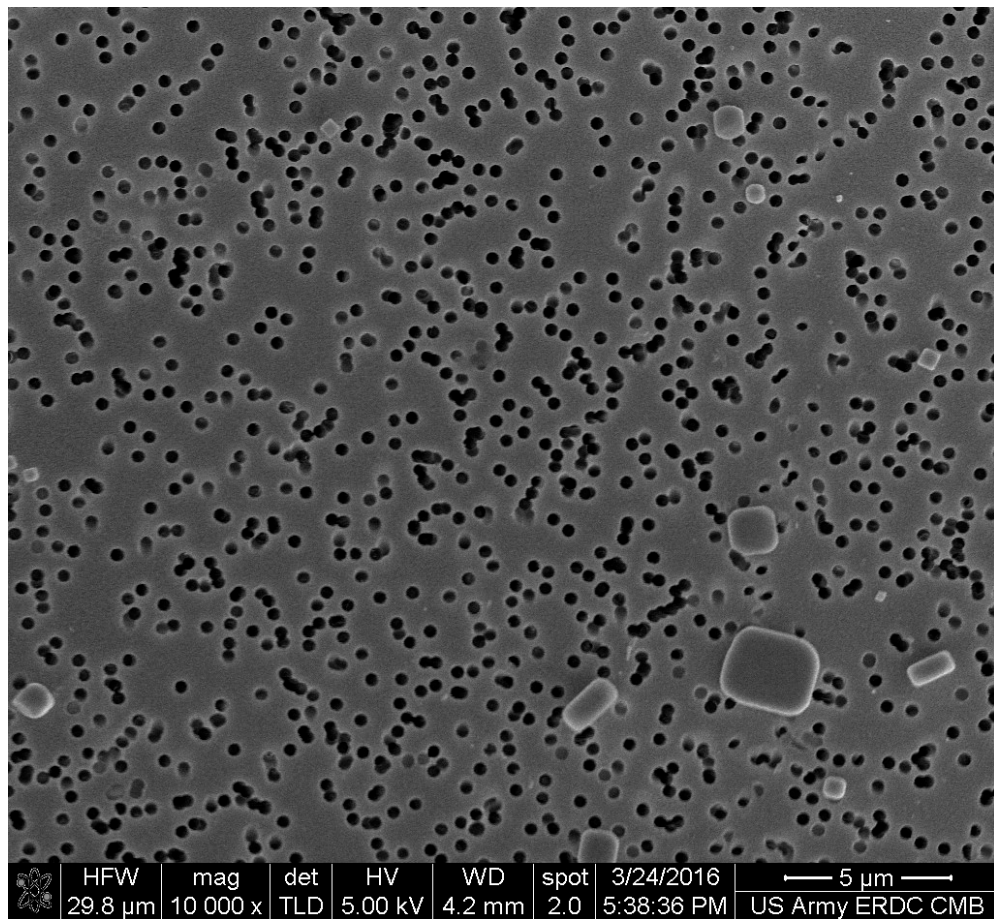
(b) 50kX SEM micrograph



(c) 100kX SEM micrograph

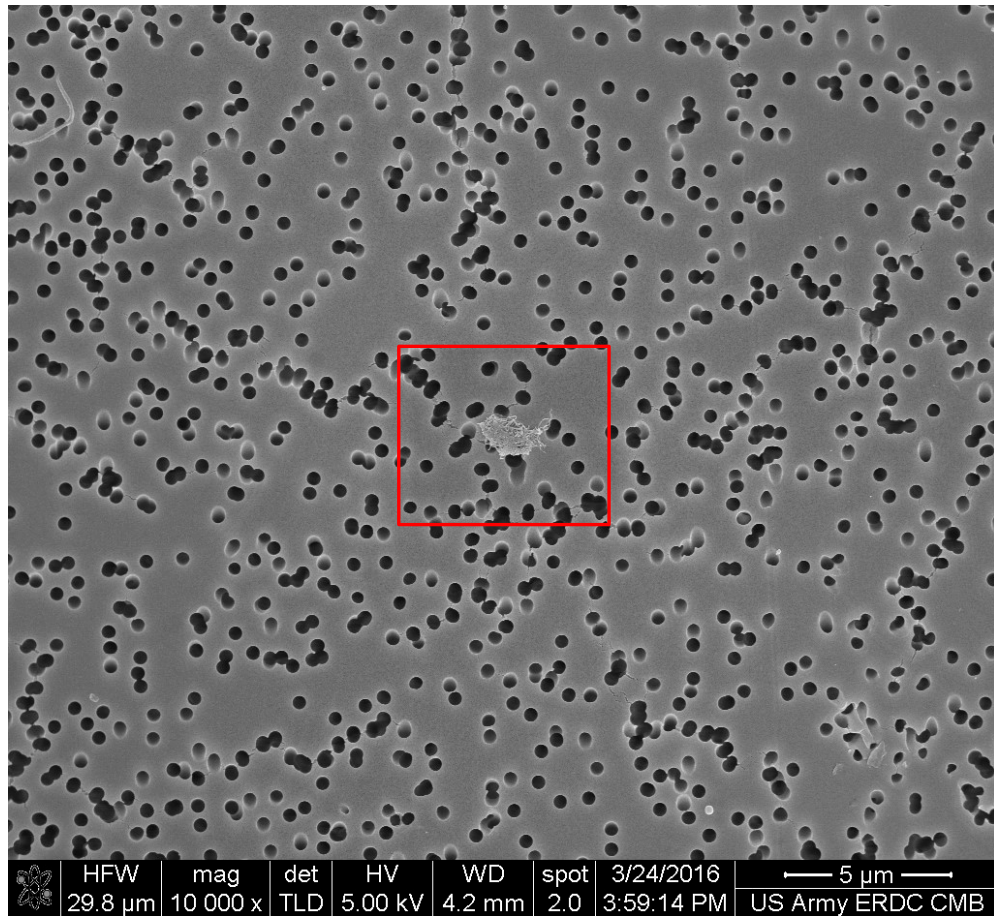
Figure 16. SEM micrographs obtained from the liquid exposure of a compromised pristine coupon in DI water solution. (a) Low magnification SEM image of the membrane filter showing a release product. (b)-(c) High magnification SEM images of the surface of the release product revealing

the presence of partially embedded CNTs. Note: the dark “specks” on the background are the randomly distributed pores of the membrane filter.

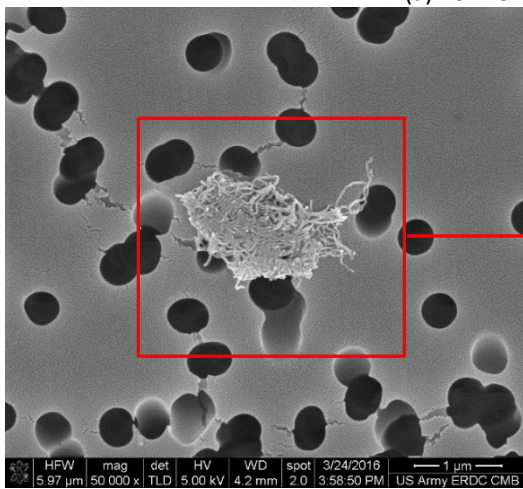


10kX SEM micrograph

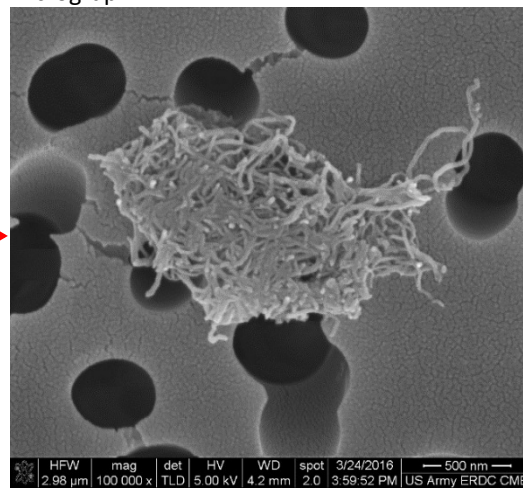
Figure 17. SEM micrograph obtained from the liquid exposure of a compromised pristine coupon in ocean water substitute solution. Salt crystals of various sizes and shape are observed on the filter but no release products from the coupon were identified.



(a) 10kX SEM micrograph

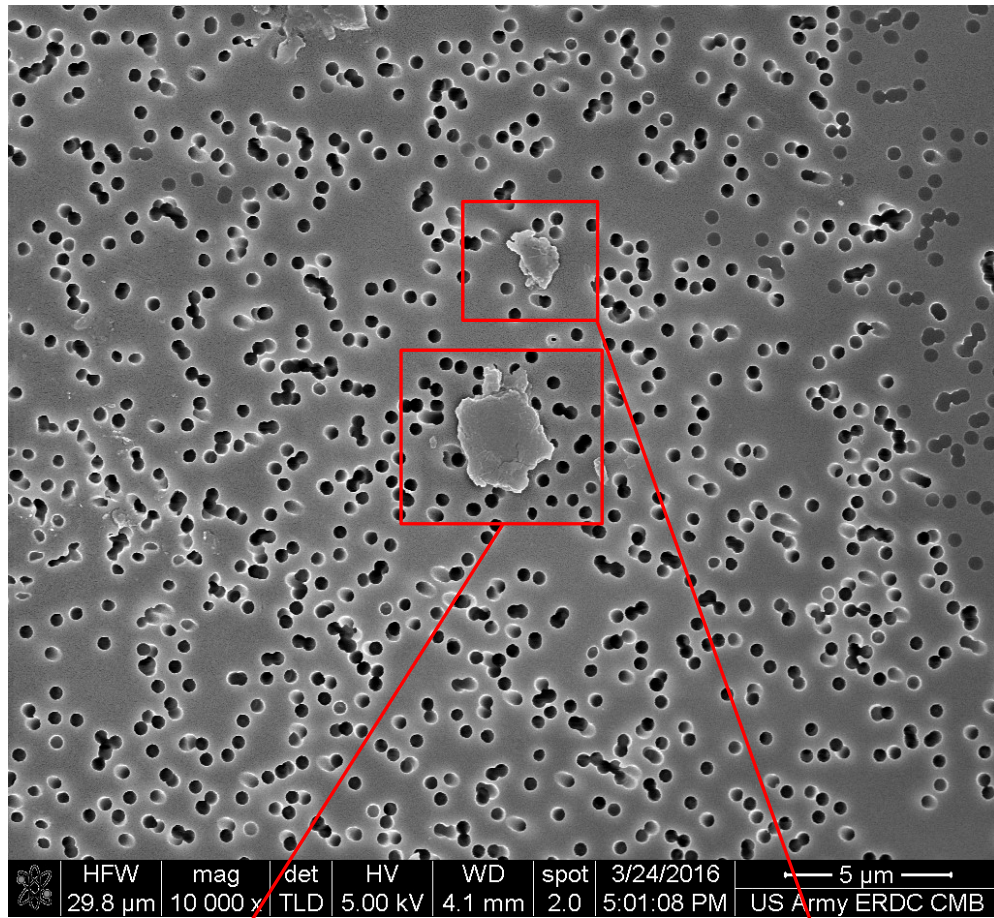


(b) 50kX SEM micrograph

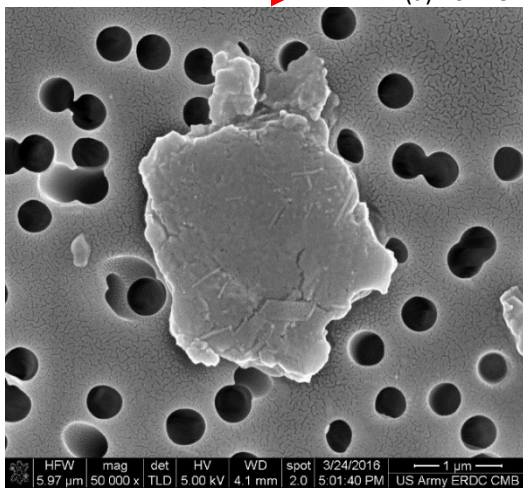


(c) 100kX SEM micrograph

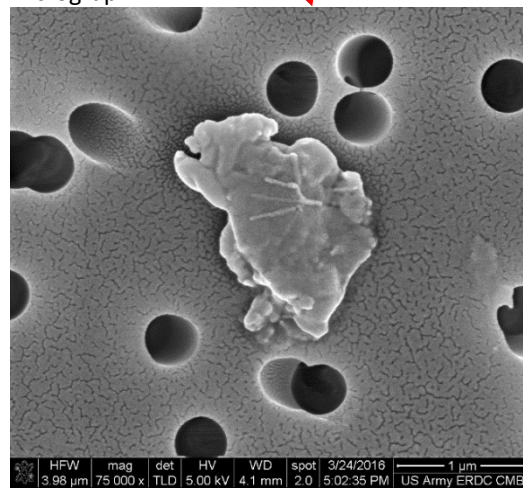
Figure 18. SEM micrographs obtained from the liquid exposure of a compromised pristine coupon in the citric acid solution. (a) Low magnification SEM image of the membrane filter showing a release product. (b)-(c) High magnification SEM images of the release product in (a). The morphology of the release product is consistent with that of an agglomerated CNT bundle.



(a) 10kX SEM micrograph

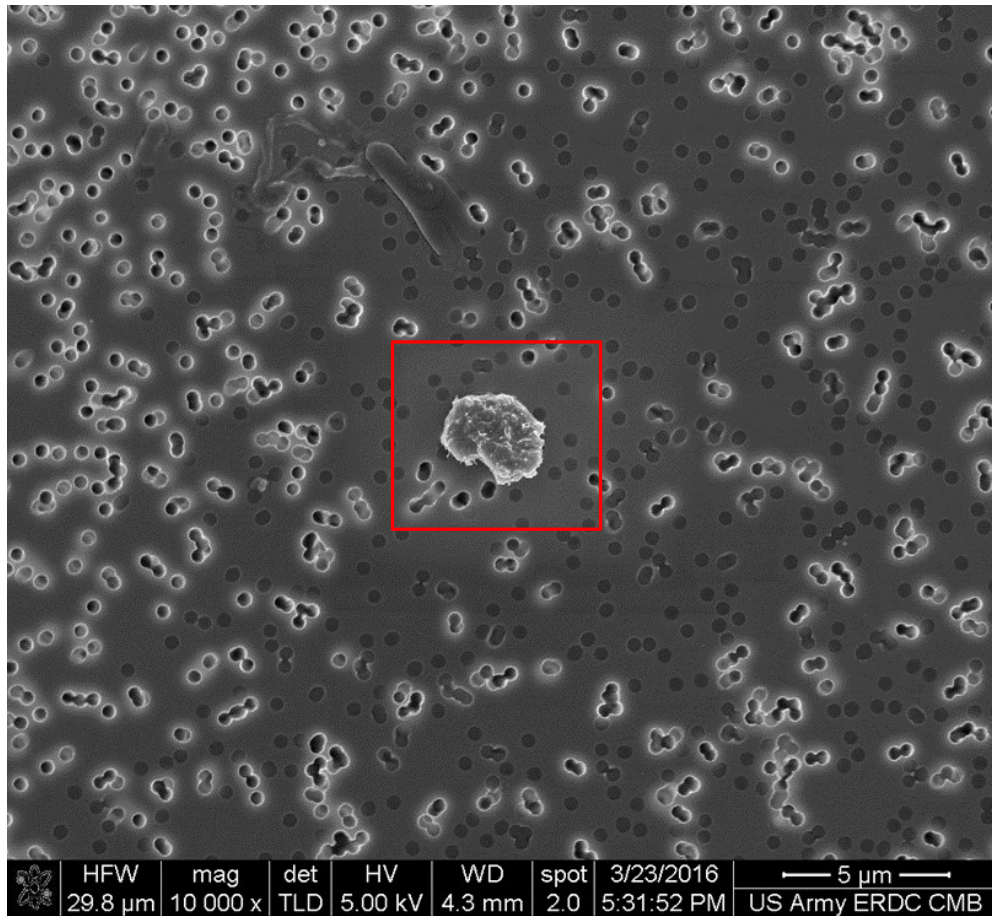


(b) 50kX SEM micrograph

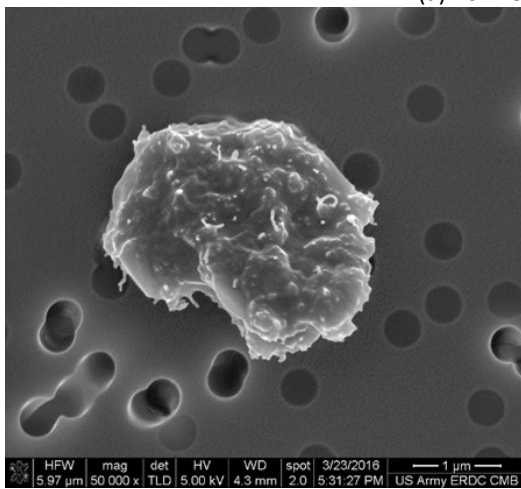


(c) 75kX SEM micrograph

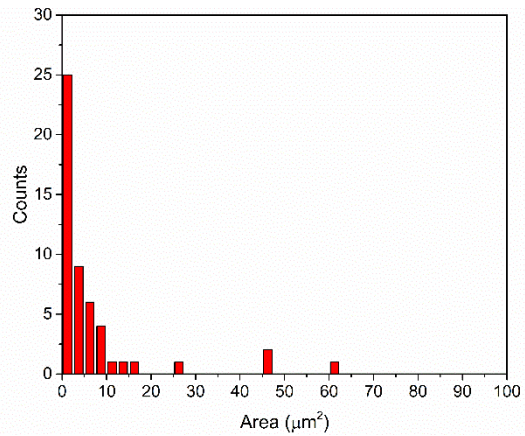
Figure 19. SEM micrographs obtained from the liquid exposure of a compromised pristine coupon in the phosphoric acid solution. (a) Low magnification SEM image of the membrane filter showing release products. (b)-(c) High magnification SEM images of the release products shown in (a). Both of the release products exhibit high aspect ratio features on their surfaces but we cannot conclusively determine if they are CNTs or not.



(a) 10kX SEM micrograph



(b) 50kX SEM micrograph



(c) Particle area distribution curve

Figure 20. SEM micrographs and particle area distribution curve obtained from washing a compromised pristine coupon with the SDS solution. (a) Low magnification SEM image of the membrane filter with release products. (b) High magnification SEM image of the indicated release product. The release product is a micron sized polymer cluster with protruding CNTs. (c) Particle area distribution curve obtained from sampling $n = 52$ release products with visible CNTs.

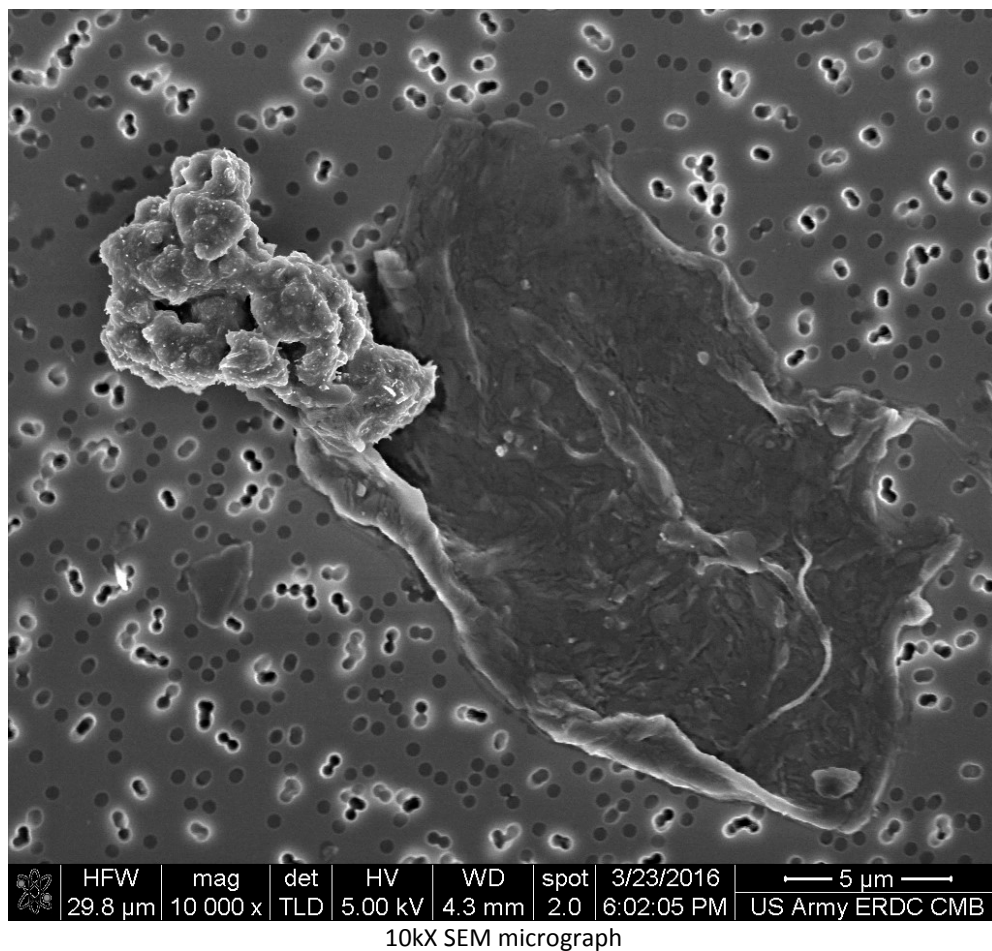
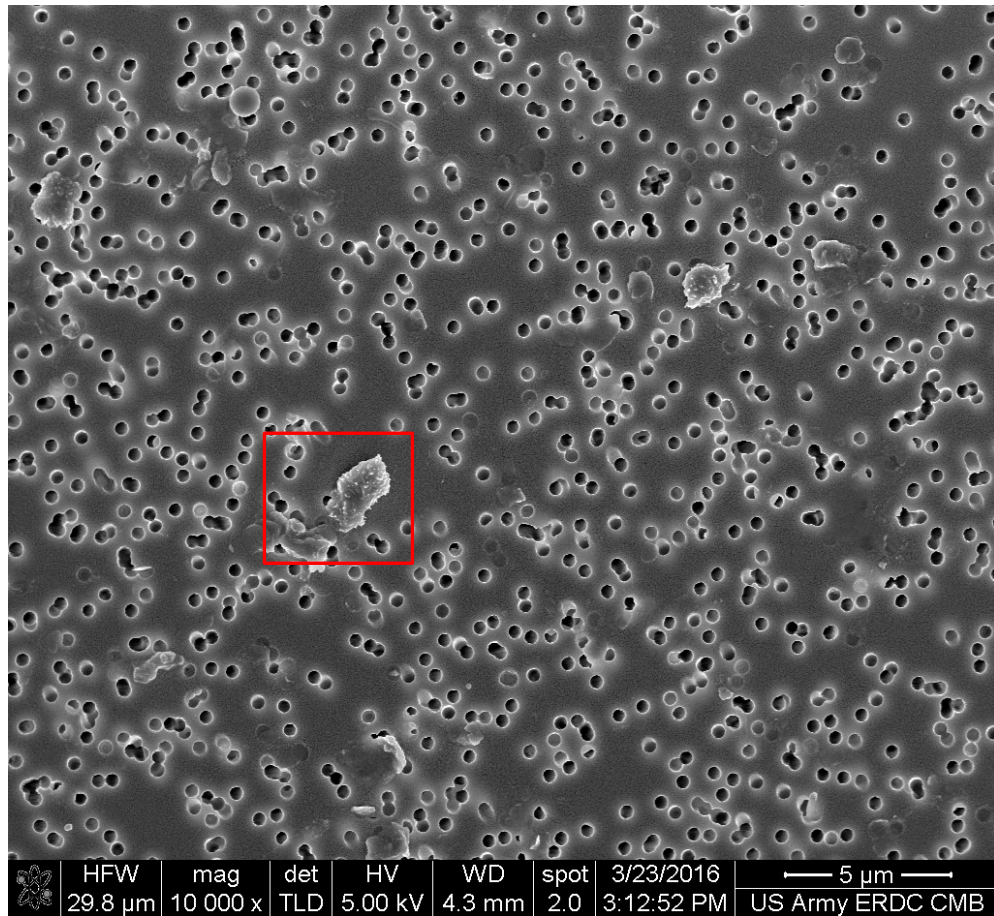
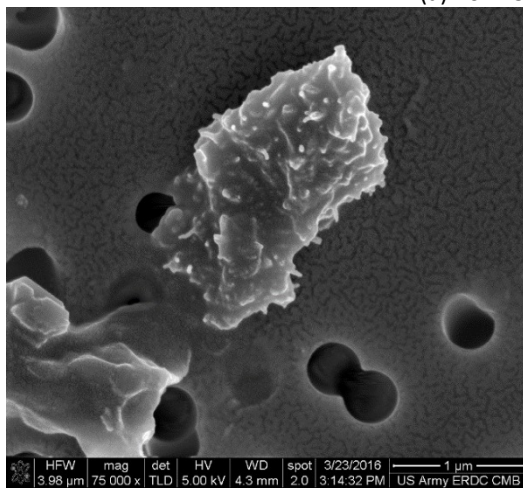


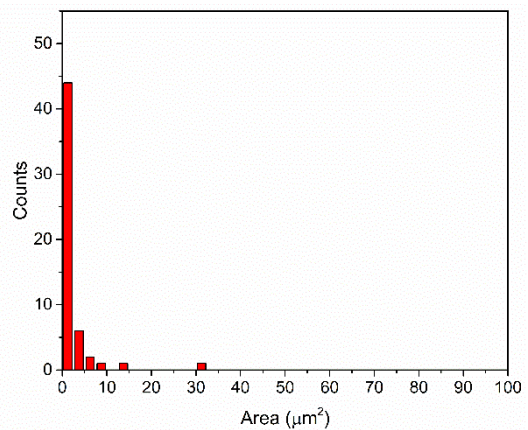
Figure 21. SEM micrograph of the membrane filter obtained from the liquid exposure, with washing-induced wear simulation, of a compromised pristine coupon in the SDS solution. The SEM image shows a release product consisting of a CNT-rich cluster (upper left portion) attached to a sheet of material (possibly a Kevlar strand).



(a) 10kX SEM micrograph

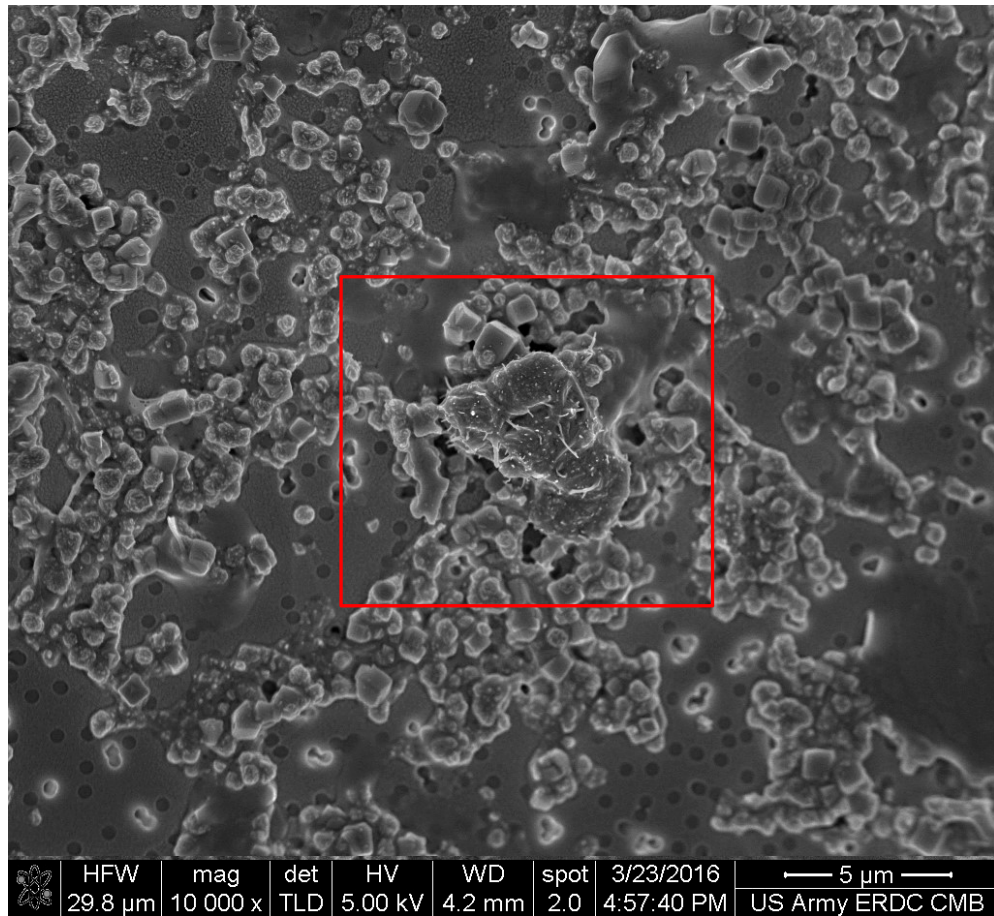


(b) 75kX SEM micrograph

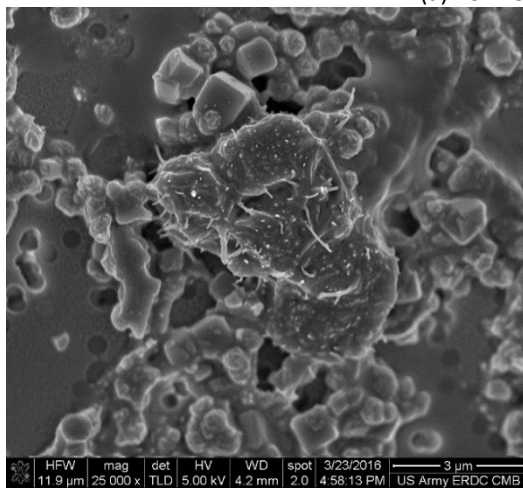


(c) Particle area distribution curve

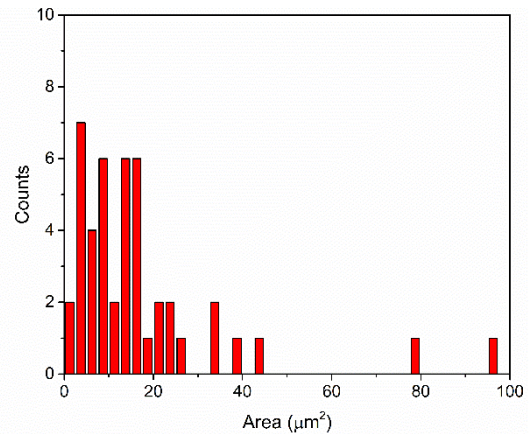
Figure 22. SEM micrographs and particle area distribution curve obtained from the liquid exposure, with washing-induced wear simulation, of a compromised pristine coupon in the Borax solution. (a) Low magnification SEM image of the membrane filter showing release products. (b) High magnification SEM image of the particle highlighted in (a). The particle has partially embedded CNTs protruding from its surface. (c) Particle area distribution curve obtained from sampling $n = 55$ release products with visible CNTs.



(a) 10kX SEM micrograph

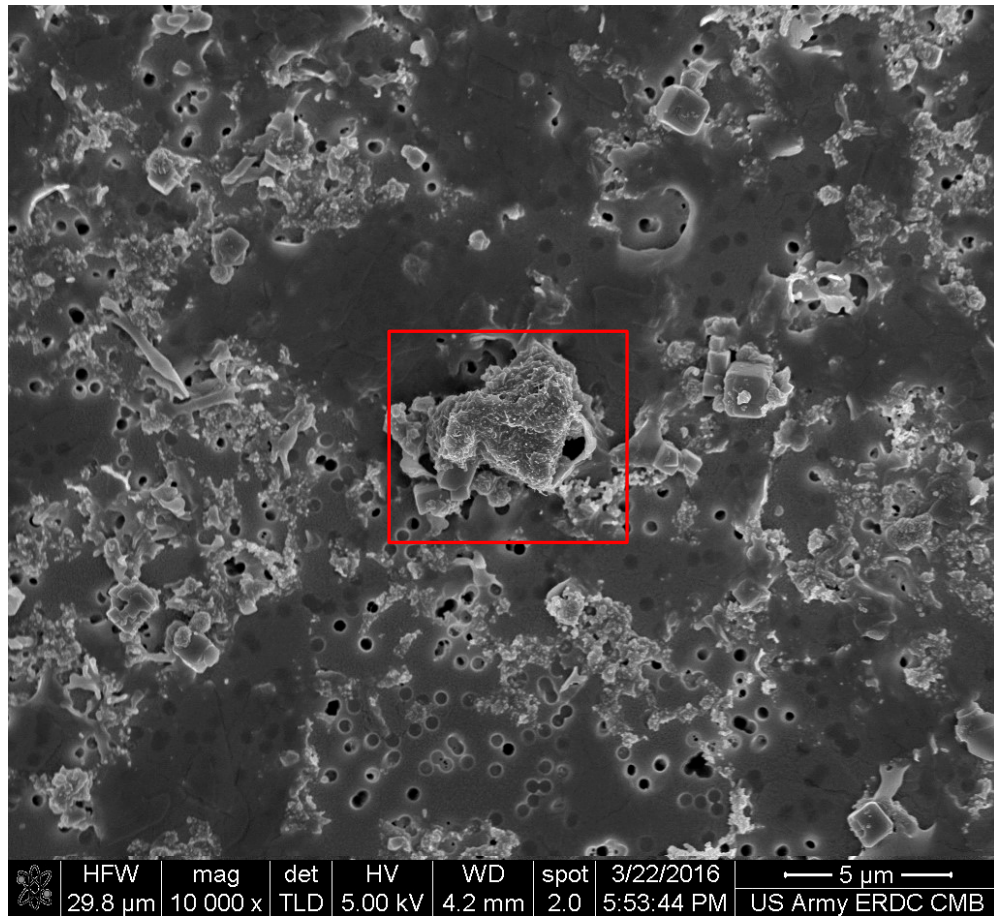


(b) 25kX SEM micrograph

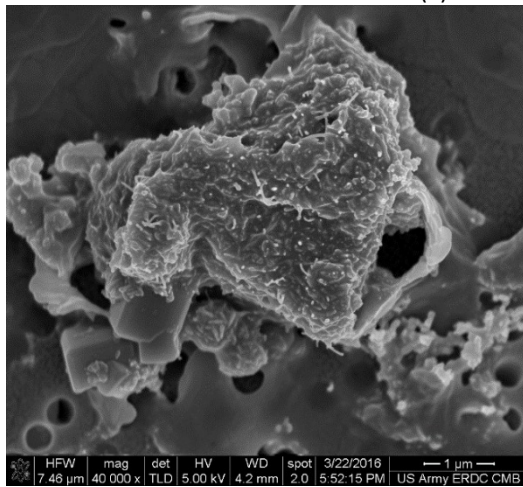


(c) Particle area distribution curve

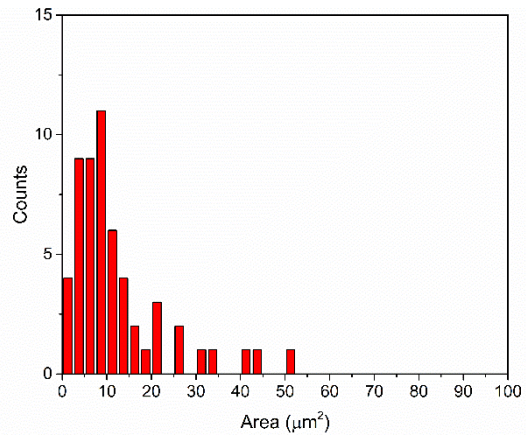
Figure 23. SEM micrographs and particle area distribution curve obtained from the liquid exposure, with washing-induced wear simulation, of a compromised pristine coupon with the ECE-(A) solution. (a) Low magnification SEM image of the membrane filter showing release products as well as a large amount of detergent (e. g. zeolites). (b) High magnification SEM image of the particle highlighted in (a). The particle has partially embedded CNTs protruding from its surface. (c) Particle are distribution curve obtained from sampling $n = 45$ release products with visible CNTs.



(a) 10kX SEM micrograph



(b) 40kX SEM micrograph

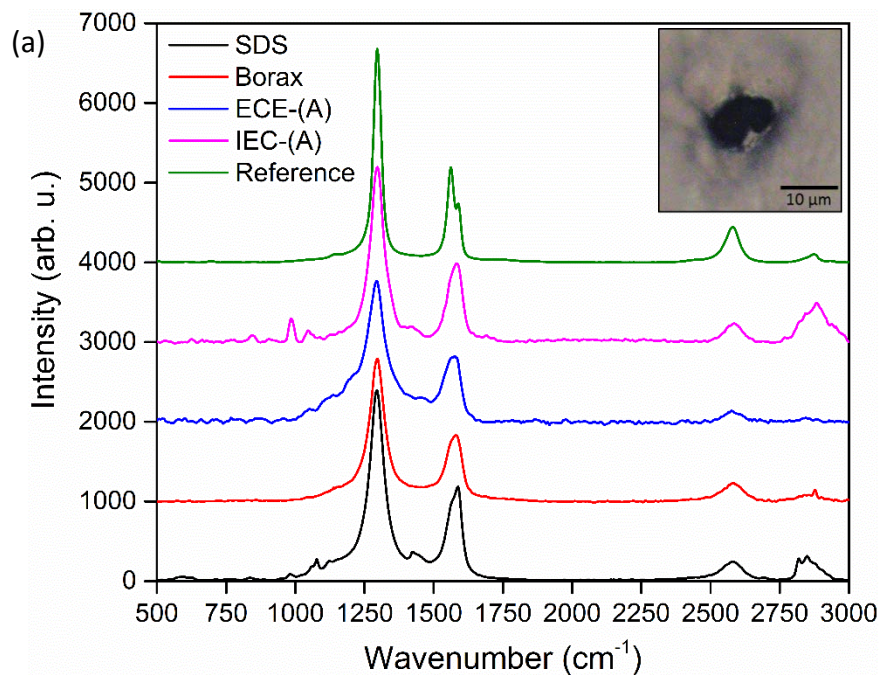


(c) Particle area distribution curve

Figure 24. SEM micrographs and particle area distribution curve obtained from the liquid exposure, with washing-induced wear simulation, of a compromised pristine coupon in the IEC-(A) solution. (a) Low magnification SEM image of the membrane filter showing release products as well as a large amount of detergent (e.g. zeolites). (b) High magnification SEM image of the particle highlighted in (a). The particle has partially embedded CNTs protruding from its surface. (c) Particle area distribution curve obtained from sampling $n = 56$ release products with visible CNTs.

RAMAN SPECTROSCOPY

Raman spectra obtained from dried unfiltered aliquots of test solution that were drop-cast on gold coated silicon wafers are shown in Figure 25(a). Raman spectra indicative of CNTs were not observed in the DI water, ocean water, citric acid and phosphoric acid solutions. In the case of DI water, citric acid and phosphoric acid the lack of positive Raman results can be attributed to the scarcity of the release products and the difficulty of locating individual CNTs under 100× optical magnification. On the other hand, all of the solutions from the washing simulations contained micron sized release particles easily observed under 100× optical magnification. As shown in Figure 25(a), Raman spectra collected from these particles exhibit peaks characteristic of CNTs (D, G, D' and G' peaks) indicating the presence of CNTs in the area probed by the laser beam. No RBM modes were observed between 150-300 cm^{-1} , verifying that the observed CNTs are indeed MWCNTs (see Appendix 6.4.3). The inset of Figure 25(a) shows an optical image of a release particle obtained from the ECE-(A) solution under 100× magnification. The same particle was later imaged with SEM and is shown in Figure 25(b)-(c), where it is verified that its surface has partially exposed CNTs.



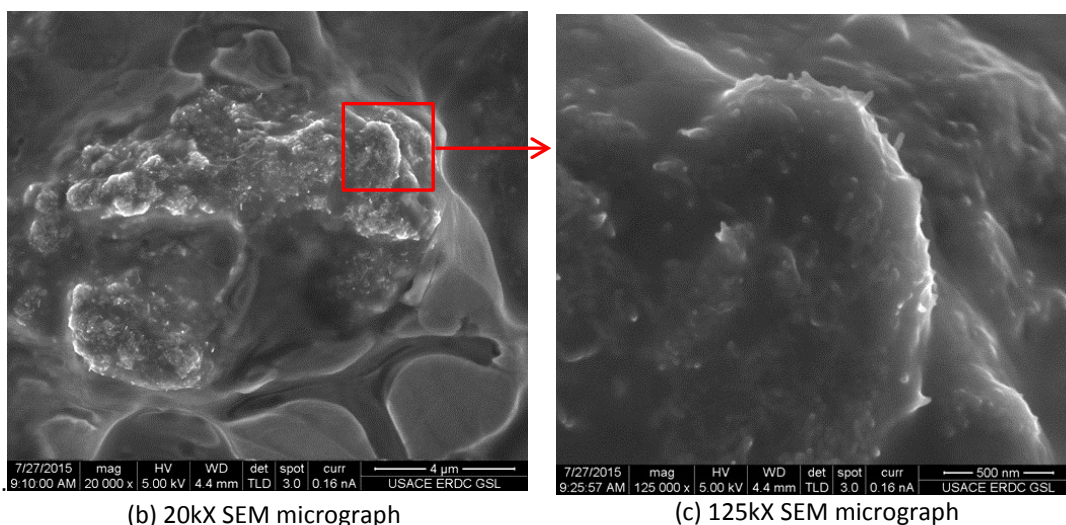


Figure 25. (a) Raman spectra collected from release products in unfiltered solutions obtained from washing compromised pristine coupons indicating the presence of CNTs. Inset: 100× optical image of the particle from the ECE-(A) solution where the Raman measurement was carried out. (b) SEM micrograph of the particle shown in the inset of (a) with partially embedded protruding CNTs. (c) Higher magnification SEM of highlighted area in (b) showing in more detail the CN- rich surface of the particle. The Raman spectra are background subtracted and vertically shifted.

TOTAL METALS ANALYSIS

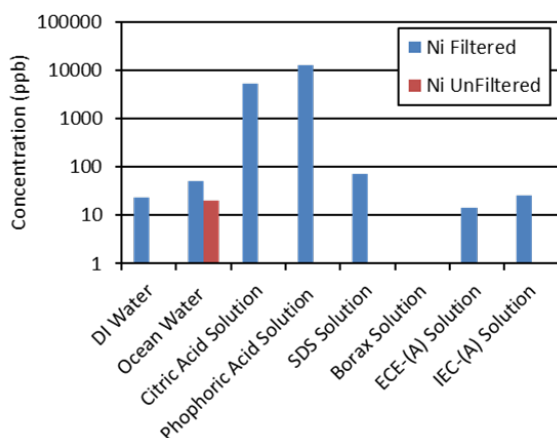
Figure 26 and Figure 27 show the concentration of nickel and zinc present in the filtered and unfiltered solutions obtained from pristine coupons with and without digestion. The results are shown both with a logarithmic and linear y-axis. Starting with the digested samples, the increased amount of nickel observed in the filtered solutions can be attributed to nickel leaching from the stainless steel filter holder (304 type), which typically contains 8-11% nickel. Leaching of nickel from the stainless steel filter is significantly higher in the citric and phosphoric acid solutions likely due to their reaction with the metal holder. The unfiltered ocean water solution surprisingly exhibits the highest concentration of nickel. If we assume that the nickel originates from CNTs, then this result is in obvious disagreement with our previous SEM observations where no release products were observed on the ocean water filter indicative of a low probability of release in ocean water.

For zinc, the highest concentrations, for both filtered and unfiltered solutions, were observed in the citric acid and phosphoric acid solutions. In some liquids, the amount of zinc in the filtered solution was higher than that in the unfiltered solution (DI water, ocean water, citric acid, SDS, and ECE-(A)). However, we expect that the unfiltered solutions have a larger amount of release products, and therefore a higher amount of zinc when compared to the filtered solutions. This discrepancy with the experimental data could indicate that the measured zinc concentration is, in part or entirely, not originating from CNT catalysts. This conclusion is also supported by the observation that the liquid exposure solutions (DI water, ocean water, citric acid, phosphoric

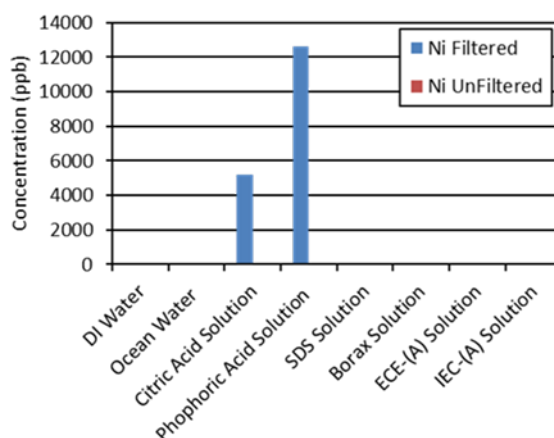
acid) have comparable or higher zinc concentrations than the washing solutions (SDS, Borax, ECE-(A), IEC-(A)) even though our SEM observations show that the washing solutions have a larger amount of release products with CNTs. For this reason, we do not believe that the nickel observed in the ocean water solution originates from catalyst particles in CNTs.

The effect of sample digestion is shown in Figure 27. Digestion should aid in increasing the amount of detected metals by dissolving or “loosening” the polymer matrix and thereby creating more free CNTs or more exposed CNTs in the solution. For nickel, the concentration of the filtered digested samples is similar to that of the filtered undigested samples with the highest concentration observed for the two acid solutions. This suggests that the observed nickel is leaching from the stainless steel filter assembly. Again, unfiltered substitute ocean water exhibits the highest concentration of nickel, followed by phosphoric and citric acid, Borax, IEC-(A), ECE-(A), DI water and SDS. As previously discussed the high nickel concentration in ocean water is surprising and likely not originating from CNT catalysts. Also, the higher nickel (unfiltered) and zinc (filtered, unfiltered) concentration in phosphoric and citric acid when compared to the washing solutions (SDS, Borax, IEC-(A), ECE-(A)) is suspicious for the same reasons presented in the case of undigested Zn.

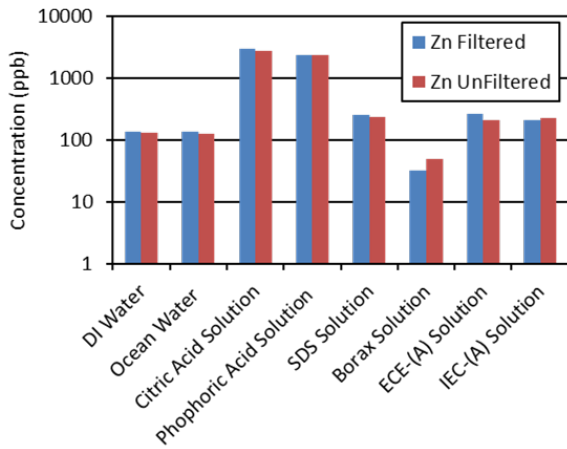
Overall, a different experimental strategy is needed in order to obtain meaningful and statistically relevant results from this technique. In terms of experimental error, filtering the solutions with a disposable plastic filter holder would eliminate the issues with nickel leaching. In addition, having access to the exact type of CNTs used in the particular product is needed in order to obtain a calibration curve of the amount of relevant trace metals as function of CNT concentration.



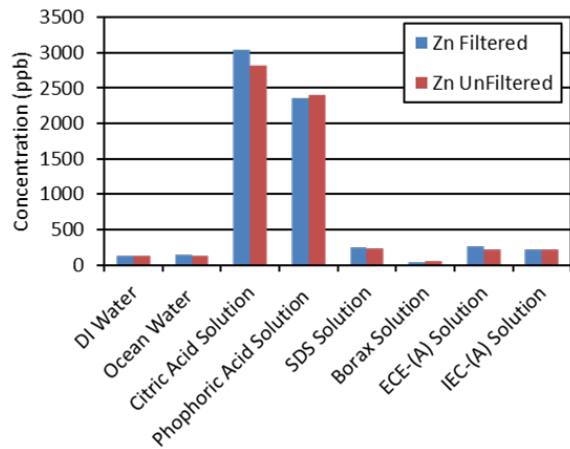
(a) Nickel with digestion; log scale



(b) Nickel with digestion; linear scale

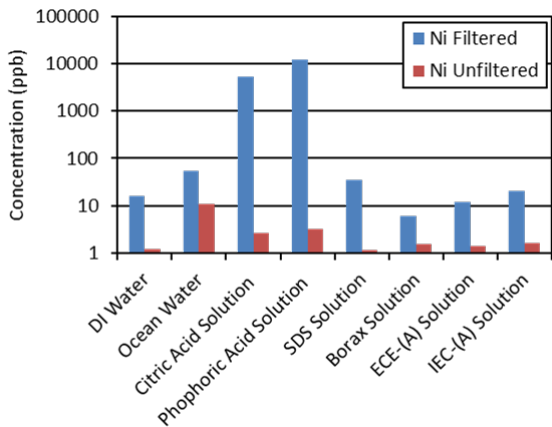


(c) Zinc with digestion; log scale

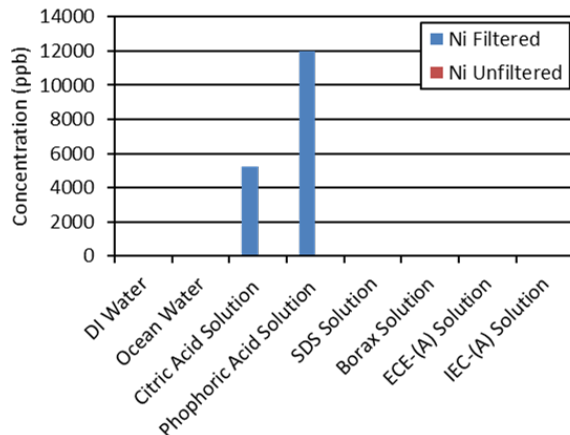


(d) Zinc with digestion; linear scale

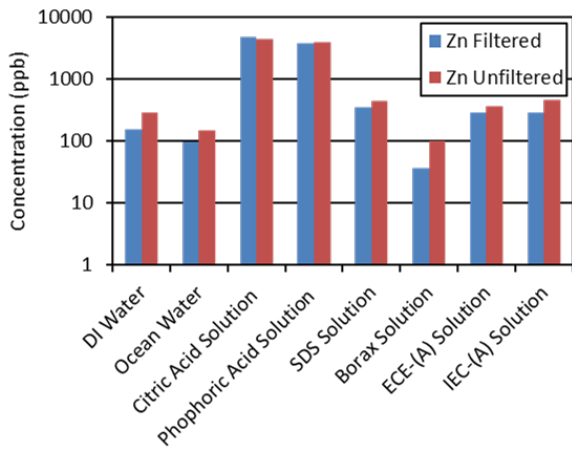
Figure 26. Nickel and zinc concentrations obtained from total metals analysis of filtered and unfiltered solutions from pristine coupons with digestion. (a) and (c) y-axis log scale, (b) and (d) y-axis linear scale. The presence of higher amounts of nickel in the filtered solutions when compared to the unfiltered solutions is indicative of leaching from the stainless steel filter assembly.



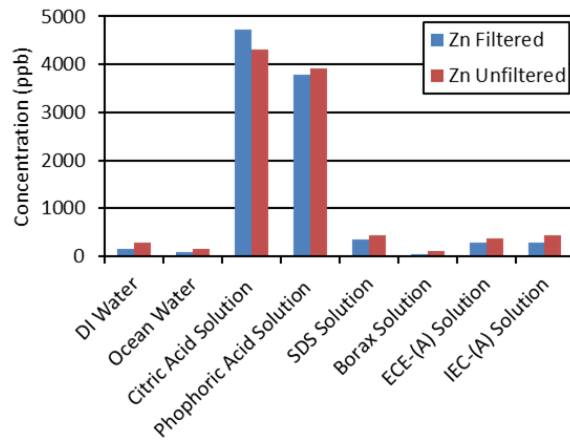
(a) Nickel without digestion; log scale



(b) Nickel without digestion; linear scale



(c) Zinc without digestion; log scale



(d) Zinc without digestion; log scale

Figure 27. Nickel and zinc concentrations obtained from total metals analysis of filtered and unfiltered solutions from pristine coupons without digestion. (a) and (c) y-axis log scale, (b) and (d) y-axis linear scale. The presence of higher amounts of nickel in the filtered solutions when compared to the unfiltered solutions is indicative of leaching from the stainless steel filter assembly.

UV-VIS SPECTROSCOPY AND DIGITAL IMAGE INTENSITY ANALYSIS FOR QUANTITATIVE ESTIMATION OF RELEASE PRODUCTS

Figure 28 shows an optical image of the OH functionalized MWCNTs dispersed in DI water with concentration varying from 0.05 mg/mL to 0.00125 mg/mL (left to right). The UV-VIS absorption spectra from these solutions along with a few additional concentrations are shown in Figure 29(a). The spectra were smoothed with a 10 point adjacent averaging smoothing operation. Figure 29 (b) shows the absorbance (points) at 250 nm, 500 nm, 700 nm and 800 nm plotted as function of OH-MWCNT concentration with corresponding linear fits (lines). The R^2 values of the linear fits ($y = mx + b$, where b was set to zero) are 0.999 for the 250 nm fit, 0.9985 for the 500 nm fit, 0.9983 for the 700 nm fit and 0.9981 for the 800 nm fit.

Representative UV-VIS absorption spectra collected from the unfiltered solutions from the liquid exposure/washing of pristine coupons are shown in Figure 30. The absorption spectra of the unfiltered solutions and their corresponding neat solutions were referenced with respect to DI water. For the DI water, ocean water, citric acid, phosphoric acid, SDS, and Borax solutions the amount of released CNTs was estimated by direct comparison of their spectra with the absorption spectra obtained from dispersing known amounts of MWCNTs in DI water as previously discussed. The DI water, ocean water, citric acid, phosphoric acid, SDS and Borax solutions contain less than 1.25 $\mu\text{g/mL}$ of MWCNTs with the DI water solution exhibiting the highest potential amount of release products (see Appendix 6.6.1). For the ECE-(A) and IEC-(A) solutions it is important to note that the variability in the amount of detergent present in the solutions, can be an important factor in the observed baseline shifts. The reference solutions, for both detergents, have higher absorbance than the solutions collected after washing the coupons, which indicates either a higher amount of detergent present in the reference solutions or faster settling of the detergent in the washing solutions or both. It is worth pointing out, that the initial amount of detergent for all solutions is nominally the same (typically within 0.2 mg). Therefore, despite our best efforts, subsampling after washing (for the UV-VIS measurements) leads to variations in the amount of detergent present in the solutions, as evidenced by the absorbance spectra. Further, the absorbance spectra of the ECE-(A) and IEC-(A) solutions are dominated by their turbidity (scattering). Therefore, for the ECE-(A) and IEC-(A) solutions, UV-VIS measurements alone cannot reliably estimate the amount of release products (or CNTs) in the solutions. For these solutions (ECE-(A) and IEC-(A)) an alternative approach, such as visual comparison of the color of the detergent solutions, must be considered.

A summary of the upper CNT release estimates based on the UV-VIS absorbance analysis of two runs (Runs 1 and 2 of the compromised pristine coupons) is shown in Table 1 and in Table 2. In Table 1 the CNT release is given in $\mu\text{g/mL}$, whereas in Table 2 the CNT release is given in mg/m^2 , where the total solution volume was 25 mL, and the area $2.58064 \times 10^{-3} \text{ m}^2$.

Table 1. Estimated amount of CNT release, in $\mu\text{g/mL}$, due to washing of compromised pristine coupons based on UV-VIS absorbance spectra of the unfiltered solutions. “Base-line shift” indicates that the absorbance spectrum is shifted with respect to the neat solution. “UV absorbance increase” refers to changes (increase) in the < 400 nm spectral region of the washing solutions.

	DI water	Ocean Water	Citric Acid Solution	Phosphoric Acid Solution	SDS Solution	Borax Solution	ECE-(A) solution	IEC-(A) solution
Run 1 UV-VIS	< 1.25, with base-line shift	< 1.25, no base-line shift	< 1.25, small base-line shift	< 1.25, small base-line shift	< 1.25, with base-line shift	< 1.25, with base-line shift	N/A	N/A
	UV absorbance increase	UV absorbance increase	UV absorbance increase	UV absorbance increase	UV absorbance increase	UV absorbance increase	N/A	N/A
Run 1 Digital Image Analysis	1.75 ± 0.3	0.74 ± 0.65	0.96 ± 0.67	0.48 ± 0.59	0.91 ± 0.58	1.17 ± 0.60	N/A*	6.97 ± 0.78
Run 2 UV-VIS	< 1.25, with base-line shift	< 1.25, small base-line shift	< 1.25, with baseline shift	< 1.25, no base-line shift	> 2.5 and < 3.75, with base-line shift	< 1.25, with base-line shift	N/A	N/A
	UV absorbance increase	UV absorbance increase	UV absorbance increase	UV absorbance increase	UV absorbance increase	UV absorbance increase	N/A	N/A
Run 2 Digital Image Analysis	1.69 ± 0.3	0.49 ± 0.62	0.65 ± 0.64	0.45 ± 0.62	1.16 ± 0.58	1.07 ± 0.51	3.29 ± 0.78	3 ± 0.79

* mean intensity less than that of neat solution

Table 2. Estimated amount of CNT release, in mg/m^2 , due to washing of compromised pristine coupons based on UV-VIS absorbance spectra of the unfiltered solutions. “Base-line shift” indicates that the absorbance spectrum is shifted with respect to the neat solution. “UV absorbance increase” refers to any change (increase) in the < 400 nm spectral region of the washing solutions.

	DI water	Ocean Water	Citric Acid Solution	Phosphoric Acid Solution	SDS Solution	Borax Solution	ECE-(A) solution	IEC-(A) solution
Run 1 UV-VIS	< 12.11, with base-line shift	< 12.11, no base-line shift	< 12.11, small base-line shift	< 12.11, small base-line shift	< 12.11, with base-line shift	< 12.11, with base-line shift	N/A	N/A
	UV absorbance increase	UV absorbance increase	UV absorbance increase	UV absorbance increase	UV absorbance increase	UV absorbance increase	N/A	N/A
Run 1 Digital Image Analysis	16.95 ± 2.9	7.20 ± 6.32	9.33 ± 6.47	4.60 ± 5.73	8.81 ± 5.62	11.34 ± 5.85	N/A*	67.55 ± 7.56

Run 2 UV-VIS	< 12.11, with base- line shift	< 12.11, small base- line shift	< 12.11, with base- line shift	< 12.11, no base-line shift	> 24.2 and < 36.33, with base- line shift	< 12.11, with base- line shift	N/A	N/A
	UV absorbance increase	UV absorbance increase	UV absorbance increase	UV absorbance increase	UV absorbance increase	UV absorbance increase	N/A	N/A
Run 2 Digital Image Analysis	16.37 ± 3.3	4.76 ± 6.02	6.26 ± 6.24	4.37 ± 5.97	11.27 ± 5.58	10.32 ± 4.95	31.85 ± 7.53	29.07 ± 7.65

* mean intensity less than that of neat solution

Figure 31 shows the digital image intensity analysis for the DI water Run 1 of a compromised pristine coupon. A similar analysis was carried out for each of the unfiltered solutions. First, a color image was obtained with all the known standards and the unknown concentration solution. Next, the image is converted to grayscale and the mean intensity and standard deviation are obtained with ImageJ. Defects such as bubbles or floating debris in the solutions were avoided when calculating the mean intensities. The linear fit (red line) and the 95% prediction band (high-lighted area) of the mean grayscale intensities (black points) versus MWCNT concentration is shown in Figure 31(c). The blue point corresponds to the intensity of the DI water Run 1 solution and its mapped CNT concentration. A summary of the results obtained from digital image intensity analysis is provided in Table 1 and Table 2.

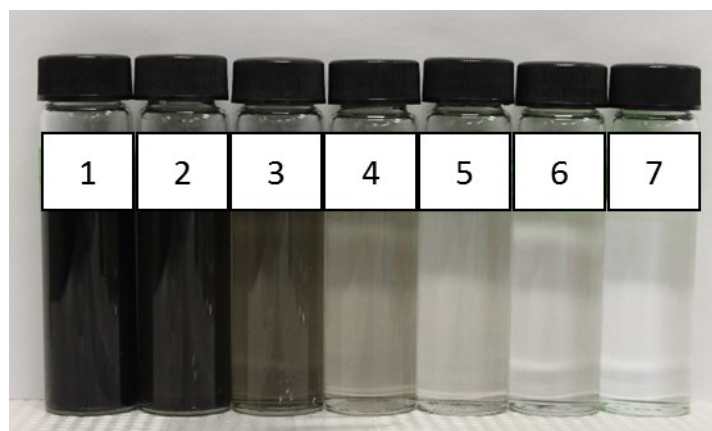


Figure 28. Representative DI water solutions of OH functionalized MWCNTs with known concentration. From left to right: 1-0.05 mg/mL, 2-0.025 mg/mL, 3-0.0125 mg/mL, 4-0.005 mg/mL, 5-0.0025 mg/mL, 6-0.00125 mg/mL and 7-DI water.

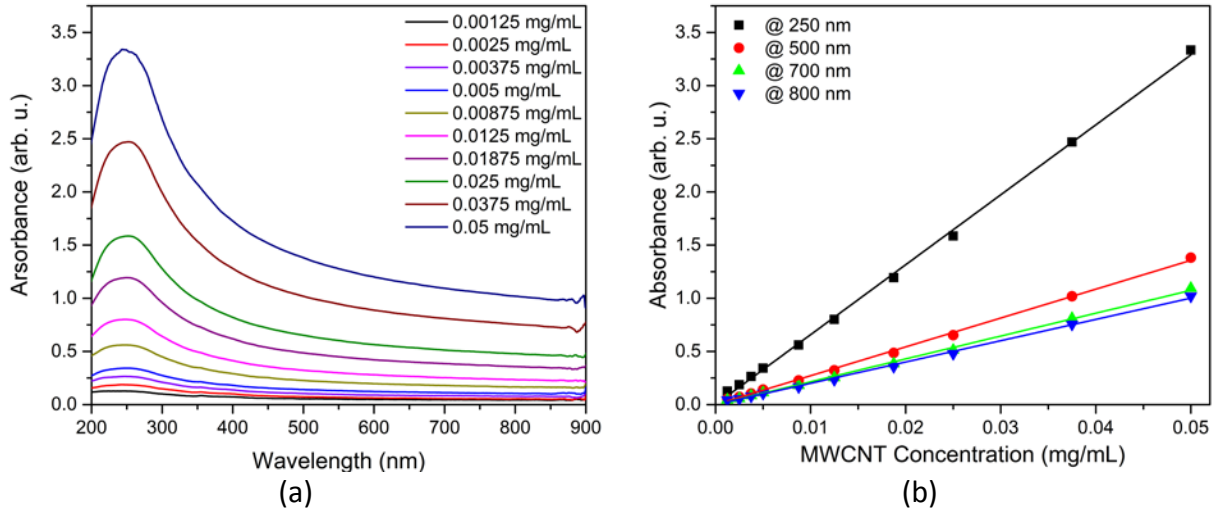


Figure 29. UV-VIS spectra of OH functionalized MWCNTs in DI water, (a) absorbance spectra of OH functionalized MWCNTs in DI water as function of MWCNT concentration, (b) Absorbance at 250 nm, 500 nm, 700 nm and 800 nm as function of MWCNT concentration with corresponding linear fits.

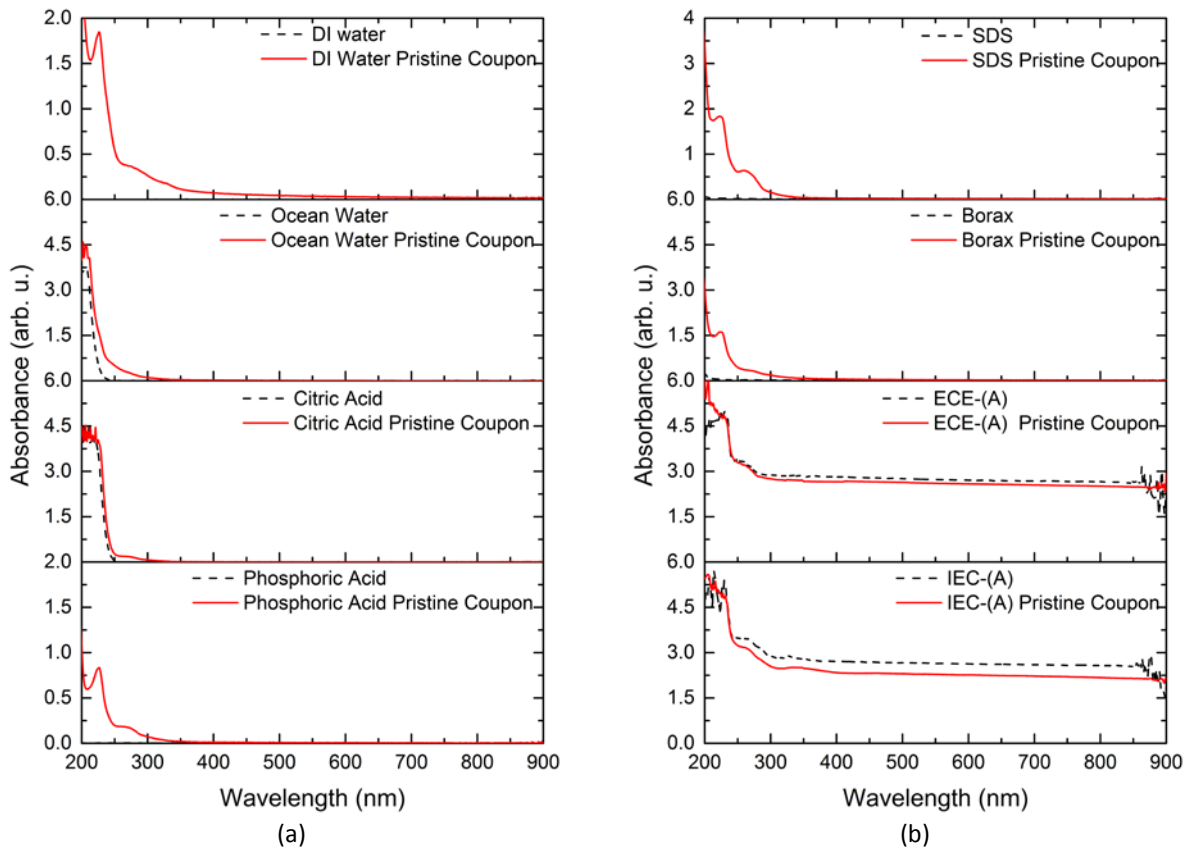
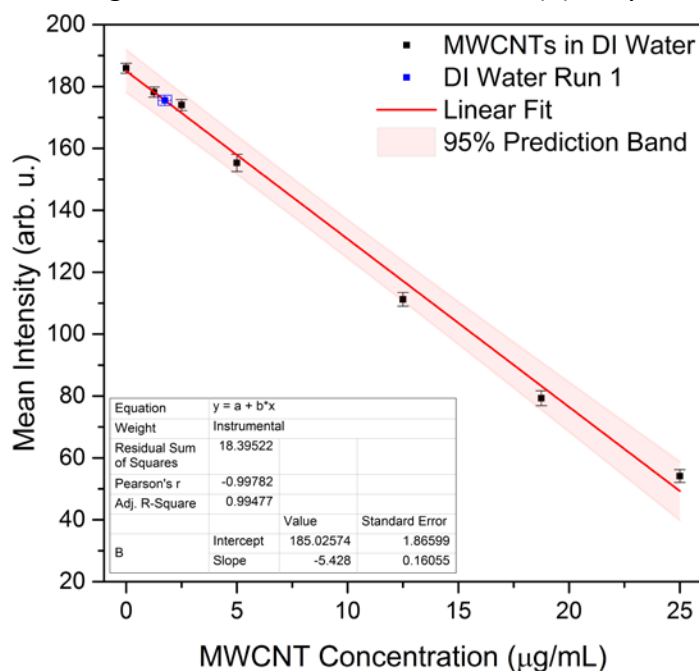


Figure 30. UV-VIS absorption spectra (Run 1) of unfiltered solutions obtained from washing compromised pristine coupons with respect to DI water. (a) UV-VIS absorbance spectra from liquid exposure solutions (DI water, ocean water substitute, citric acid and phosphoric acid solutions) and (b) UV-VIS absorbance spectra from solutions with washing-induced wear simulation (SDS, Borax, ECE-(A) and IEC-(A) solutions). The absorbance spectra of the corresponding neat (unwashed) solutions are also shown.



(a) Color image

(b) Grayscale image



(c) Calibration plot

Figure 31. Digital image intensity analysis for estimation of unknown CNT concentration in unfiltered solutions. (a) Original digital image of MWCNT standards and DI water solution (Run 1). From left to right the solutions are: 25 µg/mL, 18.75 µg/mL, 12.5 µg/mL, 5 µg/mL, 2.5 µg/mL, 1.25 µg/mL, 0 (neat DI water) and DI water Run 1 (unknown concentration). (b) Grayscale conversion of (a). (c) Extracted mean grayscale intensity as function of MWCNT concentration, and estimation of unknown CNTs. In this case, the CNT release in DI water Run 1 was estimated to be 1.75±0.30 µg/mL.

4.1.3. COMPROMISED UV-AGED MATERIAL

4.1.3.1. ANALYSIS OF COMPROMISED UV-AGED MATERIAL PRIOR TO LIQUID EXPOSURE/WASHING SIMULATION

WEIGHT LOSS DUE TO UV-AGING

The mass of 4 pristine coupons was measured before, immediately after UV-aging and 14 days after UV-aging in order to allow equilibration of the UV-aged samples with the ambient laboratory environmental conditions. These results are shown in Table 3. The majority of the initial mass loss observed @0 days after UV-aging is attributed to water loss during the UV-aging test since the masses of all the UV-aged coupons recover when measured again @14 days post UV-aging. Therefore an estimation of the mass loss due to UV-aging can be obtained from the difference between the pristine mass and the mass measured 14 days after UV-aging; the average from all four coupons is calculated to be 1.7 ± 0.4 mg or 658 ± 78 mg/m² given a surface area of 2.58064×10^{-3} m².

Table 3. Mass loss of coupons due to UV-aging.

Coupon #	Pristine mass (mg)	mass @0 days post UV-aging (mg)	mass @14 days post UV-aging (mg)
1	722.7	712.3	721.3
2	776.4	764.9	774.5
3	731.0	720.3	728.9
4	769.7	758.9	768.3

FTIR ANALYSIS

Figure 32 shows the FTIR spectra obtained from a pristine and a UV-aged coupon by placing the coupon surface in contact with the ATR crystal. The FTIR spectra were collected after equilibration of the UV-aged sample with the ambient laboratory environmental conditions. Spectral changes between the pristine and UV-aged coupon were observed in the 1446 cm⁻¹ peak (CH₂ deformation peak), the carbonyl band from 1520-1800 cm⁻¹ as well as the hydroxyl peaks present in the 3000-3500 cm⁻¹ range.

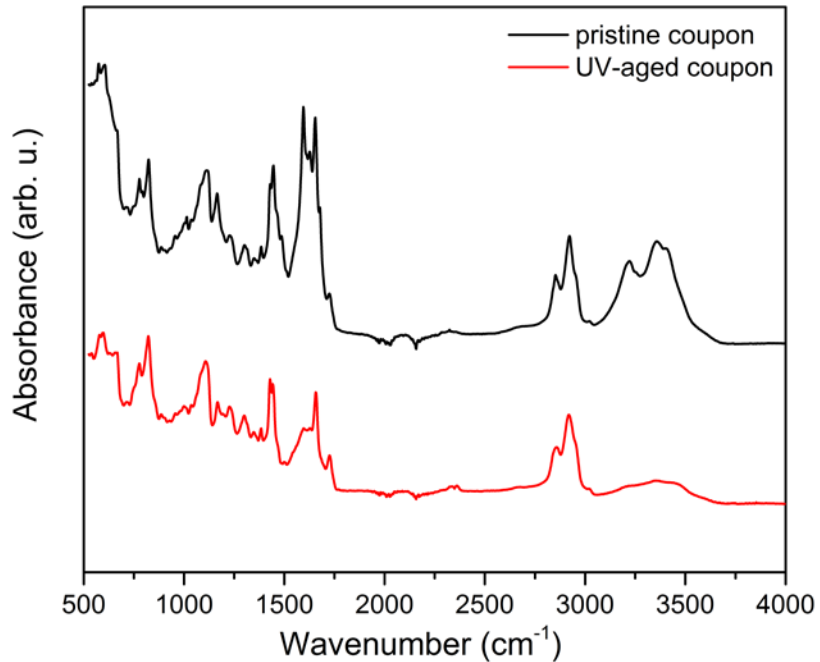


Figure 32. FTIR spectra of pristine and UV-aged coupon. Spectral changes between the pristine and UV-aged coupon were observed in the 1446 cm^{-1} peak (CH_2 deformation peak), the carbonyl band from $1520\text{-}1800\text{ cm}^{-1}$ as well as the hydroxyl peaks present in the $3000\text{-}3500\text{ cm}^{-1}$ range.

SEM ANALYSIS

Representative SEM micrographs from a UV-aged coupon are shown in Figure 33 and Figure 34. Additional micrographs from the UV-aged coupon are provided in Appendix 6.9.1. Analysis of the surface morphology reveals that the polymer matrix undergoes photodegradation resulting in cracking and accumulation of CNTs onto its surface. Surface accumulation and aggregation of CNTs after UV irradiation of polymer matrices containing CNTs has been previously observed (Kingston et al. 2014). Further, the cross sectional surfaces of the cracked polymer contain exposed CNTs; these are shown in more detail in Figure 33(c) and Figure 34(c)-(d).

Cracking of the surface renders the matrix more susceptible to particle release and disintegration by pieces breaking off during abrasion. Further, when compared to pristine samples, the UV-aged coupons have more exposed CNTs due to CNT surface aggregation and cracking which significantly increases the amount of exposed CNT rich surfaces. Therefore, larger CNT release would be expected from the UV-aged coupons when compared to the pristine coupons.

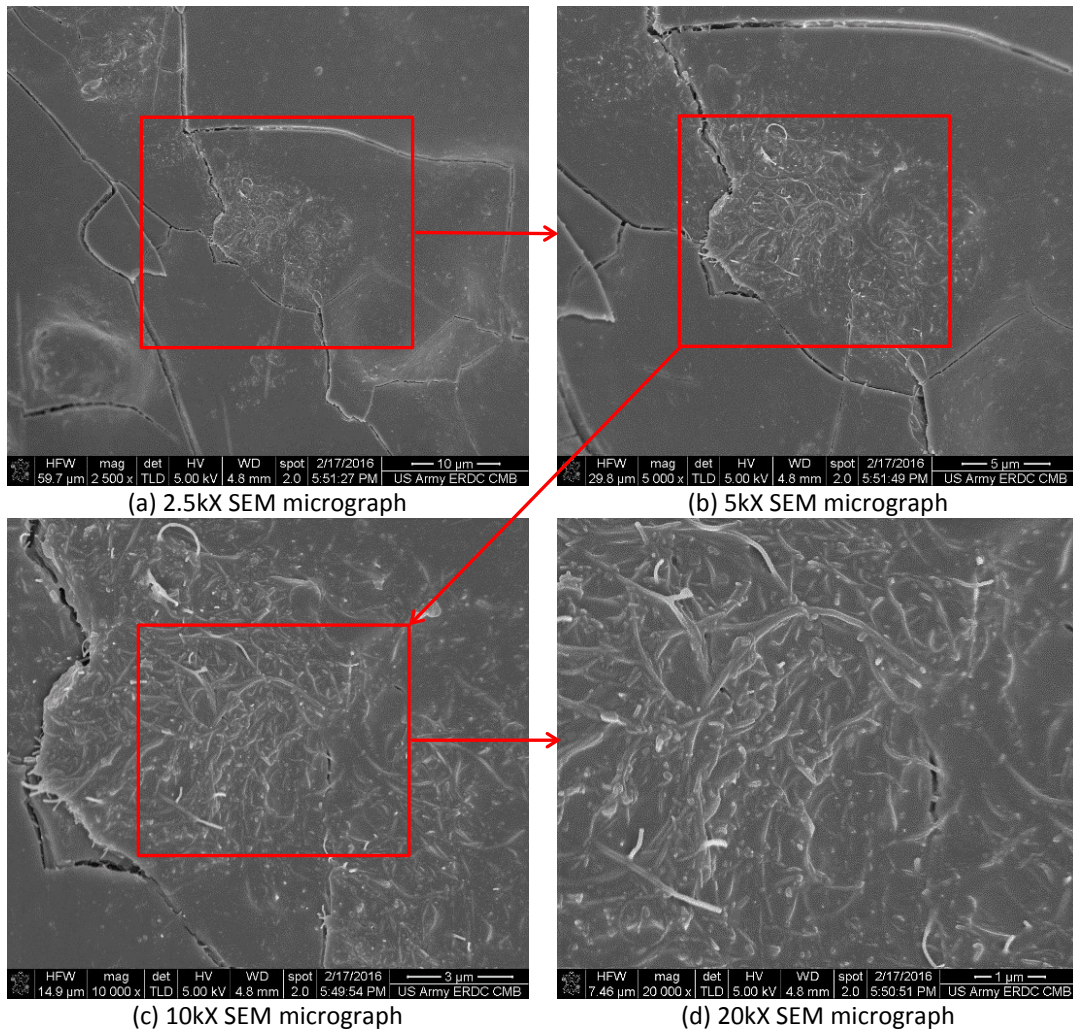


Figure 33. SEM micrographs of a UV-aged coupon exhibiting cracking and CNT surface aggregation. (a) Low magnification SEM image of a cracked area on the coupon. (b)-(d) Successively higher magnification SEM images of the area highlighted in (a). In addition to cracking and CNT surface aggregation, exposed CNTs are also visible on the cross sectional surfaces along the cracks (e.g. on the right portion of (c)).

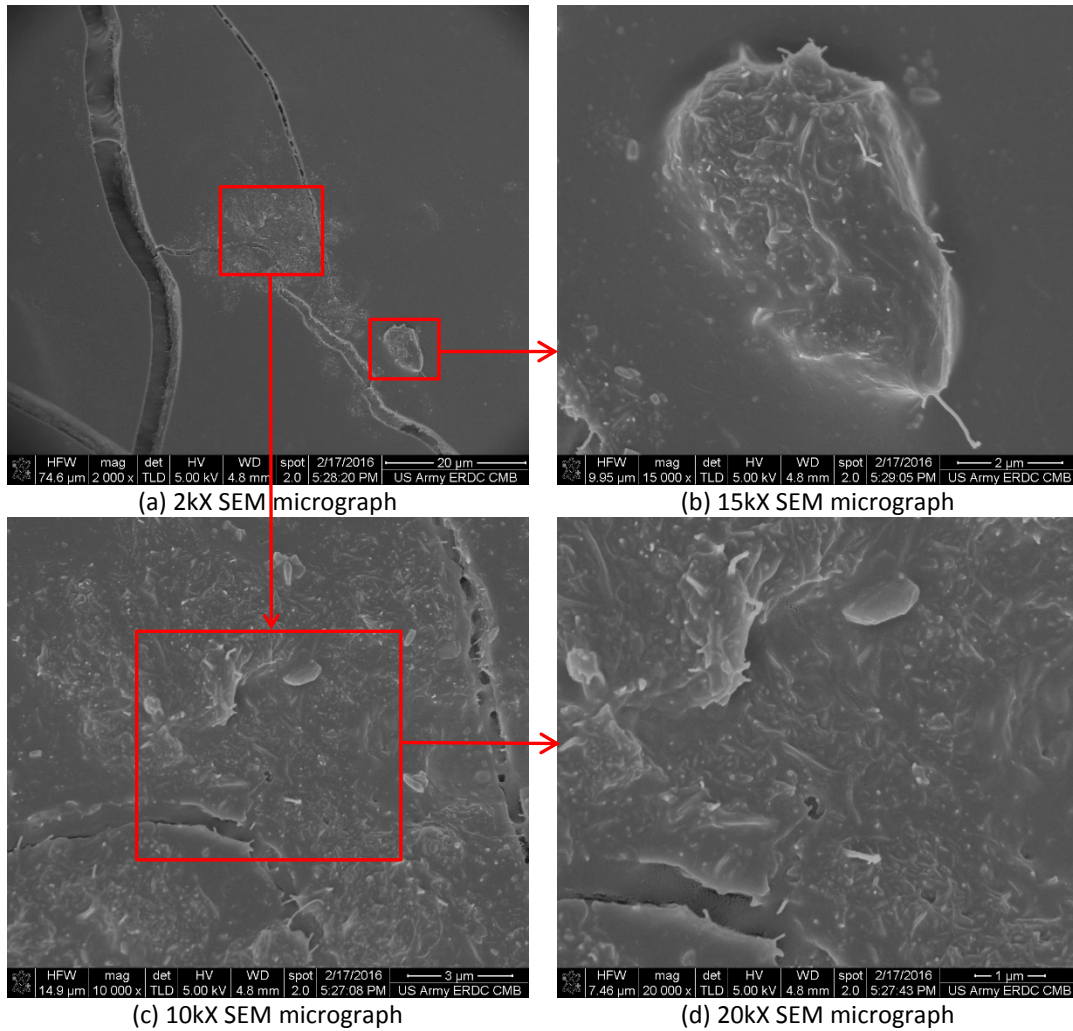


Figure 34. Additional SEM micrographs of a UV-aged coupon exhibiting cracking and CNT surface aggregation. (a) Low magnification SEM image of a cracked area on the coupon. (b) Higher magnification SEM image of the surface defect highlighted in (a). The surface defect is consistent with CNT-rich clusters obtained from poor dispersion of CNT during processing. (c) and (d) Successively higher magnification SEM images of the area highlighted in (a) showing CNT surface agglomeration and exposed CNTs visible on the cross sectional surfaces of the cracks.

4.1.3.2. EVALUATION OF RELEASE FROM UV-AGED MATERIAL BASED ON ADHESION TEST.

SEM ANALYSIS

A representative SEM micrograph of the surface of the adhesive copper tape after the adhesion test is shown in Figure 35. A variety of release particles were observed, some of which did not have visible CNTs, whereas others had visible CNTs protruding from their surface, as shown in more detail in Figure 35 (c) and (d). Additional micrographs from the adhesion test are provided in Appendix 6.9.1. It is noted these samples are primarily imaging the “back” side of the attached particles because the front side or surface is attached to the tape. The particle area distribution curve obtained from Figure 35(a) is shown in Figure 35(d). The area distribution curve was obtained with ImageJ using intensity threshold analysis.

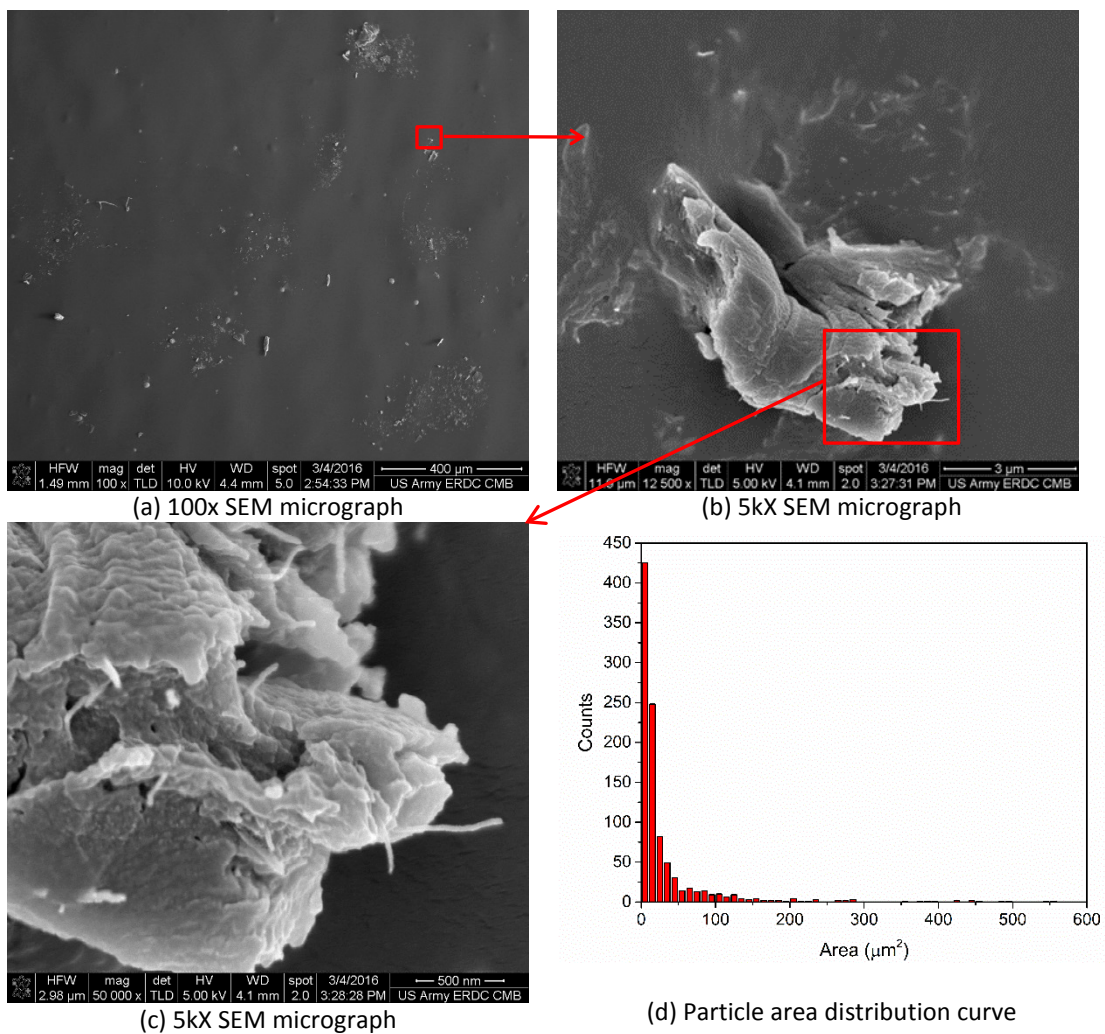


Figure 35. Evaluation of release from UV-aged coupon after adhesion test with adhesive copper tape. (a)-(c) SEM of the copper taper with increasing magnifications, (d) particle area distribution curve obtained from (a).

4.1.3.3. ANALYSIS OF RELEASE PRODUCTS FROM COMPROMISED UV-AGED MATERIAL AFTER LIQUID EXPOSURE/WASHING SIMULATION

OPTICAL MICROSCOPY

Optical images of the dried filters from the UV-aged coupons are shown in Figure 36. When compared to the filters obtained from the pristine coupons, the filters from the UV-aged coupons exhibit colorations consistent with release of material from the UV-aged matrix. The filters for DI water, citric acid and phosphoric acid look mostly clear indicative of Occasional release from the coupons (note the dark streak on the citric acid filter). The ocean water, SDS and Borax filters have light brown or brown/dark areas consistent with material release. Similarly, the ECE-(A) and IEC-(A) filters show deposition of a relatively large amount of release products in addition to the detergent.

Figure 37 shows the unfiltered solutions obtained from the UV-aged coupons. The DI water, ocean water, citric acid, phosphoric acid and SDS solutions are visually clear, whereas the Borax, ECE-(A) and IEC-(A) solutions have yellow/brown color. The filtered solutions retain the yellow color (see Appendix 6.3).

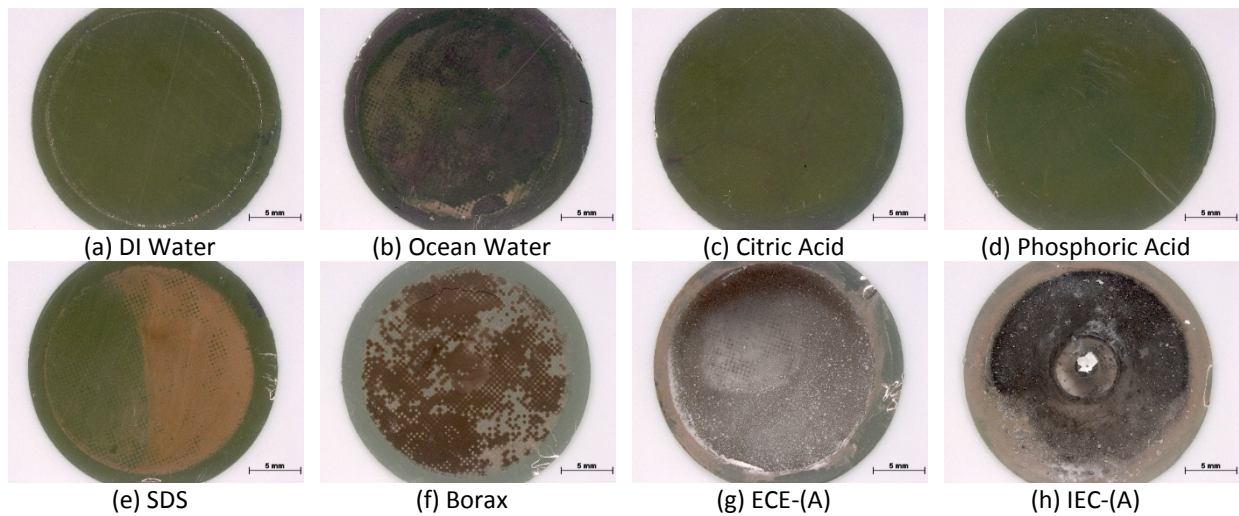


Figure 36. Optical images of filters obtained from compromised UV-aged coupon liquid exposure/washing simulations.

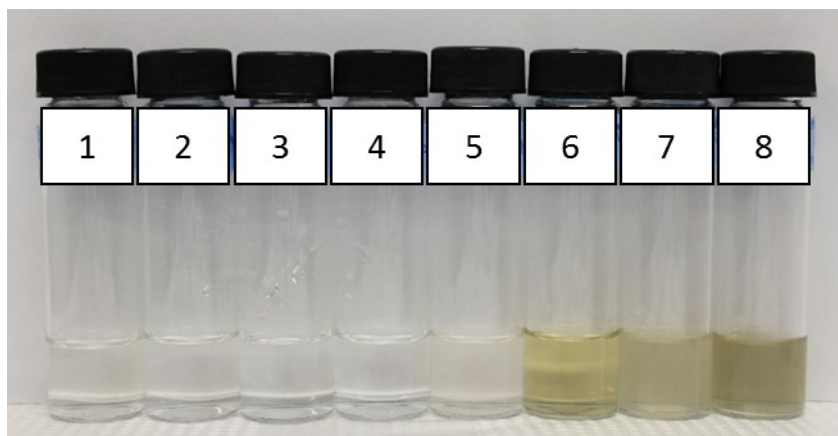


Figure 37. Optical image of unfiltered solutions obtained from the liquid exposure/washing simulation of compromised UV-aged coupons. From left to right: 1-DI water, 2-ocean water substitute, 3-citric acid solution, 4-phosphoric acid solution, 5-SDS solution, 6-Borax solution, 7-ECE-(A) solution and 8-IEC-(A) solutions. The cloudiness of the ECE-(A) and IEC-(A) is due to the presence of undissolved detergent in the solutions.

SEM ANALYSIS

4.1.3.3.1. DI WATER

A representative SEM micrograph obtained from the DI water filter is shown in Figure 38. Additional micrographs are provided in Appendix 6.9.1. High aspect ratio particles, such as the ones shown in Figure 38, were observed throughout the surface of the filter. The morphology of some of these particles is consistent with that of CNTs, but we cannot conclusively determine from SEM alone that they are indeed CNTs. In addition, SEM imaging of the unfiltered DI water solution, revealed larger release particles as shown in Figure 39.

4.1.3.3.2. OCEAN WATER

A representative SEM micrograph obtained from the ocean water filter is shown in Figure 40. Additional micrographs are provided in Appendix 6.9.1. We cannot definitively determine that these high aspect ratio features are CNTs.

4.1.3.3.3. CITRIC ACID SOLUTION

An SEM micrograph obtained from the citric acid solution filter is shown in Figure 41. Additional micrographs are provided in Appendix 6.9.1. We cannot definitively determine that these high aspect ratio features are CNTs.

4.1.3.3.4. PHOSPHORIC ACID SOLUTION

Figure 42 shows an SEM micrograph obtained from the phosphoric acid solution filter. Additional micrographs are provided in Appendix 6.9.1. The morphology of some of the release particles is consistent with that of CNTs, but we cannot definitively determine from SEM alone that these high aspect ratio features are CNTs.

4.1.3.3.5. SDS SOLUTION

SEM micrographs of the release products collected on the SDS filter are shown in Figure 43. Additional micrographs are provided in Appendix 6.9.1. Overall, more release products were observed on the SDS filter when compared to the DI water, ocean water, citric acid and phosphoric acid filters. Figure 43(b) and Figure 43(c) are higher magnification SEM micrographs of some of the observed release products. The morphology of these particles is consistent to that of CNTs. As shown in Figure 44, larger size release products were observed with SEM carried out on dried unfiltered SDS solution. As opposed to the detergent solutions obtained from the pristine coupons, the UV induced disintegration of the polymer matrix and compaction of the release products made it impossible to observe individual, micron-sized release particles with protruding CNTs; therefore we could not obtain a particle area distribution curve.

4.1.3.3.6. BORAX SOLUTION

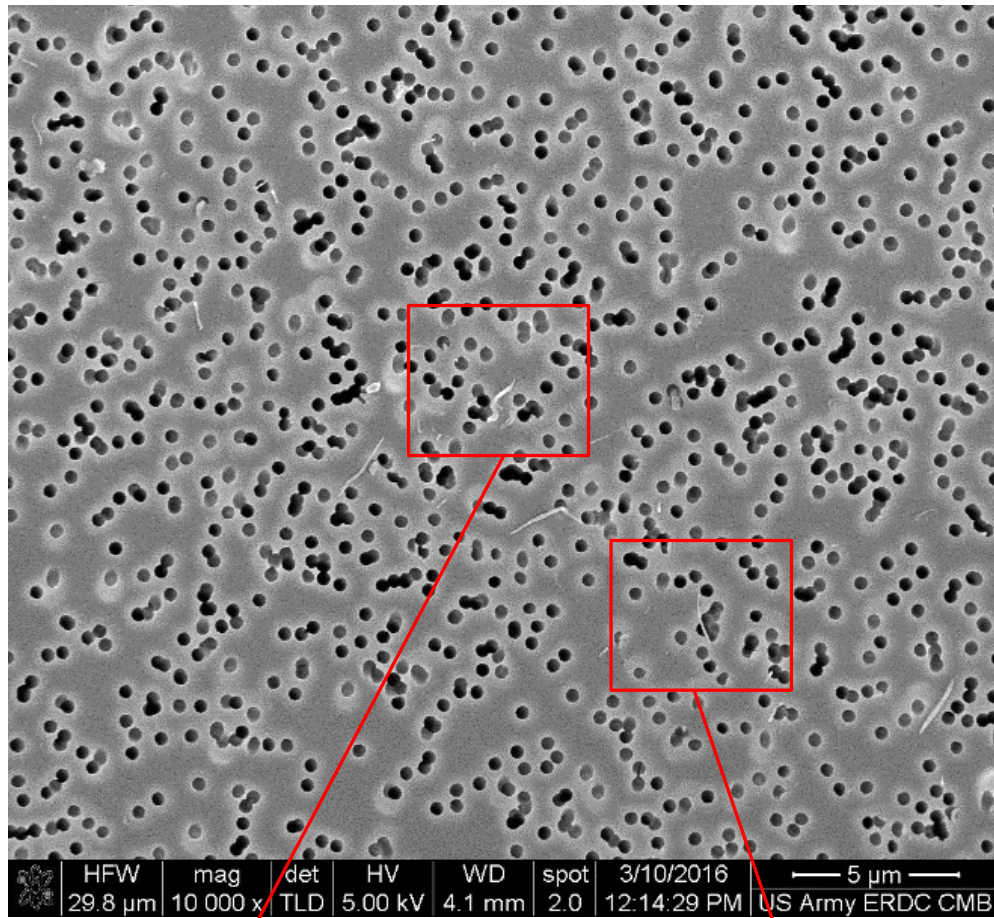
SEM micrographs of the release products on the Borax filter are shown in Figure 45. Additional micrographs are provided in Appendix 6.9.1. Similar to the SDS filter, more release products were observed on the Borax filter when compared to the DI water, ocean water, citric acid and phosphoric acid filters. Figure 45(b) and Figure 45(c) are higher magnification SEM micrographs of some of the release products. The morphology of these particles (especially for the one shown in Figure 45(c)), is consistent to that of CNTs. As shown in Figure 46, larger size release products were observed with SEM carried out on dried unfiltered Borax solution.

4.1.3.3.7. ECE-(A) SOLUTION

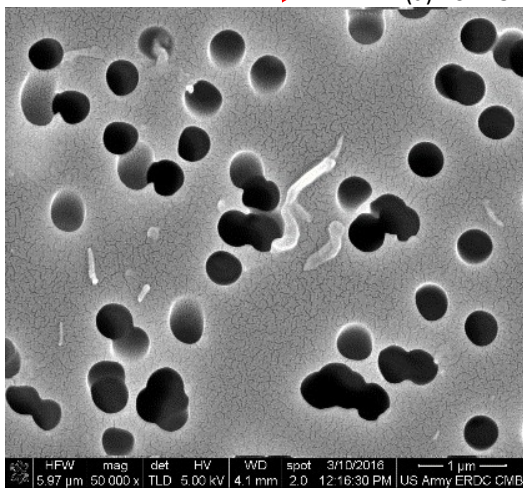
Representative SEM micrographs of the release products obtained from the unfiltered ECE-(A) solution are shown in Figure 47. Additional micrographs are provided in Appendix 6.9.1. Due to large amount of release material observed on the wafer, we focused our SEM imaging on areas of lower density allowing for imaging of small release products. Release products such as the ones shown in Figure 47 were commonly observed throughout the surface of the wafer. The morphology of the release products, shown in Figure 47(b) and Figure 47 (c) is consistent with that of CNTs. However, it is not clear from the SEM whether the released CNTs are free or still partially bound to portions of the polymer matrix (dark background behind CNTs in Figure 47).

4.1.3.3.8. IEC-(A) SOLUTION

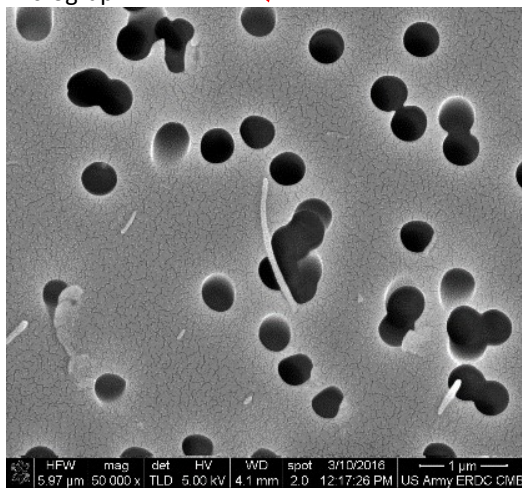
Representative SEM micrographs of the release products obtained from the unfiltered the IEC-(A) solution are shown in Figure 48. Additional micrographs are provided in Appendix 6.9.1. Our SEM observations are similar to the ones for the ECE-(A) solution, namely, an abundance of either free or partly bound CNTs.



(a) 10kX SEM micrograph

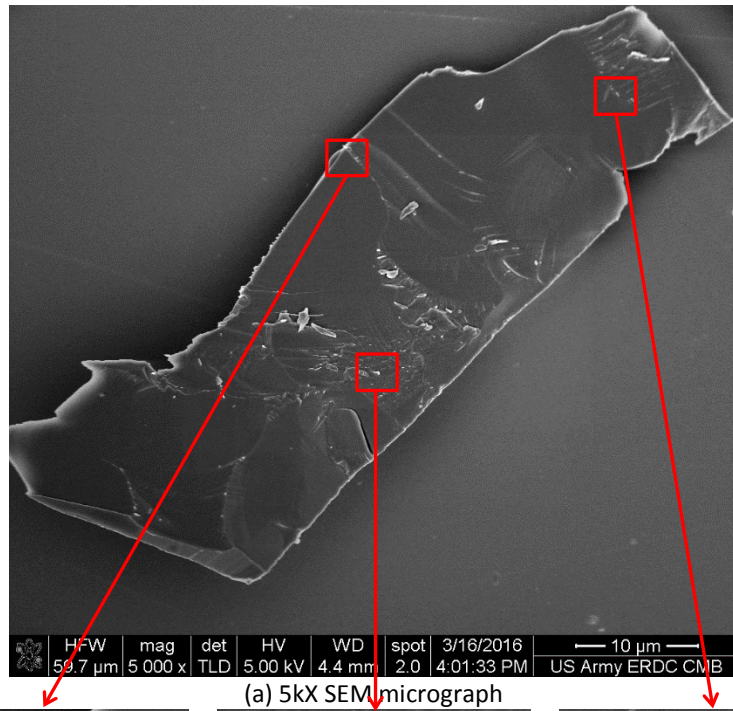


(b) 50kX SEM micrograph

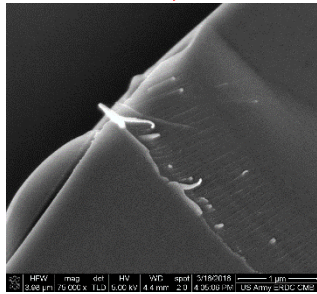


(c) 50kX SEM micrograph

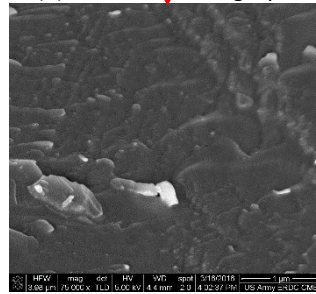
Figure 38. SEM micrographs obtained from the liquid exposure, with washing-induced wear simulation, of a UV-aged compromised coupon in DI water solution. (a) Low magnification SEM image of the membrane filter showing release products. (b)-(c) High magnification SEM images of the highlighted areas in (a) showing high aspect ratio release products, which are likely CNTs.



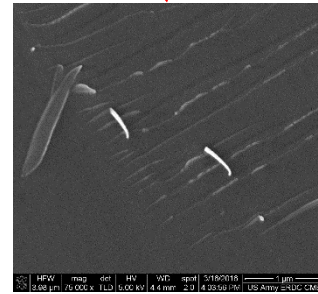
(a) 5kX SEM micrograph



(b) 75kX SEM micrograph

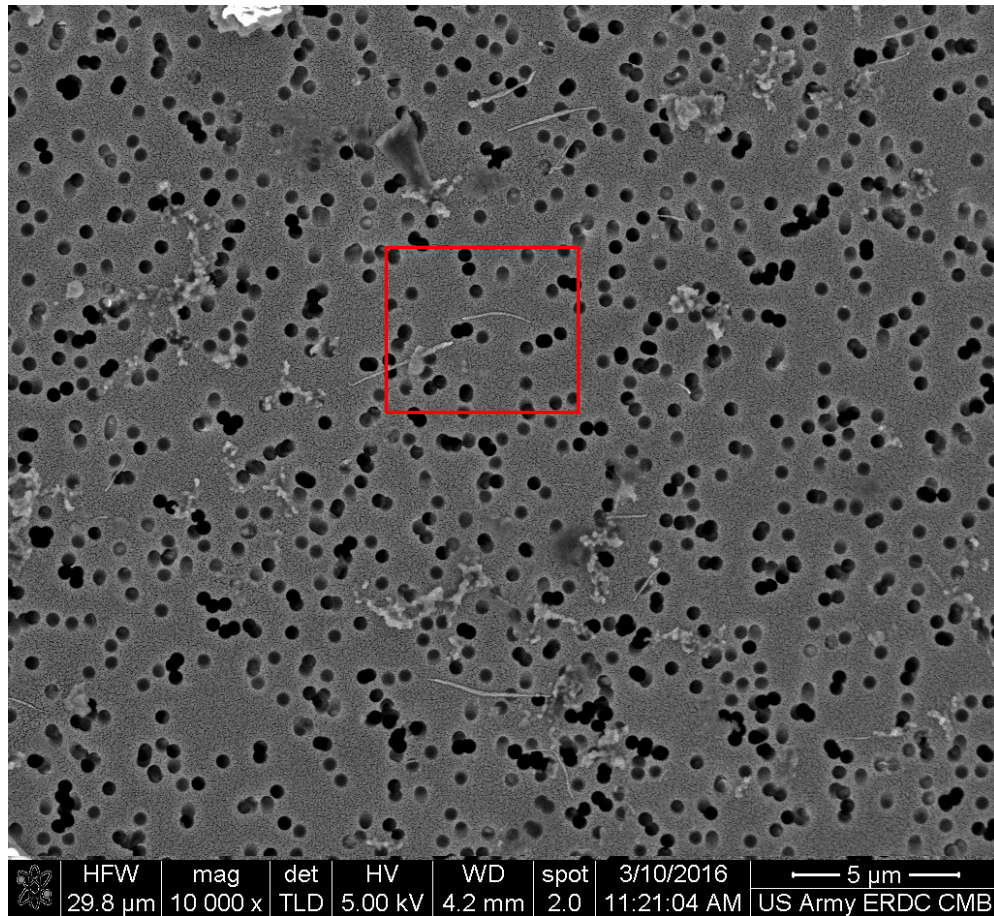


(c) 75kX SEM micrograph

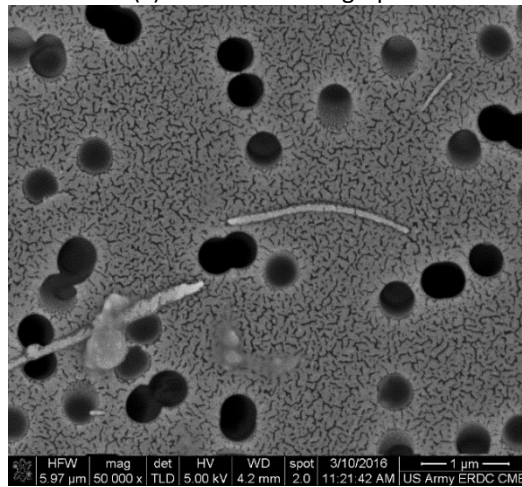


(d) 75kX SEM micrograph

Figure 39. SEM micrographs of a release product obtained from washing a UV-aged compromised coupon with the DI water solution and imaging aliquots of the unfiltered solution. (a) Low magnification SEM image showing the release product. (b)-(d) High magnification SEM images of the highlighted areas in (a) showing partially protruding CNTs located at various locations on the surface of the release product.

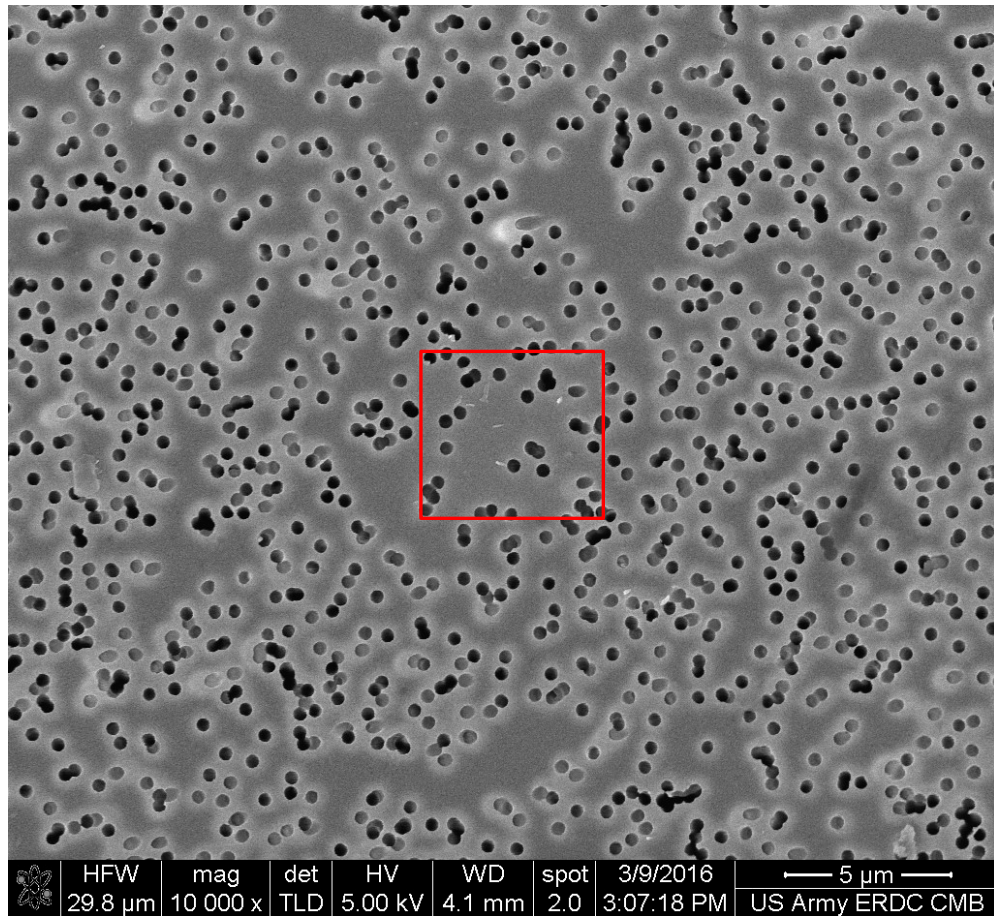


(a) 10kX SEM micrograph

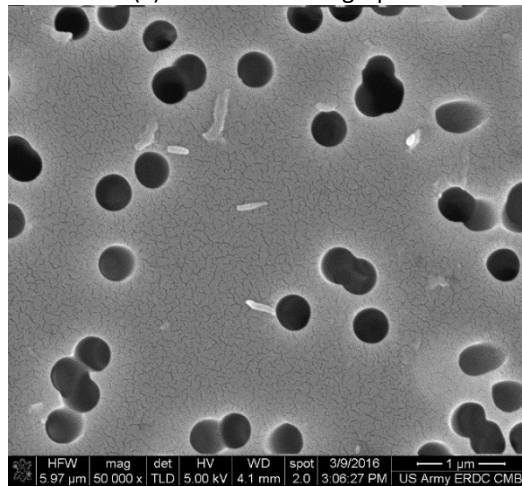


(b) 50kX SEM micrograph

Figure 40. SEM micrographs obtained from the liquid exposure, with washing-induced wear simulation, of a UV-aged compromised coupon in the ocean water substitute solution. (a) Low magnification SEM image of the membrane filter showing release products. (b) High magnification SEM image of the highlighted area in (a) showing high aspect ratio release products. We cannot conclusive determine if these are CNTs.

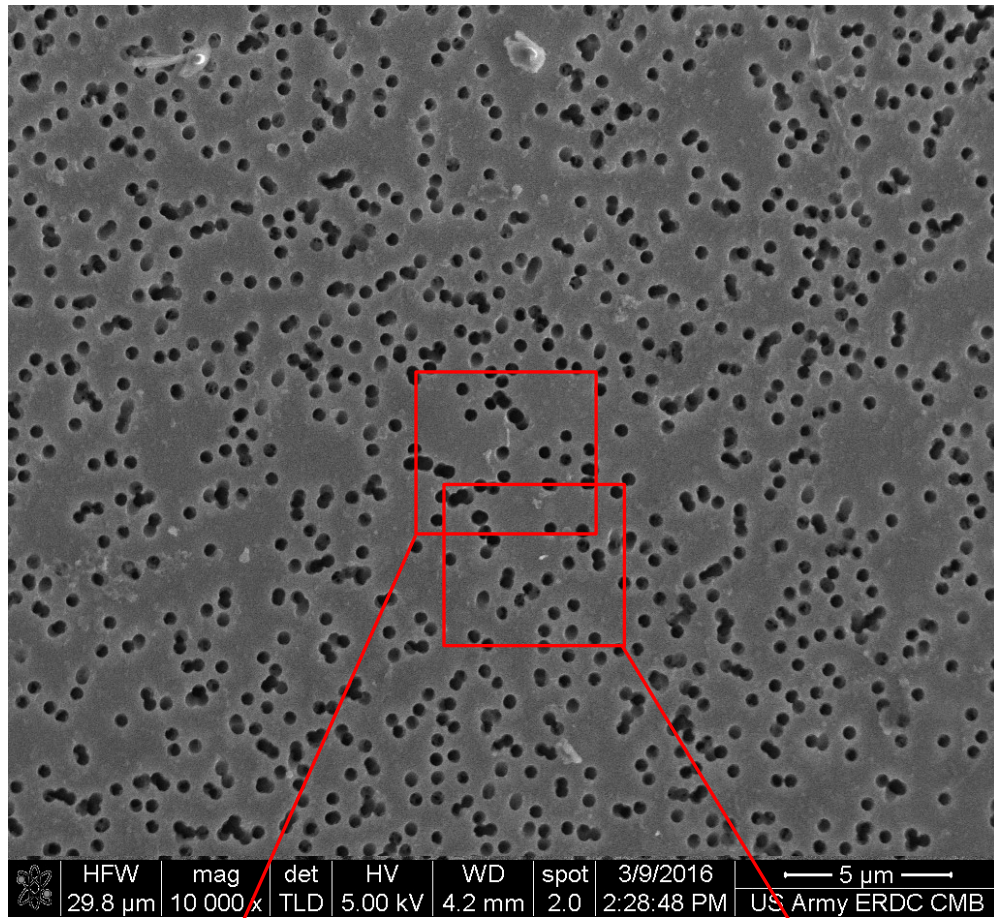


(a) 10kX SEM micrograph

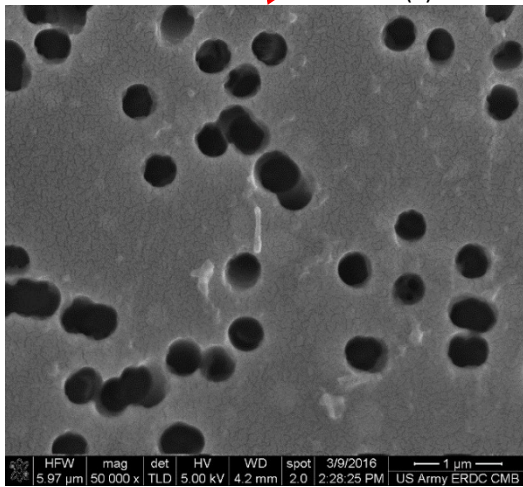


(b) 50kX SEM micrograph

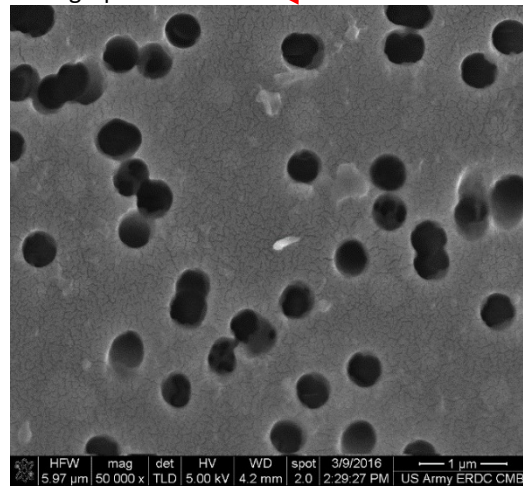
Figure 41. SEM micrographs obtained from the liquid exposure, with washing-induced wear simulation, of a UV-aged compromised coupon in the citric acid solution. (a) Low magnification SEM image of the membrane filter showing release products. (b) High magnification SEM image of the highlighted area in (a) showing high aspect ratio re-lease products. We cannot conclusive determine if these are CNTs.



(a) 10kX SEM micrograph

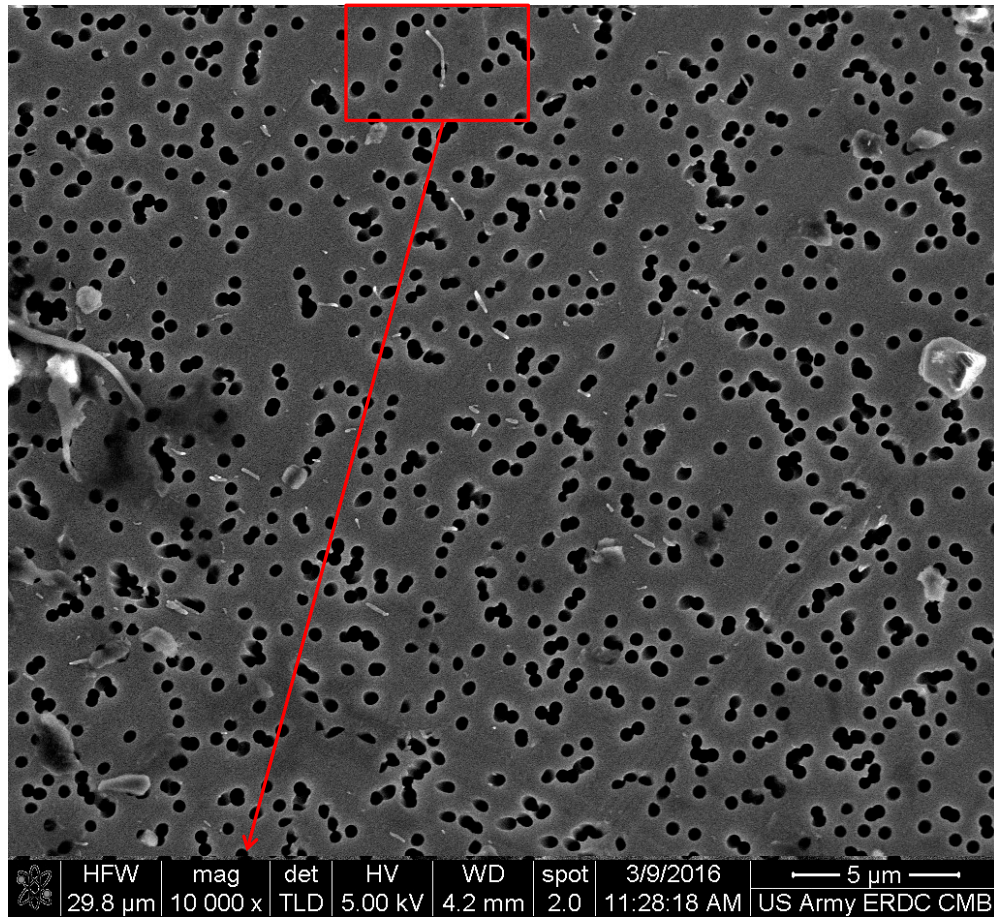


(b) 50kX SEM micrograph

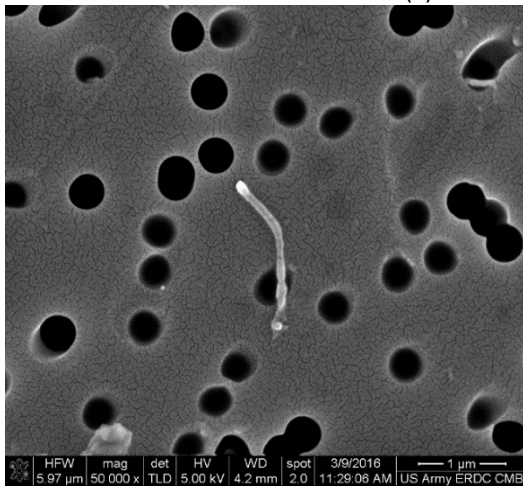


(c) 50kX SEM micrograph

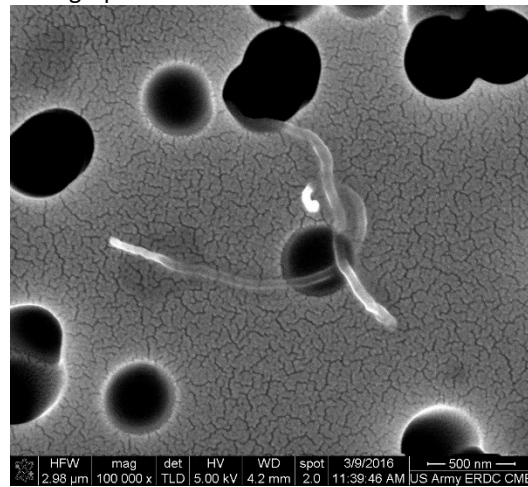
Figure 42. SEM micrographs obtained from the liquid exposure, with washing-induced wear simulation, of a UV-aged compromised coupon in the phosphoric acid solution. (a) Low magnification SEM image of the membrane filter showing release products. (b)-(c) High magnification SEM images of the highlighted areas in (a) showing high aspect ratio release products. We cannot conclusive determine if these are CNTs.



(a) 10kX SEM micrograph



(b) 50kX SEM micrograph



(c) 100kX SEM micrograph

Figure 43. SEM micrographs obtained from the liquid exposure, with washing-induced wear simulation, of a UV-aged compromised coupon in the SDS solution. (a) Low magnification SEM image of the membrane filter showing release products. (b) High magnification SEM image of the highlighted area in (a) showing high aspect ratio release products. (c) High magnification SEM image of a release product observed at a different location. The morphology of the release products is consistent with that of CNTs.

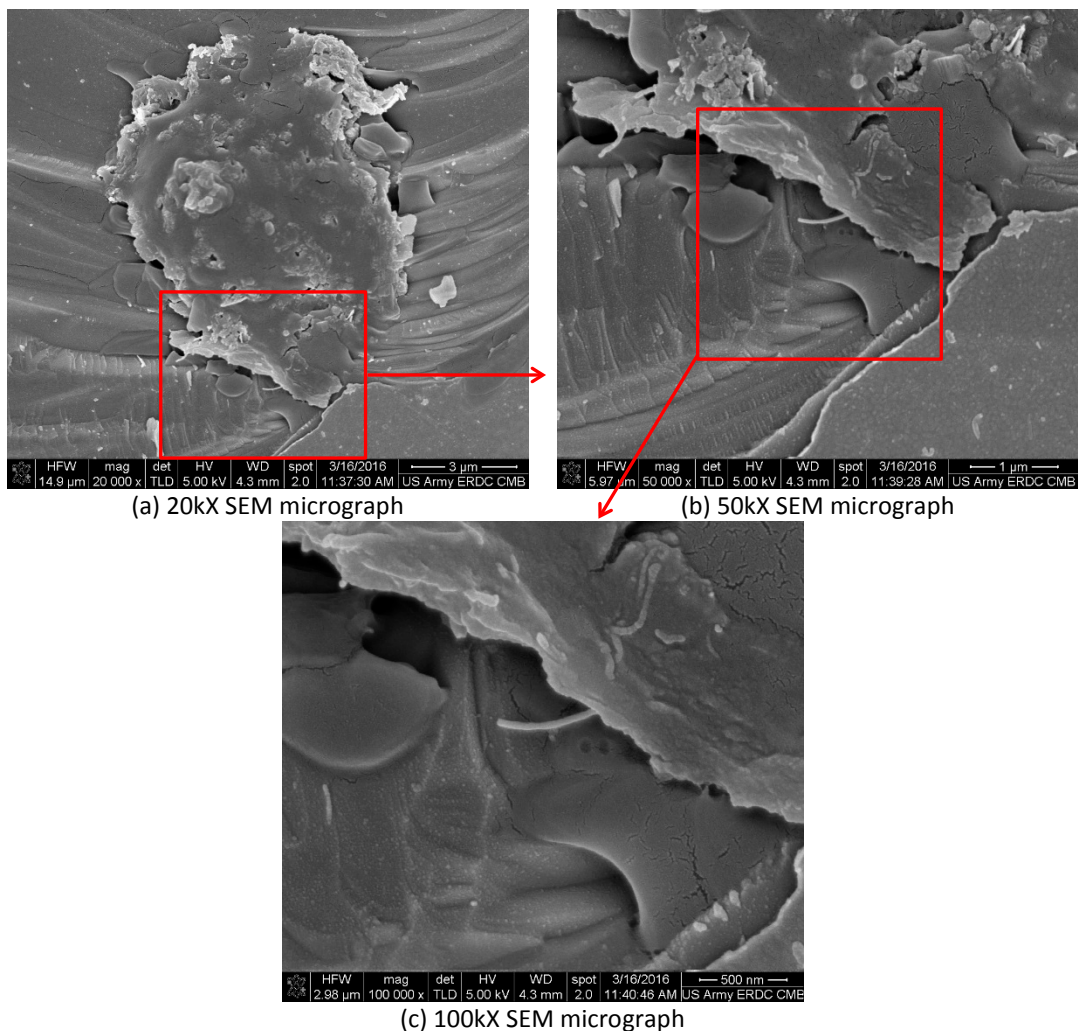
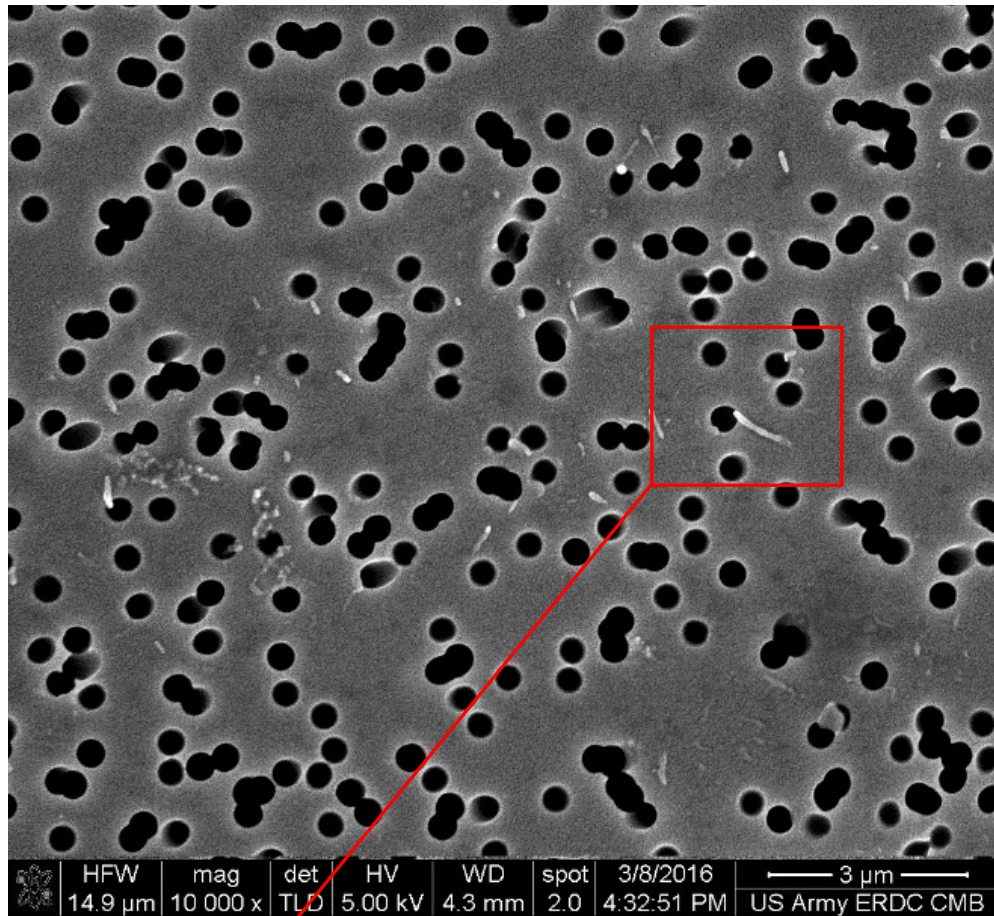
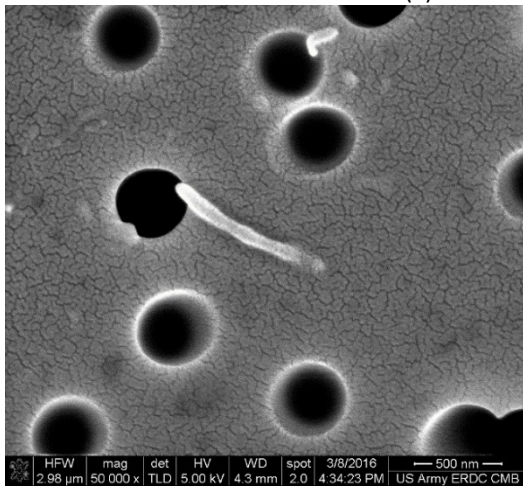


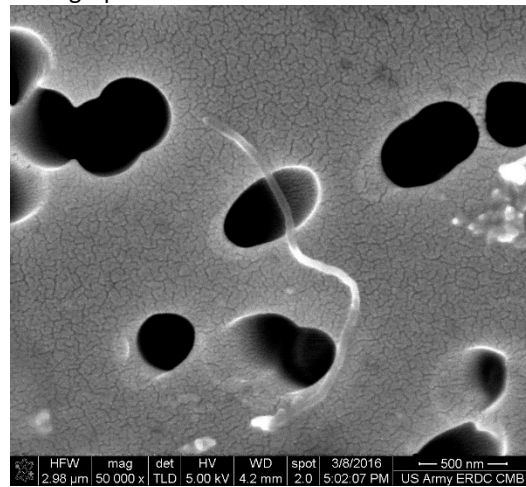
Figure 44. SEM micrographs of a release product obtained from the liquid exposure, with washing-induced wear simulation, of a UV-aged compromised coupon in the SDS solution and imaging aliquots of the unfiltered solution. (a) Low magnification SEM image showing the release product. (b)-(c) Successively higher magnification SEM images of the highlighted area in (a) showing protruding CNTs from the surface of the release product.



(a) 10kX SEM micrograph



(b) 50kX SEM micrograph



(c) 50kX SEM micrograph

Figure 45. SEM micrographs obtained from the liquid exposure, with washing-induced wear simulation, of a UV-aged compromised coupon in the Borax solution. (a) Low magnification SEM image of the membrane filter showing release products. (b) High magnification SEM image of the highlighted area in (a) showing high aspect ratio release products. (c) High magnification SEM image of a release product observed at a different location. The morphology of the release products is consistent with that of CNTs.

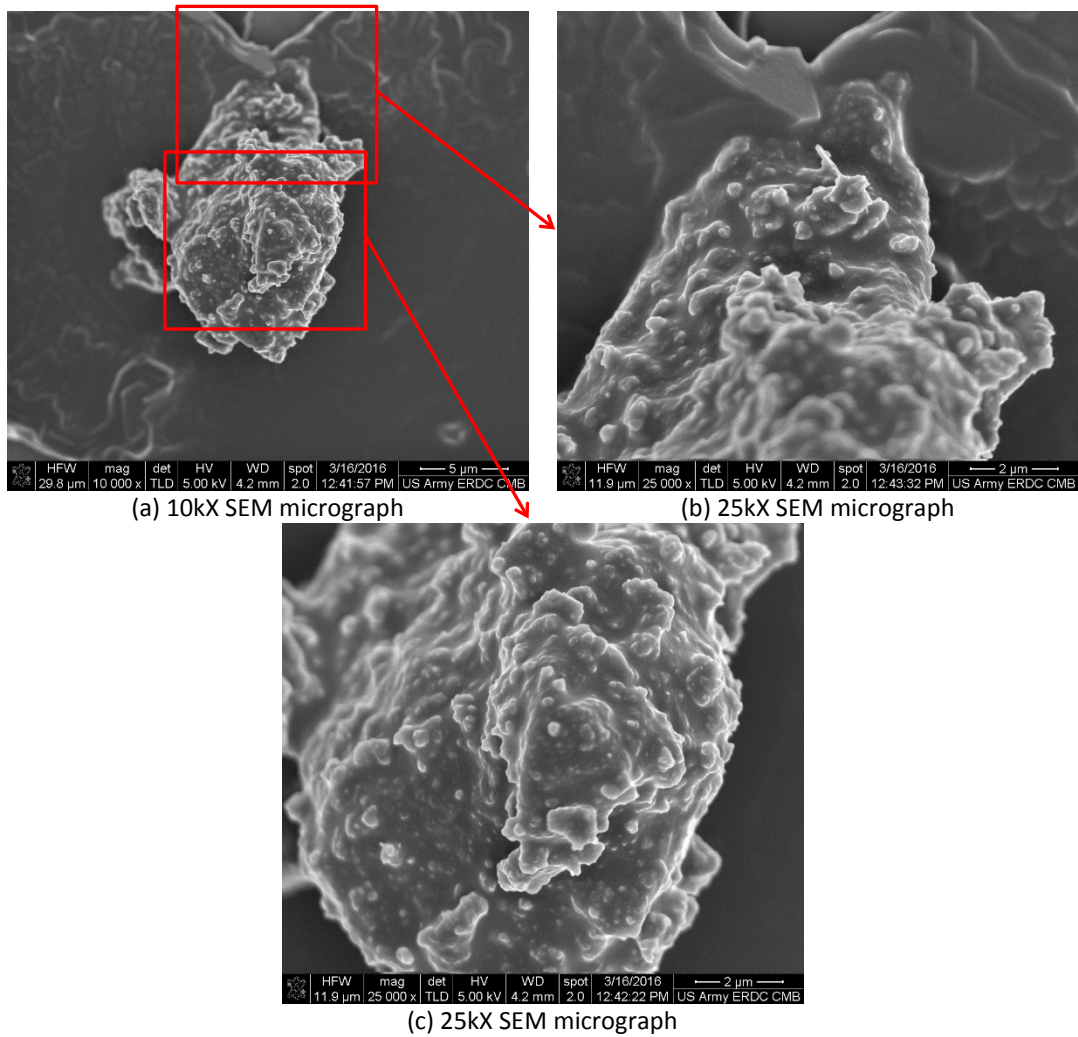
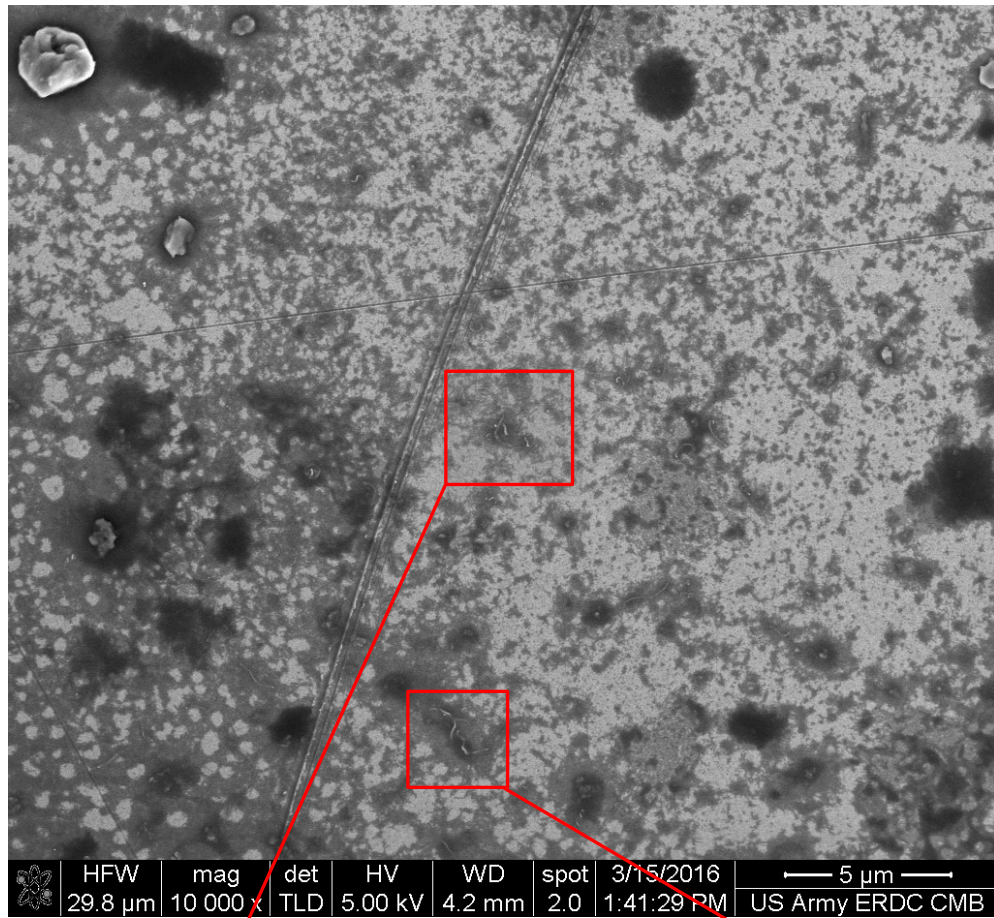
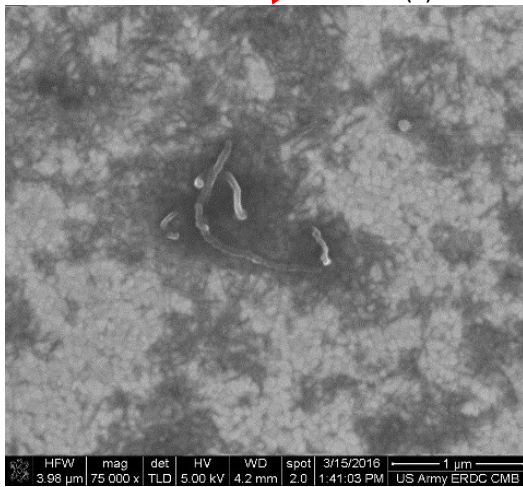


Figure 46. SEM micrographs of a release product obtained from the liquid exposure, with washing-induced wear simulation, of a UV-aged compromised coupon in the Borax solution and imaging aliquots of the unfiltered solution. (a) Low magnification SEM image showing the release product. (b)-(c) High magnification SEM images of the highlighted areas in (a) showing partially embedded CNTs from the surface of the release product.



(a) 10kX SEM micrograph

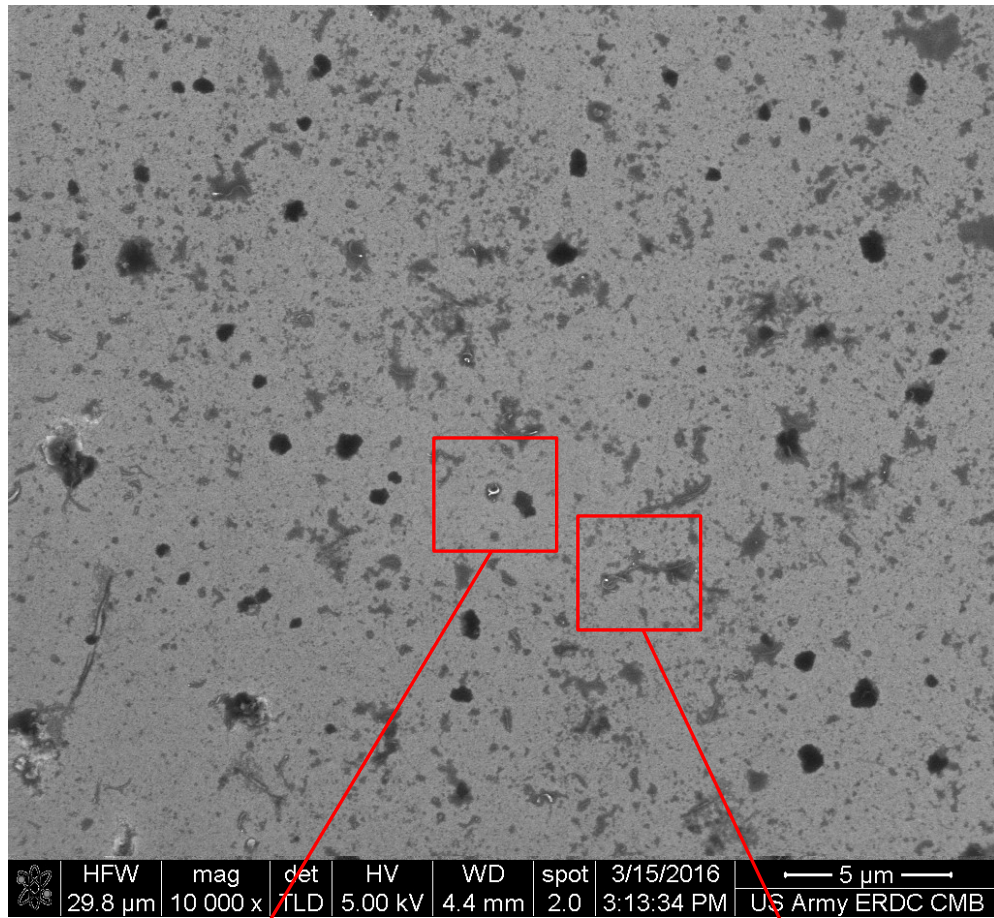


(b) 75kX SEM micrograph

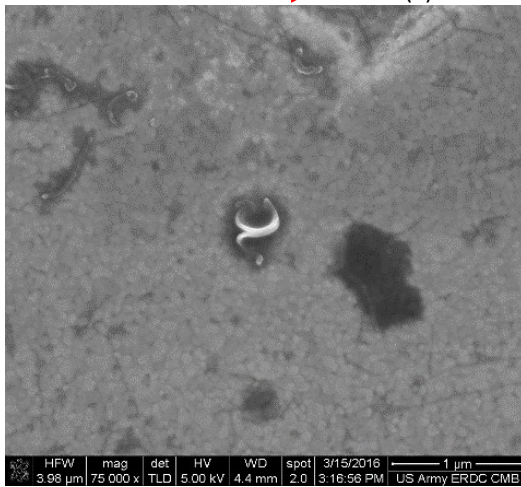


(c) 100kX SEM micrograph

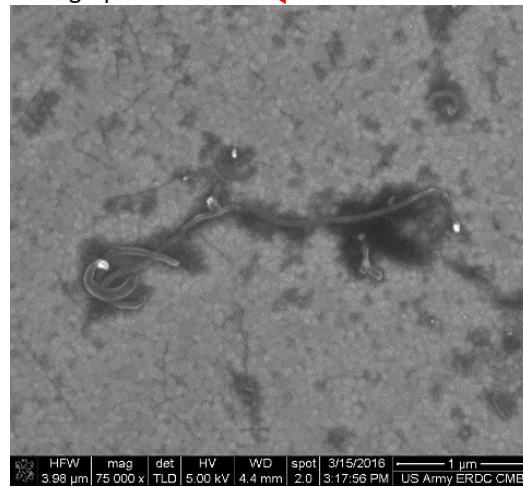
Figure 47. SEM micrographs of release products obtained from the liquid exposure, with washing-induced wear simulation, of a UV-aged compromised coupon in the ECE-(A) solution and imaging aliquots of the unfiltered solution. (a) Low magnification SEM image showing the release products. (b)-(c) High magnification SEM images of the highlighted areas in (a) showing released CNTs.



(a) 10kX SEM micrograph



(b) 75kX SEM micrograph



(c) 75kX SEM micrograph

Figure 48. SEM micrographs of the release products obtained from the liquid exposure, with washing-induced wear simulation, of a UV-aged compromised coupon in the IEC-(A) solution and imaging aliquots of the unfiltered solution. (a) Low magnification SEM image showing the release products. (b)-(c) High magnification SEM images of the highlighted areas in (a) showing released CNTs.

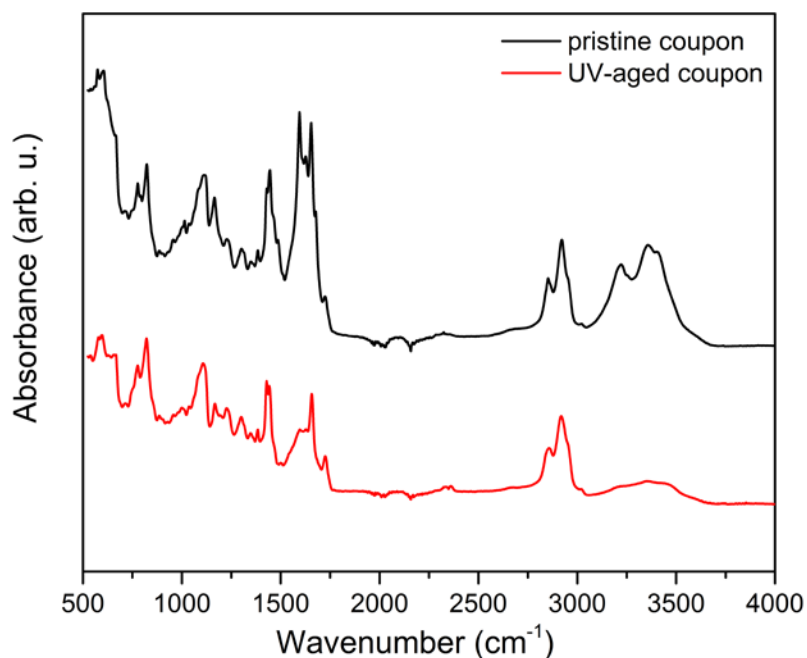


Figure 49. FTIR spectra obtained from the coating of pristine and UV-aged coupons.

RAMAN SPECTROSCOPY

Raman spectra obtained from dried unfiltered aliquots drop-cast on gold coated silicon wafers are shown in Figure 50. Raman spectra indicative of CNTs were not observed in the ocean water, citric acid and phosphoric acid solutions. All of the washing solutions (SDS, Borax, ECE-(A) and IEC-(A)) as well as the DI water exhibit Raman spectra characteristic of MWCNTs. The spectra were collected at areas of interest featuring micron size release particles, and therefore originate from release products with CNTs protruding but bound to the polymer matrix. Locating individual CNTs under optical magnification (100 \times) is challenging; therefore Raman spectra were not obtained from individual free CNTs.

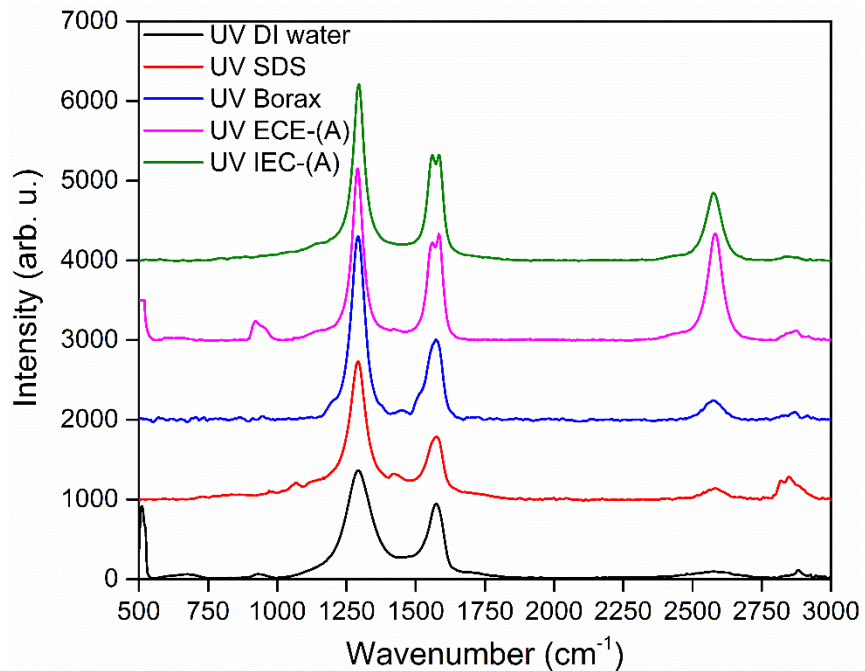


Figure 50. Raman spectra obtained from release products in unfiltered solutions obtained from washing UV-aged coupons indicating the presence of CNTs. The Raman spectra are background subtracted and vertically shifted.

UV-VIS SPECTROSCOPY AND DIGITAL IMAGE INTENSITY ANALYSIS FOR QUANTITATIVE ESTIMATION OF RELEASE PRODUCTS

The UV-VIS absorption spectra measured from the unfiltered solutions obtained from the UV-aged coupons are shown in Figure 51. All of the absorption spectra are referenced with respect to DI water. For the DI water, ocean water, citric acid, phosphoric acid, SDS, and Borax solutions the amount of released CNTs was estimated by direct comparison of their spectra with the absorption spectra obtained from dispersing known amounts of MWCNTS in DI water as discussed in further detail above. Based on this analysis, the DI water, ocean water, citric acid and phosphoric acid solutions could contain at most 1.25 $\mu\text{g/mL}$ of MWCNTs, the SDS solution at most 8.75 $\mu\text{g/mL}$ and the Borax solution at most 3.75 $\mu\text{g/mL}$. As previously described in detail, the estimation of CNTs in the ECE-(A) and IEC-(A) solutions cannot be reliably carried out from the UV-VIS absorbance spectra. A summary of the upper CNT release estimates, based on the UV-VIS absorbance analysis (Run 1 UV-aged coupons) is shown in Table 4 and in Table 5. In Table 3 the release is given in $\mu\text{g/mL}$, whereas in Table 4 the release is given in mg/m^2 , where the total solution volume was 25 mL, and the area is $2.58064 \times 10^{-3} \text{ m}^2$. The release estimations based on digital image grayscale intensity analysis are also included in Table 4 and Table 5. When compared to the UV-VIS release estimations, the yellow color of the UV-aged Borax solution appears to dominate the grayscale intensity estimation, shifting the release estimation to a higher amount than that of the colorless SDS solution (in UV-VIS measurements, the baseline of the SDS solution was higher than that of Borax suggesting larger CNT release). The release estimates for the IEC-(A) Run 3 based on digital image colorimetry is $8.9 \pm 0.84 \mu\text{g/mL}$ or $86.25 \pm 8.17 \text{ mg/m}^2$. The average release from all three runs of washing UV-aged coupons in the IEC-(A) solution is $6.29 \pm 1.28 \mu\text{g/mL}$ or $60.93 \pm 12.4 \text{ mg/m}^2$.

Table 4. Estimated amount of CNT release, in $\mu\text{g/mL}$, due to washing of compromised UV-aged coupons based on UV-VIS absorbance spectra of the unfiltered solutions. “Base-line shift” indicates that the absorbance spectrum is shifted with respect to the neat solution. “UV absorbance increase” refers to changes (increase) in the $< 400 \text{ nm}$ spectral region of the washing solutions.

	DI water	Ocean Water	Citric Acid Solution	Phosphoric Acid Solution	SDS Solution	Borax Solution	ECE-(A) solution	IEC-(A) solution
Run 1 UV-VIS	< 1.25, with base-line shift	< 1.25, no base-line shift	< 1.25, no base-line shift	< 1.25, no base-line shift	> 8.75 and < 12.5, with baseline shift	> 3.75 and < 5, with base-line shift	N/A	N/A
	UV absorbance increase	UV absorbance increase	UV absorbance increase	UV absorbance increase	UV absorbance increase	UV absorbance increase	N/A	N/A
Run 1 Digital Image Analysis	1.13 ± 0.48	-	-	0.01 ± 0.6	2.88 ± 0.65	4.46 ± 0.64	3.21 ± 0.79	6.97 ± 0.78

Table 5. Estimated amount of CNT release, in mg/m², due to washing of compromised UV-aged coupons based on UV-VIS absorbance spectra of the unfiltered solutions. “Base-line shift” indicates that the absorbance spectrum is shifted with respect to the neat solution. “UV absorbance increase” refers to any change (increase) in the < 400 nm spectral region of the washing solutions.

	DI water	Ocean Water	Citric Acid Solution	Phosphoric Acid Solution	SDS Solution	Borax Solution	ECE-(A) solution	IEC-(A) solution
Run 1 UV-VIS	< 12.11, with base-line shift	< 12.11, no base-line shift	< 12.11, no base-line shift	< 12.11, no base-line shift	> 84.76 and < 121.1, with baseline shift	> 36.33 and < 48 with base-line shift	N/A	N/A
	UV absorbance increase	UV absorbance increase	UV absorbance increase	UV absorbance increase	UV absorbance increase	UV absorbance increase	N/A	N/A
Run 1 Digital Image Analysis	10.93 ± 4.65	-	-	0.11 ± 5.82	27.91 ± 6.28	43.17 ± 6.24	31.17 ± 7.67	67.55 ± 7.56

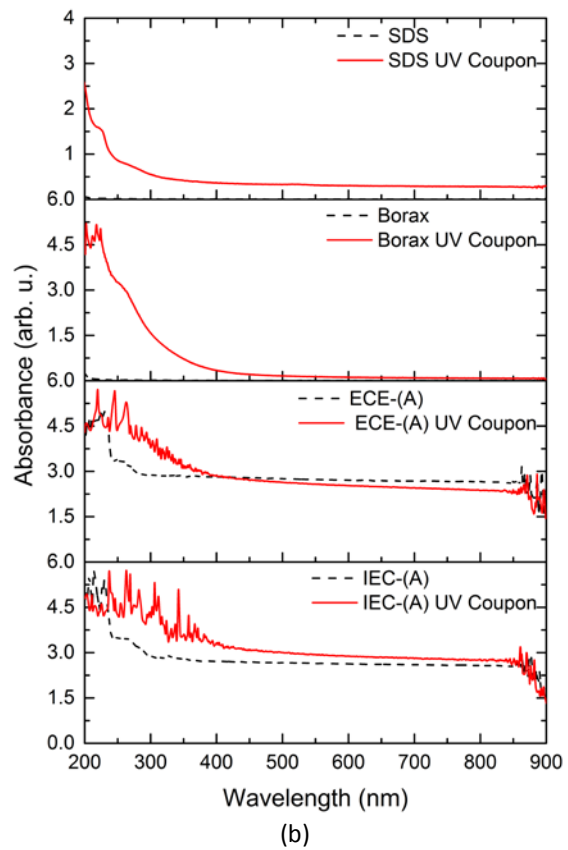
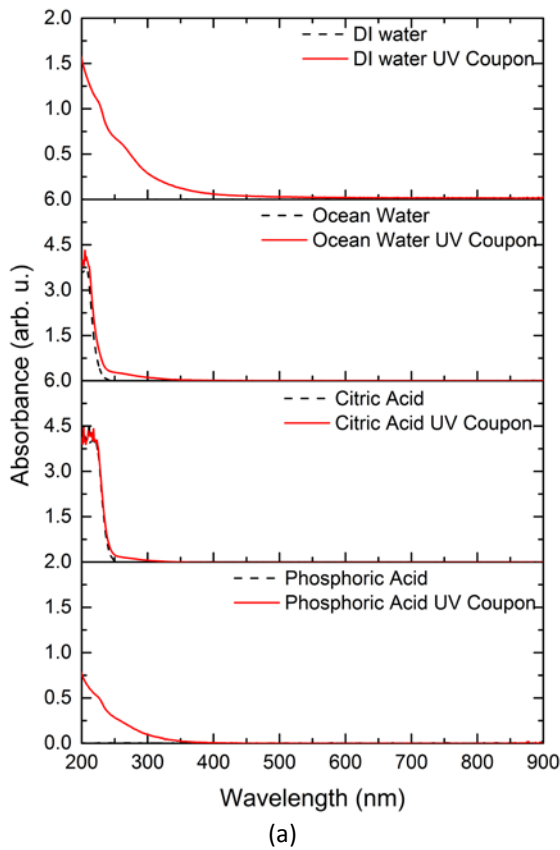


Figure 51. UV-VIS absorption spectra of unfiltered solutions (Run 1) obtained from UV-aged coupons. (a) UV-VIS absorbance spectra from liquid exposure solutions (DI water, ocean water substitute, citric acid and phosphoric acid solutions) and (b) UV-VIS absorbance spectra from solutions with washing-induced wear simulation (SDS, Borax, ECE-(A) and IEC-(A) solutions). The absorbance spectra of the corresponding neat solutions are also shown.

4.2. SUMMARY AND CONCLUSIONS

4.2.1. METHOD DEVELOPMENT

Very few standard methods exist in characterizing liquid exposure/washing release of CNTs from complex matrices. In general, quantification of CNT release is a difficult task, which becomes even more complicated when evaluating realistic release scenarios. Some of the recent work reporting quantification of CNT release (Doudrick *et al.* 2012 and Reed *et al.* 2013) are based on an initial calibration with a known type of CNT which is then incorporated into complex matrices or solutions. In this study, the challenge is that CNTs were already embedded into the polymer matrix and the chemical resilience of the matrix prevented extraction of CNTs for any type of initial calibration for our analytical techniques. We are not aware of any technique which can unambiguously extrapolate the amount of MWCNTs dispersed in a composite without extensive *a priori* knowledge of the synthesis conditions.

We employed multiple complementary techniques such as SEM, Raman spectroscopy, UV-VIS and digital image intensity analysis. Analysis of the release products by electron microscopy was limited both in the case of low and high release. For low release, the main problem was probing the large size (tens of mms) of the filtration area while attempting to find nano-sized release products or in other words looking for the “needle in the haystack.” For high release, the main issue was that the deposition of release products created a dense, compact mass which made identification of individual CNTs almost impossible. Similarly, Raman spectroscopy is a great tool for proving the existence of CNTs but it is not ideal for their quantification in complex media. In addition, since the areas of interest for the Raman measurements were identified under optical microscopy, we were essentially limited to probing micron sized particles with CNTs and not fully released CNTs. UV-VIS spectroscopy was successfully employed in estimating an upper limit in the potential amount of CNTs in unfiltered solutions but did not work well for the IEC-(A) and ECE-(A) solutions due to the variability in the amount of detergent in the solutions. Estimation of the release products collected on the IEC-(A) and ECE-(A) filters by weighing was also not successful due to variability in the amount of detergent collected on reference filters.

4.2.2. CLOSING REMARKS

By combining complimentary characterization techniques such as SEM and Raman spectroscopy we unambiguously identified CNTs as one of the release products from the coupons. A combination of UV-VIS absorbance and digital image intensity analysis allowed us to estimate the upper bounds of CNT release in the unfiltered solutions from the UV-aged coupons, with the ECE-(A) and IEC-(A) detergent solutions exhibiting the highest amount of CNT release.

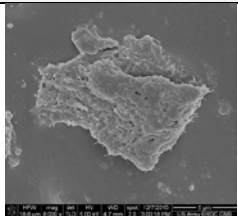
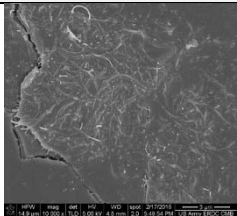
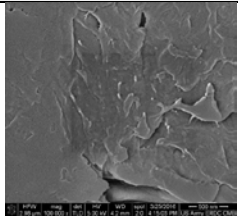
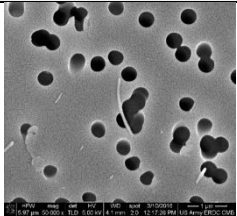
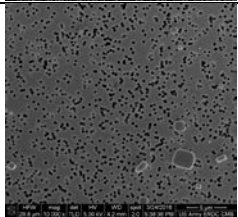
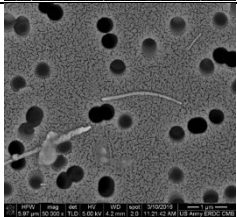
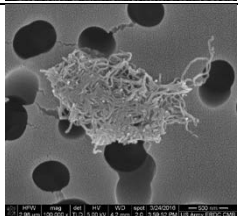
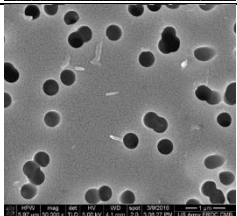
- Exposure of pristine coupons to liquid solutions leads to a modest release of MWCNTs (highest release $\sim 2 \mu\text{g/mL}$ or $\sim 19 \text{ mg/m}^2$), whereas washing simulations lead to the release of micron sized polymer MWCNT particles which are either completely released from the polymer matrix or they are still partly attached to a larger sheets of material.
- The highest estimated release for the washing solution test using the pristine coupons is $\sim 7 \mu\text{g/mL}$ ($\sim 68 \text{ mg/m}^2$). Here we assume that 100% of the material released is CNTs, which, as previously explained, is the conservative upper bound of the quantity of CNT released from the product.
- UV aging of the coupons increases the amount of exposed CNTs on the surface of the coupon. The UV-aged coupons are particularly susceptible to release during the washing simulations due to macroscopic (glass beads) and microscopic (micron sized zeolites) abrasion on the surfaces which remove material at a much higher rate than the pristine coupons. Therefore we hypothesize the dominant release mechanism for both pristine and UV-aged compromised coupons is mechanical abrasion of the surface.
- The highest release from the UV-aged coupons was associated with the IEC-(A) solution which showed visible changes in its color for two of the three runs. For UV-aged Run 1, the release was estimated to be $\sim 7 \mu\text{g/mL}$ (68 mg/m^2), for UV-aged Run 2 $\sim 3 \mu\text{g/mL}$ (29 mg/m^2), and for UV-aged Run 3 $\sim 9 \mu\text{g/mL}$ (86 mg/m^2).

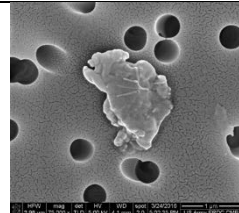
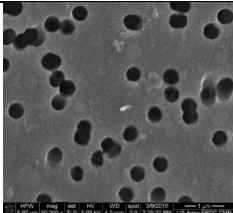
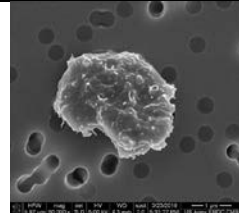
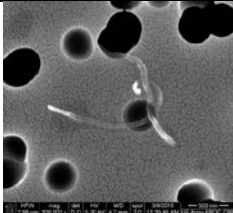
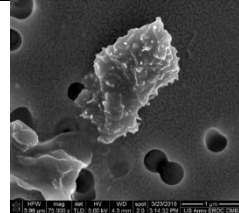
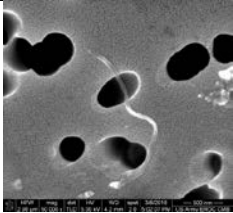
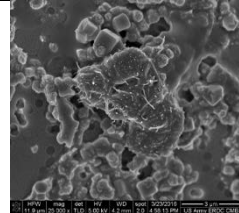
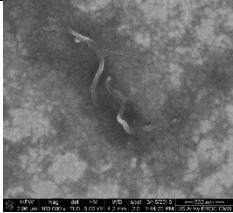
These results suggest there is release of CNT associated with the use of the ballistic backpack insert. However, these releases are only likely to occur under the most extreme conditions including removal from the protective outer casing and exposing the insert to UV light or mechanical abrasion by washing with a detergent. In order to understand the level of risk associated with this release, these results must be interpreted in the context of use, receptors, and toxicity information associated with this type of material.

5. METHODOLOGY OR PROTOCOL FOR RELEASE TESTING THAT CAN BE USED FOR EVALUATING THE PRESENCE AND RELEASE OF NANOPARTICLES FROM OTHER PRODUCTS

Please refer to the Standard Operating Procedures in Appendix 6.8 titled “Liquid Exposure, with or without Washing-induced Wear Simulation, of Products Containing Nanomaterials” and “Accelerated UV Aging of Nanomaterials to Study Potential for Release”. Even though generic, modifications to these SOPs can be made in accordance to relevant ASTM/ISO standards or specific type of material tested.

Table 6. Summary of observations for compromised materials (coupons)

	Pristine Compromised Material		UV-aged Compromised Material	
	SEM micrograph	Optical, SEM, Raman observations	SEM micrograph	Optical, SEM, Raman observations
Bulk Surface (Coupon Surface)				
Prior to liquid/washing		Surface defects with protruding MWCNTs were observed with SEM Presence of MWCNTs was verified with Raman spectroscopy		Surface cracking and aggregation of carbon nanotubes onto the surface of the polymer matrix was observed with SEM
Filter Surface				
DI Water		Filter appears clear. Very few release products were observed with SEM. No Raman confirmation of MWCNTs.		Filter appears clear. Occasional release products observed with SEM. Raman confirmation of MWCNTs in micron size clusters
Ocean water		Filter has opaque accumulations. Release products were not observed with SEM.		Filter has opaque accumulations. High aspect ratio particles observed with SEM; inconclusive as to whether these were MWCNTs. No Raman confirmation of MWCNTs.
Citric Acid Solution		Filter appears clear. Occasional release products were observed with SEM. Morphology consistent with MWCNTs. No Raman confirmation of MWCNTs.		Filter has a few dark streaks. Occasional release products were observed with SEM; inconclusive as to whether these were MWCNTs. No Raman confirmation of MWCNTs.

	Pristine Compromised Material		UV-aged Compromised Material	
	SEM micrograph	Optical, SEM, Raman observations	SEM micrograph	Optical, SEM, Raman observations
Phosphoric Acid Solution		Filter appears clear. Occasional release products were observed with SEM. No Raman confirmation of MWCNTs.		Filter appears mostly clear. Occasional release products were observed with SEM; inconclusive as to whether these were MWCNTs. No Raman confirmation of MWCNTs.
SDS Solution		Filter has opaque accumulations. Release products were frequently observed with SEM. Raman confirmation of MWCNTs in micron size clusters		Filter has light brown accumulation. Release products were frequently observed with SEM; MWCNTs were also observed. Raman confirmation of MWCNTs in micron size clusters
Borax Solution		Filter has opaque accumulations. Release products were frequently observed with SEM. Raman confirmation of MWCNTs in micron size clusters		Filter has black accumulation. Release products were frequently observed with SEM; MWCNTs were also observed. Raman confirmation of MWCNTs in micron size clusters
ECE-(A) Solution		Filter has large amount of detergent. Release products were frequently observed with SEM. Raman confirmation of MWCNTs in micron size clusters		Filter has large amount of release material. Release products were frequently observed with SEM; MWCNTs were also observed. Raman confirmation of MWCNTs in micron size clusters

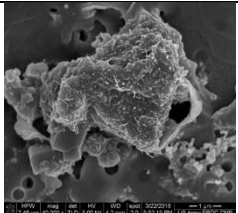
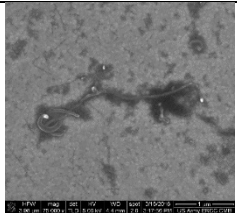
<p>IEC-(A) Solution</p>		<p>Filter has large amount of detergent. Release products were frequently observed with SEM. Raman confirmation of MWCNTs in micron size clusters</p>		<p>Filter has large amount of release material. Release products were frequently observed with SEM; MWCNTs were also observed. Raman confirmation of MWCNTs in micron size clusters</p>
--------------------------------	---	---	---	---

Table 7. Summary of experimental techniques.

Dry Material																
Technique	Pristine Compromised Material								UV-aged Compromised Material							
SEM	E								E							
Raman	Y								Y							
TGA	Y															
FTIR	N								N							
Liquid Exposure with and without Washing-Induced Wear Simulation																
Technique	DI Water		Ocean Water		Citric Acid Solution		Phosphoric Acid Solution		SDS Solution		Borax Solution		ECE-(A) Solution		IEC-(A) Solution	
	Pristine	UV	Pristine	UV	Pristine	UV	Pristine	UV	Pristine	UV	Pristine	UV	Pristine	UV	Pristine	UV
SEM	E	EF	N/A	EF	EF	EF	E	EF	E	EF	E	EF	E	EF	E	EF
Raman	N	Y	Y	N	N	N	N	N	Y	Y	Y	Y	Y	Y	Y	Y
ICP-MS																
Optical Microscopy: filters	S	S	S*	L*	S	S	S	S	L	L	L	L	L*	L*	L*	L*
Digital Image Intensity Analysis**	16.51 ± 3.10	10.93 ± 4.65	7.20 ± 6.32	-	7.80 ± 6.36	-	-	-	10.04 ± 5.6	27.91 ± 6.28	10.83 ± 5.4	43.17 ± 6.24	31.85 ± 7.53	60.93 ± 12.4	48.31 ± 7.61	67.55 ± 7.56
UV-VIS**	<12.11	<12.11	<12.11	<12.11	<12.11	<12.11	<12.11	<12.11	>12.1 and <24.22	> 84.76 and < 121.1	<12.11	>36.33 and < 48	N/A	N/A	N/A	N/A

SEM MWCNT Observation: E- Embedded MWCNT, F- free MWCNT

Bulk MWCNT Confirmation: Y/N

Release Material Observed: L- Large amount of material observed, S- Small amount of material observed

- *Salt crystals or detergent
- ** Estimated Release in mg/m^2 , average value and ignoring estimations with negative estimations

REFERENCES

ASTM D1141-98(2013), Standard Practice for the Preparation of Substitute Ocean Water, ASTM International, West Conshohocken, PA, 2013, www.astm.org

Bokobza, L.; Zhang, J., Raman Spectroscopic Characterization of Multiwall Carbon Nanotubes and of Composites, *eXPRESS Polymer Letters* **2012**, *6*, 601–608.

Bokobza, L.; Bruneel, J.-L.; Couzi, M., Raman Spectroscopic Investigation of Carbon-based Materials and their Composites. Comparison between Carbon Nanotubes and Carbon Black, *Chemical Physics Letters* **2013**, *590*, 153–159.

Doudrick, K.; Herckes, P.; Westerhoff, P., Detection of Carbon Nanotubes in Environmental Matrices Using Programmed Thermal Analysis, *Environ. Sci. Technol.* **2012**, *46*, 12246–12253.

Huang, Y. Y.; Terentjev, E. M., Dispersion and Rheology of Carbon Nanotubes in Polymers, *Int J Mater Form* **2008**, *1*, 63-74.

ISO 4892-2:2013 - Plastics -- Methods of exposure to laboratory light sources -- Part 2: Xenon-arc lamps, International Organization for Standardization, 2013.

ISO 105-C06:2010 -Textiles --Tests for colour fastness--Part C06: Colour fastness to domestic and commercial laundering, International Organization for Standardization, 2010.

Kingston, C.; Zepp, R.; Andrady, A.; Boverhof, D.; Fehir, R.; Hawkins, D.; Roberts, J.; Sayre, P.; Shelton, B.; Sultan, Y.; Vejins, V.; Wohlleben, W., Release Characteristics of Selected Carbon Nanotube Polymer Composites, *Carbon* **2014**, *68*, 33-57.

McNally, T.; Pötschke, P., Polymer-Carbon Nanotube Composites: Preparation, Properties and Applications, Woodhead Publishing **2011**, ISBN 9781845697617.

Reed, R. B.; Goodwin, D. G.; Marsh, K. L.; Capracotta, S. S.; Higgins, C. P.; Fairbrother H. D.; Ranville, J. F., Detection of single walled carbon nanotubes by monitoring embedded metals, *Environ. Sci.: Processes Impacts* **2013**, *15*, 204-213.

Soin, N.; Roy, S. S.; Rayb, S. C.; McLaughlin, J. A, Excitation Energy Dependence of Raman Bands in Multiwalled Carbon Nanotubes, *J. Raman Spectrosc.* **2010**, *41*, 1227-1233.

Schneider, C. A.; Rasband, W. S.; Eliceiri, K. W., NIH Image to ImageJ: 25 Years of Image Analysis, *Nat. Methods* **2012**, *9*, 671-675.

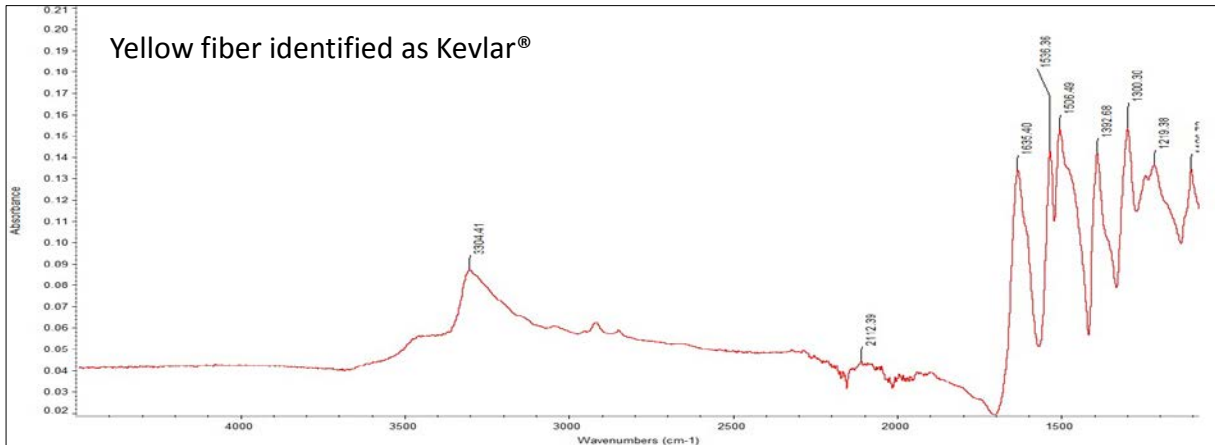
Subramaniam, K.; Das, A.; Häußler, L.; Harnisch, C.; Stöckelhuber, K.-W.; Heinrich, G., Enhanced thermal stability of polychloroprene rubber composites with ionic liquid modified MWCNTs, *Polymer Degradation and Stability* **2012**, *97*, 776-785.

“What is in Coca-Cola? A briefing on our ingredients” (<http://www.coca-colahellenic.ro/Download.aspx?ResourceId=122398>).

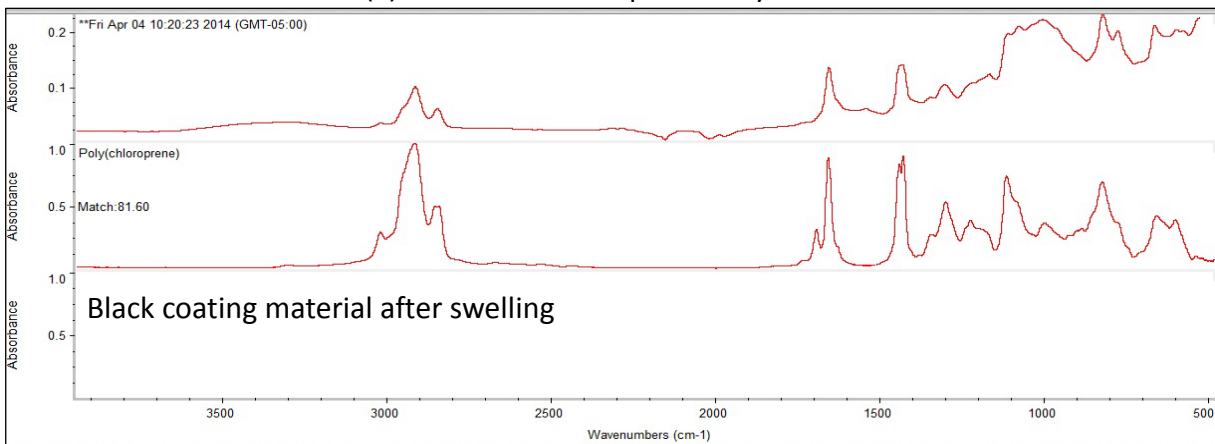
Windler, L.; Lorenz, C.; von Goetz, N.; Hungerbühler, K.; Amberg, M.; Heuberger, M.; Nowack, B; Release of Titanium Dioxide from Textiles during Washing, *Environ. Sci. Technol.* **2012**, *46*, 8181-8188.

6. APPENDICES

6.1. FTIR SPECTROSCOPY



(a) FTIR absorbance spectra of yellow fiber



(b) FTIR absorbance spectra of polychloroprene (top) and black coating (bottom)

Figure 52. Identification of ballistic insert material based on FTIR spectroscopy. (a) Peak indexed FTIR spectra identify yellow fiber as Kevlar, (b) FTIR spectra of black coating (bottom) compared to polychloroprene (top) with 81.60 % match.

6.2. REFERENCE DETERGENT COMPOSITION

Table 8. ECE (A) Reference detergent No. 2 composition.

<http://www.altraco.nl/content/altraco/producten/pdf/detergenten-test-zeepoeders.pdf>

Component	Quantity % Mass
Linear sodium alkyl benzene sulphonate (mean length of alkane chain C _{11.5})	9.7
Ethoxylated fatty alcohol C ₁₂₋₁₈ (7 EO units)	5.2
Sodium soap, chain length C ₁₂₋₁₇ 46% : C ₁₈₋₂₀ 54%	3.6
Foam inhibitor (DC-4248S)	4.5
Sodium aluminium silicate (Zeolite 4A)	32.5
Sodium carbonate	11.8
Sodium salt of copolymer from acrylic and maleic acid	5.2
Sodium silicate (SiO ₂ :Na ₂ O = 3.3 : 1)	3.4
Carboxy methyl cellulose (CMC)	1.3
Diethylene triamine penta(methylene phosphonic acid)	0.8
Sodium sulphate	9.8
Water	12.2
	TOTAL 100.0

Table 9. IEC (A) Reference detergent No. 3 composition.

<http://www.altraco.nl/content/altraco/producten/pdf/detergenten-test-zeepoeders.pdf>

Component	Quantity % Mass
Linear sodium alkyl benzene sulphonate (mean length of alkane chain C _{11.5})	9.7
Ethoxylated fatty alcohol C ₁₂₋₁₈ (7 EO units)	5.2
Sodium soap, chain length C ₁₂₋₁₇ 46% : C ₁₈₋₂₀ 54%	3.6
Foam inhibitor concentrate 8% on inorganic carrier	6.5
Sodium aluminium silicate (Zeolite 4A)	32.5
Sodium carbonate	11.8
Sodium salt of copolymer from acrylic and maleic acid	5.2
Sodium silicate (SiO ₂ :Na ₂ O = 3.3 : 1)	3.4
Carboxy methyl cellulose (CMC)	1.3
Diethylene triamine penta(methylene phosphonic acid)	0.8
Optical brightener (stilbene type)	0.3
Sodium sulphate	7.5
Water	12.2
	TOTAL 100.0

6.3. OPTICAL IMAGES OF UNFILTERED/FILTERED SOLUTIONS

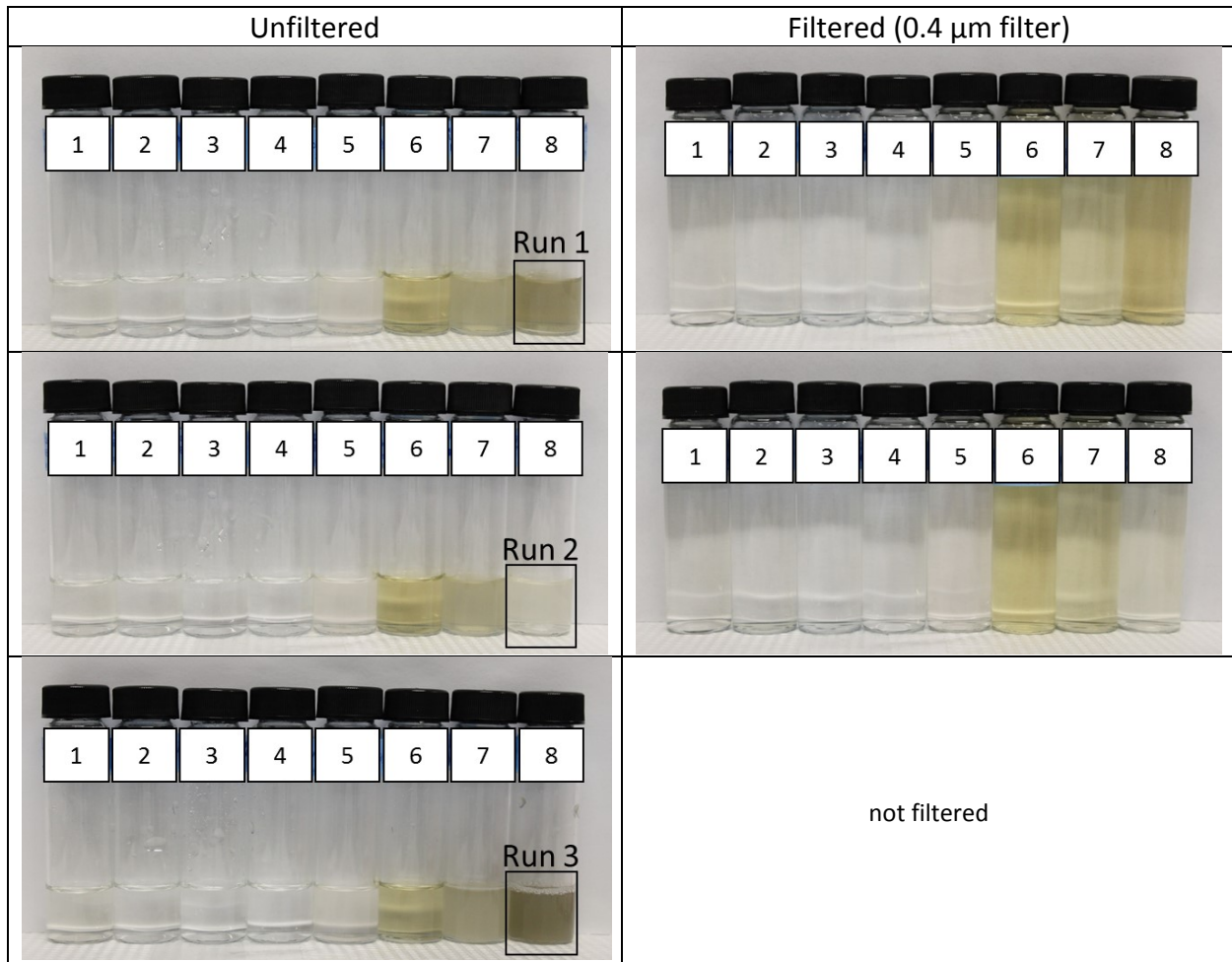


Figure 53. Optical images of the unfiltered (left column) and filtered solutions (right column) obtained from exposing UV-aged coupons to liquids with and without washing-induced wear simulation. From left to right: liquid exposure solutions: 1-DI water, 2-ocean water substitute, 3-citric acid solution, 4-phosphoric acid solution; washing simulation with beads: 5-SDS solution, 6-Borax solution, 7-ECE-(A) solution and 8-IEC-(A) solution. The IEC-(A) washing simulation was performed in triplicate.

6.4. RAMAN RESULTS

6.4.1. COMPROMISED PRISTINE MATERIAL: ECE-(A)

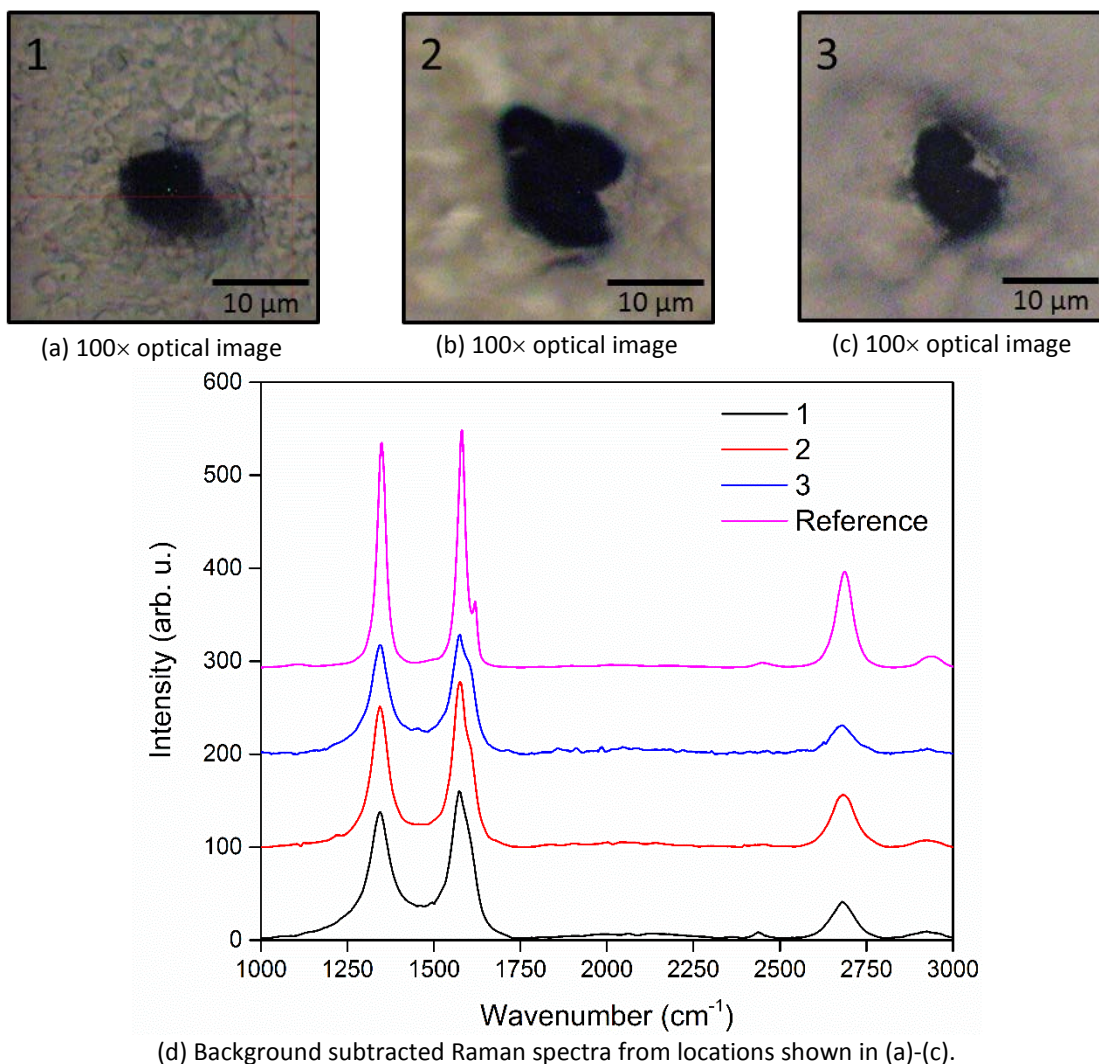


Figure 54. Raman spectra verifying the presence of CNTs in release products obtained from washing a compromised pristine coupon in the ECE-(A) solution. (a)-(c) 100× optical magnification bright-field images of release products obtained from the unfiltered ECE-(A) solution. Prior to the Raman measurements, aliquots from the solution were dried on gold coated silicon wafers. (d) Raman spectra, obtained under 532 nm laser excitation, were collected from the release products shown in (a)-(c). The observed Raman peaks are consistent with those of CNTs. Reference spectra were also obtained from the coating of an unwashed pristine compromised coupon, and they are shown in (d) for comparison. The Raman spectra were background subtracted and vertically shifted.

6.4.2. COMPROMISED PRISTINE MATERIAL IEC-(A)

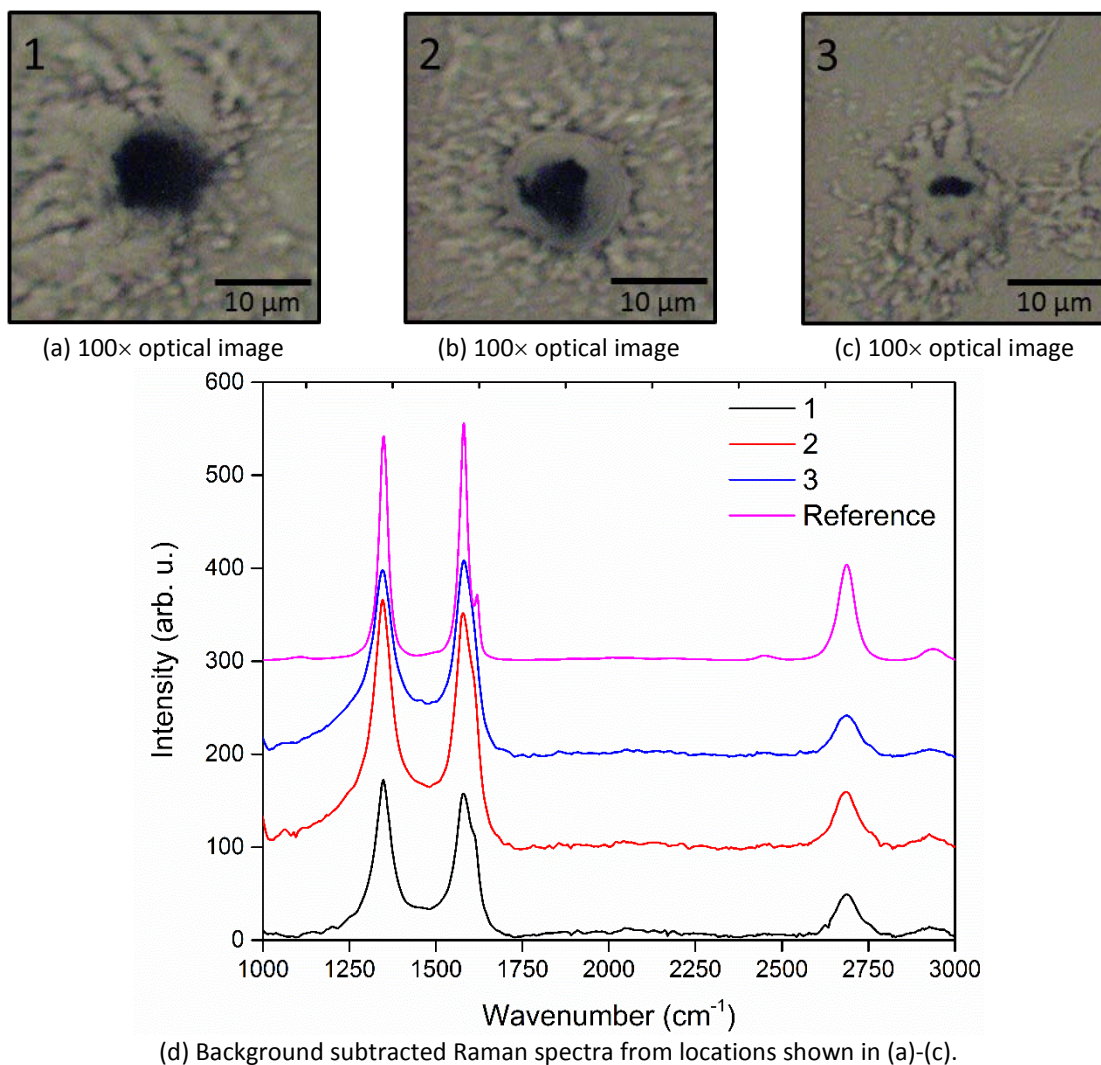


Figure 55. Raman spectra verifying the presence of CNTs in release products obtained from washing a compromised pristine coupon in the IEC-(A) solution. (a)-(c) 100× optical magnification bright-field images of release products obtained from the unfiltered IEC-(A) solution. Prior to the Raman measurements, aliquots from the solution were dried on gold coated silicon wafers. (d) Raman spectra, obtained under 532 nm laser excitation, were collected from the release products shown in (a)-(c). The observed Raman peaks are consistent with those of CNTs. Reference spectra were also obtained from the coating of an unwashed pristine compromised coupon, and they are shown in (d) for comparison. The Raman spectra were background subtracted and vertically shifted.

6.4.3. VERIFICATION OF MWCNTs IN COUPONS

The lack of RBM peaks in the 150-300 cm^{-1} spectral region is indicative of MWCNTs.

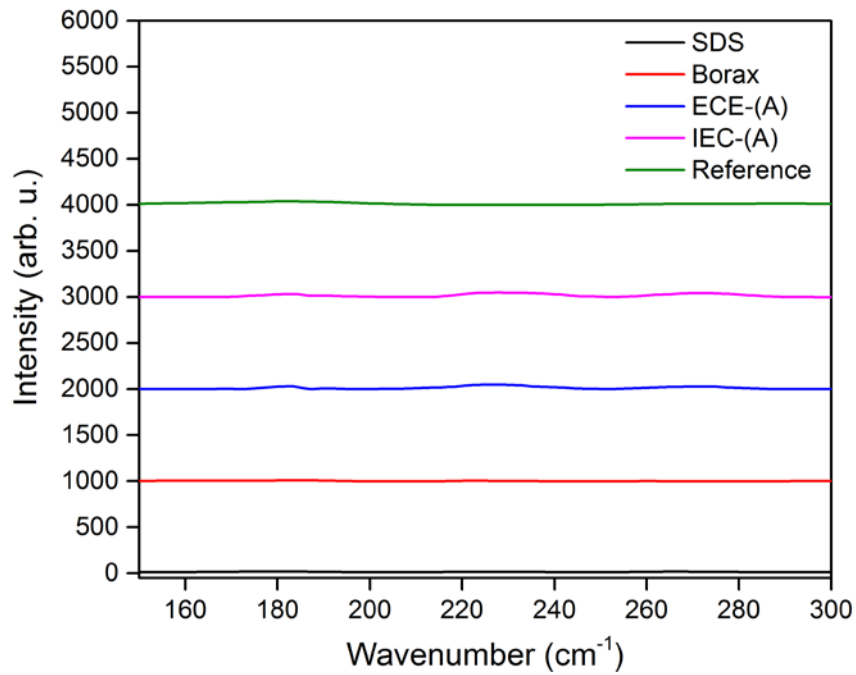
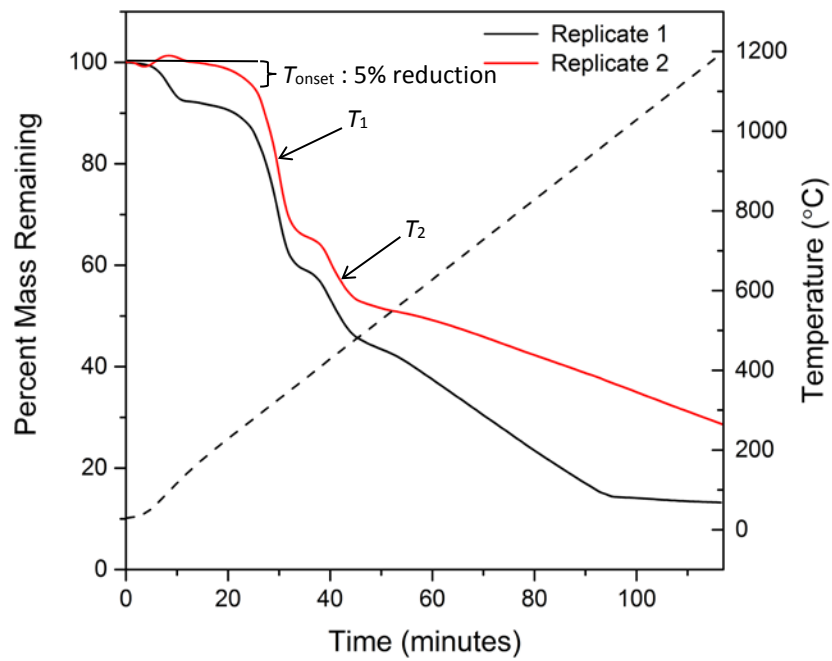
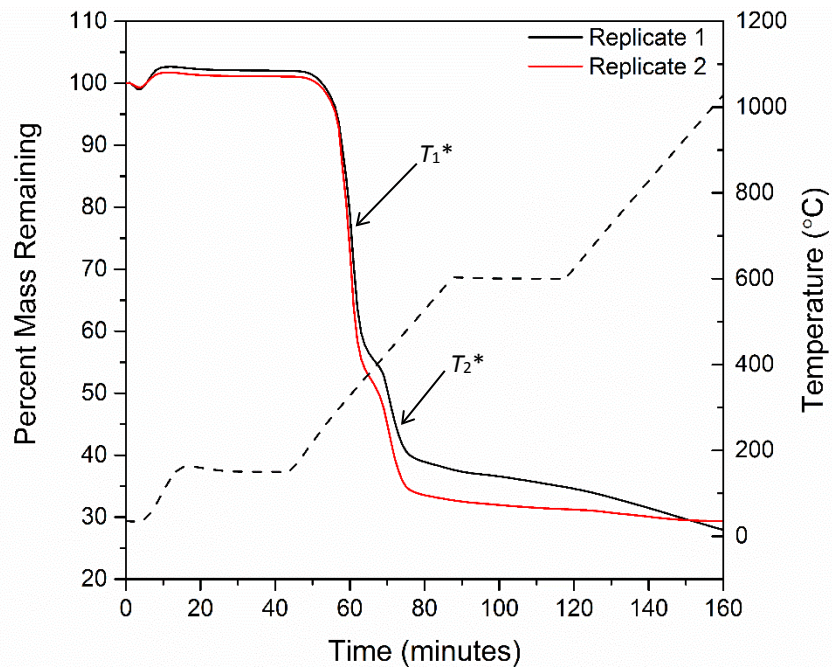


Figure 56. Raman spectra between 150-300 cm^{-1} exhibit lack of sharp peaks indicative of single-walled CNTs.

6.5. THERMOGRAVIMETRIC ANALYSIS OF COATING



(a) TGA of coating in nitrogen under continuous heating, constant ramp



(b) TGA of coating in nitrogen under custom heating ramp

Figure 57. TGA mass loss curves of coating (polymer with CNTs) in inert atmosphere (nitrogen). (a) Mass loss curves obtained under continuous heating with constant ramp. (b) Custom temperature ramp. The coating was removed from a pristine coupon after soaking the coupon in chloroform for 5-10 minutes.

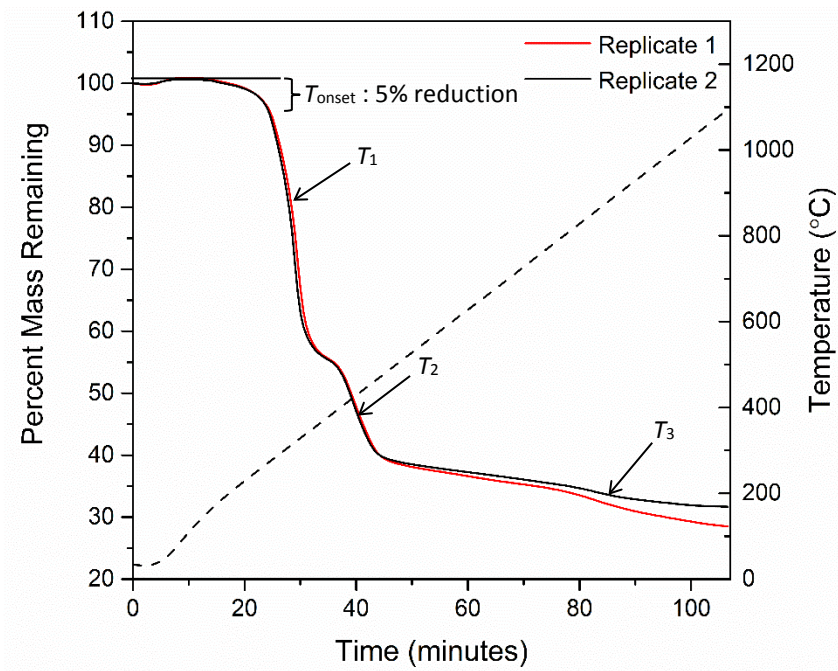


Figure 58. TGA of pristine polymer matrix with MWCNTs in oxidizing atmosphere (air) under continuous heating. The coating was removed from a pristine coupon after swelling with chloroform.

6.6. UV-VIS COMPARISON WITH OH-MWCNT SOLUTIONS

6.6.1. UV-VIS COMPARISON PRISTINE COUPONS – RUN 1

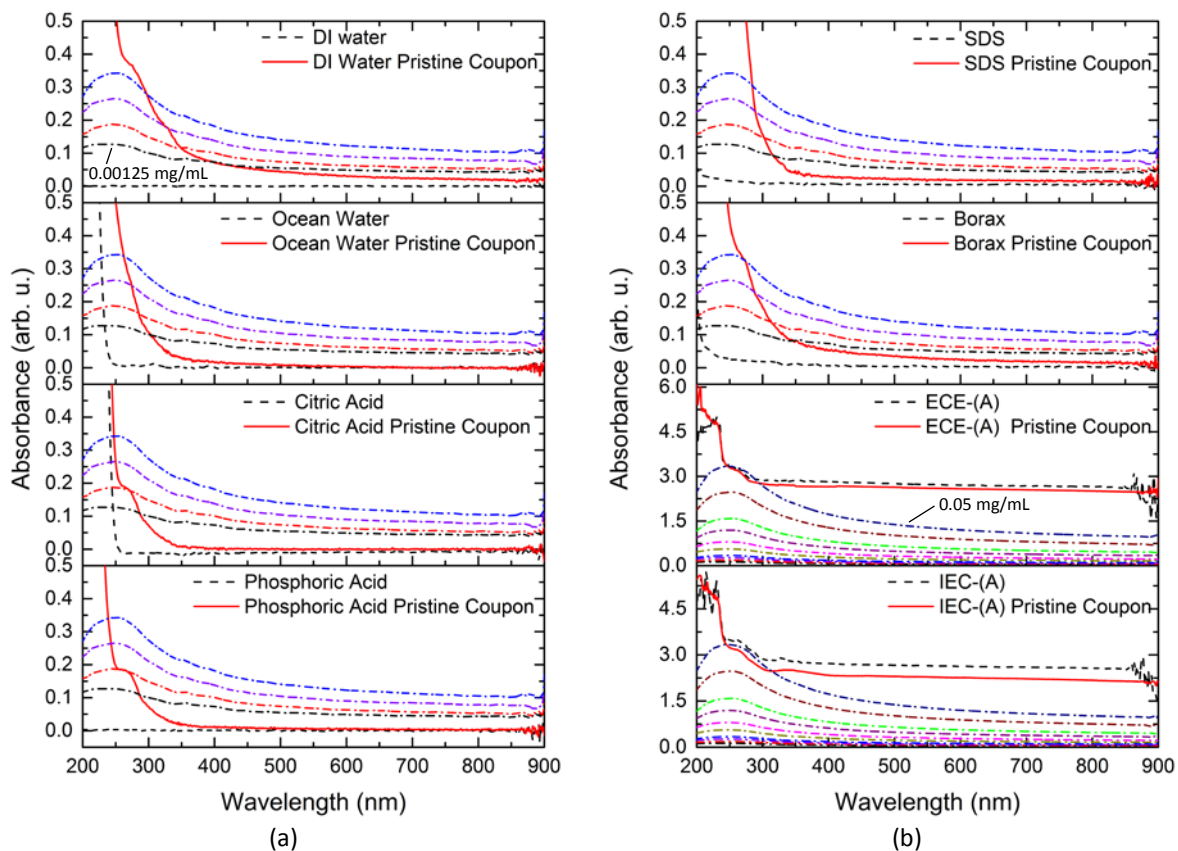


Figure 59. UV-VIS absorbance spectra of unfiltered solutions obtained from liquid exposure of compromised pristine coupons Run 1 with respect to DI water. (a) Liquid exposure without washing-induced wear simulation (DI water, ocean water substitute, citric acid and phosphoric acid), (b) washing simulation (SDS, Borax, ECE-(A) and IEC-(A) solutions with wear simulation). The absorbance spectra of the neat solutions are also shown (dashed lines). The absorbance spectra of OH-functionalized MWCNTs in DI water are also shown. The OH-MWCNT concentrations vary from 0.00125 mg/mL to 0.05 mg/mL, with pertinent concentrations indicated in the inset of the plots. The OH-MWCNT absorbance spectra shown are: 0.00125 mg/mL (dash-dot, black), 0.0025 mg/mL (dash-dot, red), 0.00375 mg/mL (dash-dot, violet), 0.005 mg/mL (dash-dot, blue), 0.00875 mg/mL (dash-dot, dark yellow), 0.0125 mg/mL (dash-dot, magenta), 0.01875 mg/mL (dash-dot, purple), 0.025 mg/mL (dash-dot, green), 0.0375 mg/mL (dash-dot, wine) and 0.05 mg/mL (dash-dot, navy).

6.6.2. UV-VIS COMPARISON PRISTINE COUPONS – RUN 2

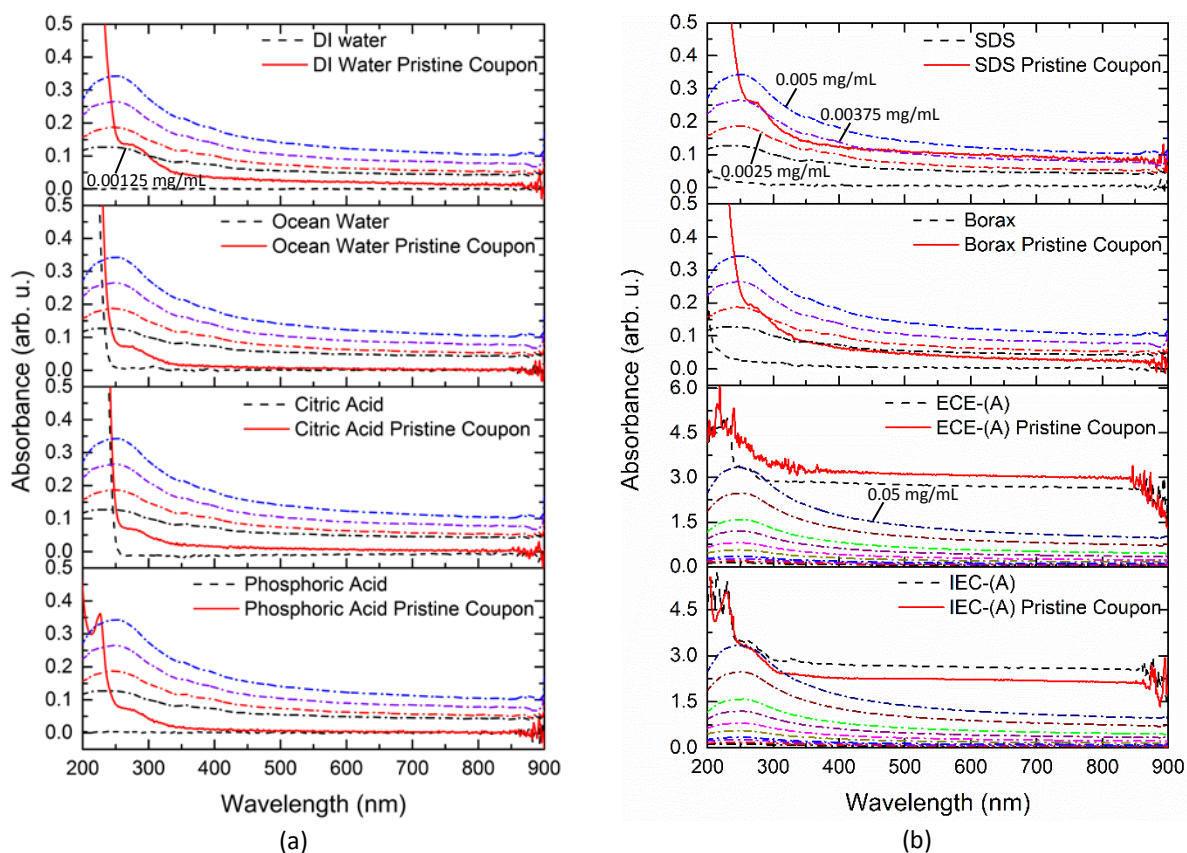


Figure 60. UV-VIS absorbance spectra of unfiltered solutions obtained from liquid exposure of compromised pristine coupons Run 2 with respect to DI water. (a) Liquid exposure without washing-induced wear simulation (DI water, ocean water substitute, citric acid and phosphoric acid), (b) washing simulation (SDS, Borax, ECE-(A) and IEC-(A) solutions with wear simulation). The absorbance spectra of the neat solutions are also shown (dashed lines). The absorbance spectra of OH-functionalized MWCNTs in DI water are also shown. The OH-MWCNT concentrations vary from 0.00125 mg/mL to 0.05 mg/mL, with pertinent concentrations indicated in the inset of the plots. The OH-MWCNT absorbance spectra shown are: 0.00125 mg/mL (dash-dot, black), 0.0025 mg/mL (dash-dot, red), 0.00375 mg/mL (dash-dot, violet), 0.005 mg/mL (dash-dot, blue), 0.00875 mg/mL (dash-dot, dark yellow), 0.0125 mg/mL (dash-dot, magenta), 0.01875 mg/mL (dash-dot, purple), 0.025 mg/mL (dash-dot, green), 0.0375 mg/mL (dash-dot, wine) and 0.05 mg/mL (dash-dot, navy).

6.6.3. UV-VIS COMPARISON UV-AGED COUPONS – RUN 1

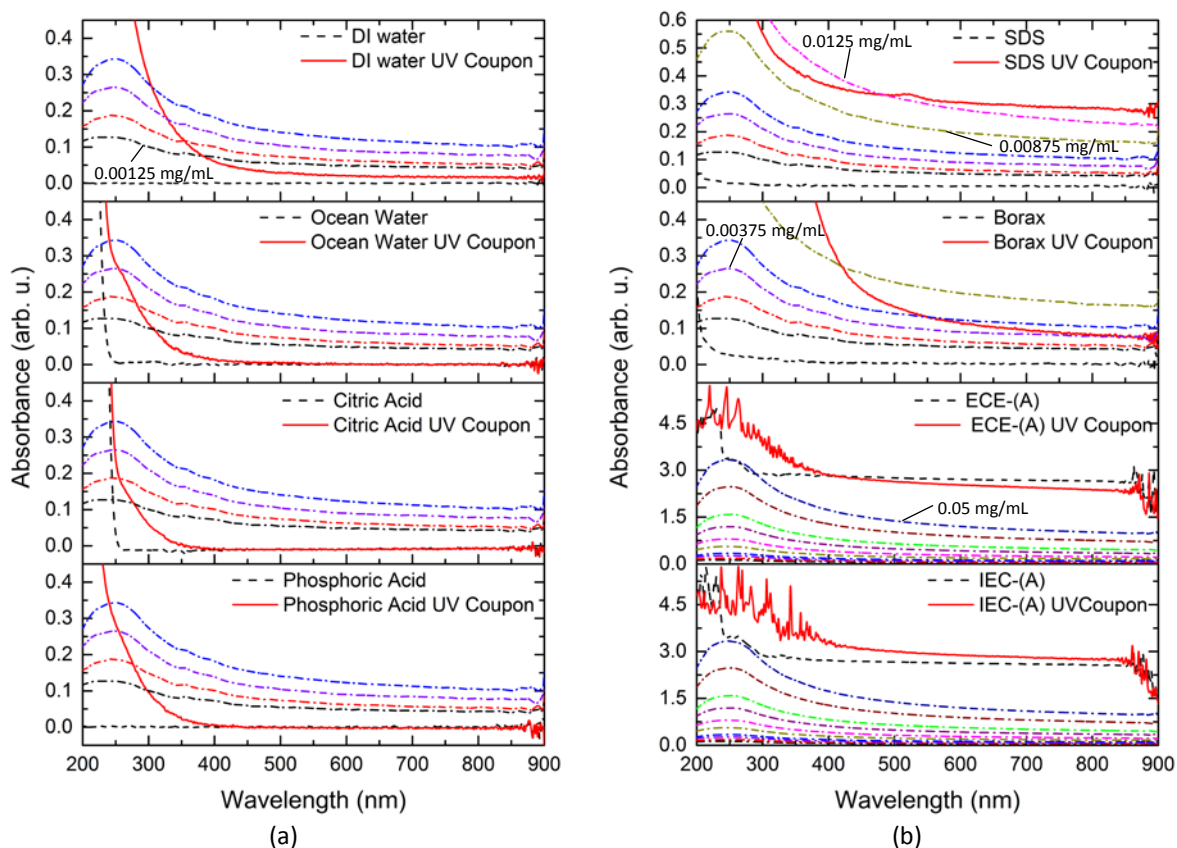


Figure 61. UV-VIS absorbance spectra of unfiltered solutions obtained from liquid exposure of compromised UV-aged coupons Run 1 with respect to DI water. (a) Liquid exposure without washing-induced wear simulation (DI water, ocean water substitute, citric acid and phosphoric acid), (b) washing simulation (SDS, Borax, ECE-(A) and IEC-(A) solutions with wear simulation). The absorbance spectra of the neat solutions are also shown (dashed lines). The absorbance spectra of OH-functionalized MWCNTs in DI water are also shown. The OH-MWCNT concentrations vary from 0.00125 mg/mL to 0.05 mg/mL, with pertinent concentrations indicated in the inset of the plots. The OH-MWCNT absorbance spectra shown are: 0.00125 mg/mL (dash-dot, black), 0.0025 mg/mL (dash-dot, red), 0.00375 mg/mL (dash-dot, violet), 0.005 mg/mL (dash-dot, blue), 0.00875 mg/mL (dash-dot, dark yellow), 0.0125 mg/mL (dash-dot, magenta), 0.01875 mg/mL (dash-dot, purple), 0.025 mg/mL (dash-dot, green), 0.0375 mg/mL (dash-dot, wine) and 0.05 mg/mL (dash-dot, navy).

6.7. STANDARD OPERATING PROCEDURE

Liquid Exposure, with or without Washing-induced Wear Simulation, of Products Containing Nanomaterials

Scope and Applicability

This SOP investigates the release of particles generated by liquid exposure with or without washing-induced wear of products containing nanomaterials. Such products include coatings with embedded CNTs or fabrics with embedded nanoparticles. During the test, samples containing nanomaterials will be exposed to liquids and periodically agitated. Washing-induced surface wear will be simulated with beads. The morphology of the release particles, their elemental/chemical composition, their size (or area) distribution and concentration under, different test conditions, can be determined with this method.

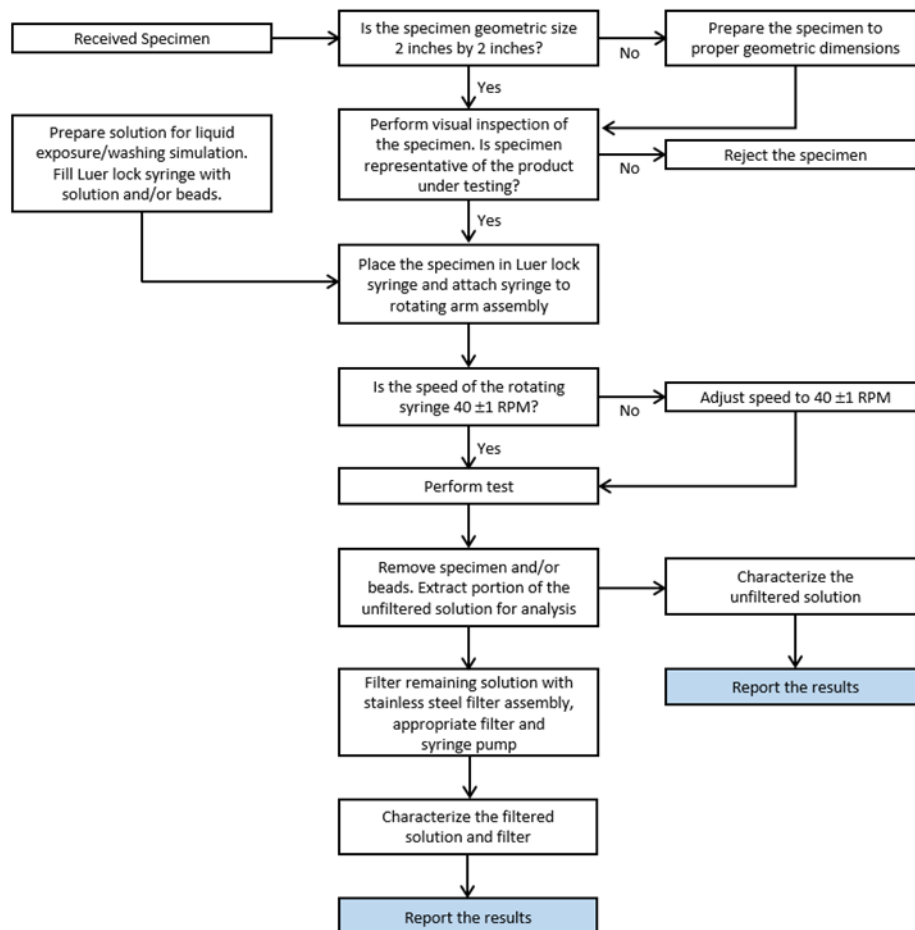


Figure SOP-1. 1. Flowchart showing testing procedure for the preparation and exposure of a specimen to a liquid with and without washing-induced wear simulation.

Terminology

Acronyms

AATCC	American Association of Textile Chemists and Colorists
cc	Cubic Centimeter
CNT(s)	Carbon Nanotube(s)
EDS	Energy Dispersive X-ray Spectroscopy
EM	Electron Microscopy
ICP-AES	Inductively Coupled Plasma Atomic Emission Spectroscopy
ICP-MS	Inductively Coupled Plasma Mass Spectrometry
ISO	International Organization for Standardization
mL	Milliliter
mm	Millimeter
PCTE	Polycarbonate Track Etch
SEM	Scanning Electron Microscopy
SOP	Standard Operating Procedure
TEM	Transmission Electron Microscopy
UV-VIS	Ultraviolet Visible

Related Documents

ISO 105-C06:2010 -Textiles --Tests for colour fastness--Part C06: Colour fastness to domestic and commercial laundering, International Organization for Standardization, 2010.

ISO 105-E04:2013-Textiles -- Tests for colour fastness -- Part E04: Colour fastness to perspiration, International Organization for Standardization, 2013.

AATCC Test Method 15-2013--Colorfastness to Perspiration, American Association of Textile Chemists and Colorists, Research Triangle Park, NC, 2013.

ISO/TS 80004-2:2015 - Nanotechnologies -- Vocabulary -- Part 2: Nano-objects, International Organization for Standardization, 2015.

ISO 4892-2:2013 - Plastics -- Methods of exposure to laboratory light sources -- Part 2: Xenon-arc lamps, International Organization for Standardization, 2013.

ASTM D1141-98-Standard Practice for the Preparation of Substitute Ocean Water, ASTM International, West Conshohocken, PA: ASTM International, 2013.

Definitions

Abrasion - wearing away: the process of wearing away by friction.

Nanomaterials-objects with one, two, or three dimensions in the size range of 1 nm to 100 nm.

Nanoparticle- objects with all three dimensions smaller than 100 nm.

Nano-scale- size range of approximately 1 nm to 100 nm.

Wear - damage, erosion, or destruction by friction or use.

Materials and Apparatus

Materials

- Coupons of the product to be tested, as shown in Figure SOP-1. 2A.
- Supplies for preparation of solutions
- Luer lock syringes (nominally 50 mL/50 cc) with caps, as shown in Figure SOP-1. 2B.
- Corrosion resistant stainless steel beads or glass beads, as shown in Figure SOP-1. 2B.
- Mechanical rotating arm assembly, as shown in Figure SOP-1. 2C.
- Tachometer and reflective tape for measuring speed of rotating arm assembly
- In-line stainless steel filter assembly, as shown in Figure SOP-1. 2A.
- Filters such as polycarbonate track etch (PCTE) membrane filter with pores (0.4 μm diameter holes), as shown in Figure SOP-1. 2A.
- Hollow steel arch punch (1 inch diameter)
- Infusion syringe pump
- Thread seal tape for sealing threads of filter assembly
- Wrenches for tightening filter assembly
- Tube level for leveling the in-line stainless steel assembly during filtering
- Disposable aluminum pans for coupon and PCTE filter drying
- Bake module or hot plate for drying filters
- Clean glass vials for storage of filtered and unfiltered solutions.
- Refrigerator for long term storage of filtered/unfiltered solutions.
- Tweezers for handling coupons and membrane filters.

Apparatus

The liquid exposure setup and example test materials are shown in Figure SOP-1. 2. The coupon shown in Figure SOP-1. 2A was obtained from an aramid woven fiber mat with CNT reinforced coating. The candidate solution, beads and coupon are sealed in a 50 ml Luer lock syringe, and then attached to the rotating arm apparatus as shown in Figure SOP-1. 2B and Figure SOP-1. 2C respectively. The rotating arm assembly is a custom built apparatus used to simulate liquid exposure, with or without washing-induced wear. The rotation speed can be adjusted with a rotary knob located above the power switch.

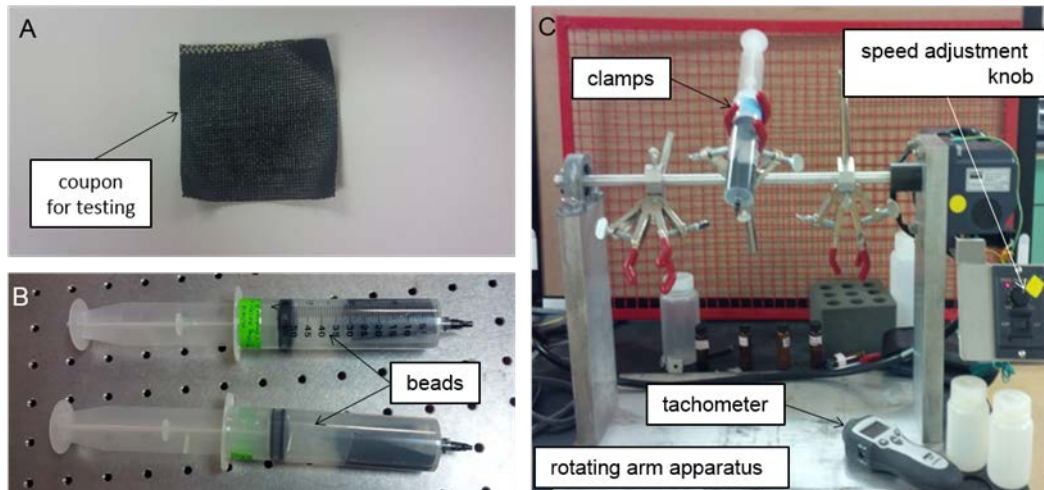


Figure SOP-1. 2. Photographs of the liquid exposure experimental setup. A. Coupon for testing. B. Filled syringes with glass beads and coupons prior to liquid exposure with washing-induced wear simulation. C. Custom rotating arm apparatus.

Filtering of the solutions is carried out with an in-line stainless steel filter attached to the syringe, which is mounted to a syringe pump as shown in Figure SOP-1. 3. The gold coated side of the membrane filter faces to-wards the inlet of the filter assembly. Both the volume of the syringe and the pump rate are required for proper operation of the syringe pump. If desired, multiple syringes can be mounted and filtered.

Note 1: Filtering with a stainless steel filter assembly leaches trace metals from the assembly into the filtered solutions. This effect is especially pronounced when filtering acidic solutions (citric acid, phosphoric acid, etc.). If metals analysis (ICP-MS, ICP-AES) is required for the filtered solutions, the use of a plastic filter assembly is recommended.

Note 2: The stainless steel mesh used to support the membrane filter has a periodic grid pattern which affects the spatial distribution of the material collected onto the membrane filter. Hence, the material collected onto the filter can exhibit a checked pattern consisting of alternating areas of low and high concentrations of material accumulation. Quantification of the collected material based on local microscopic observations must take this spatial distribution into account. Further, the support mesh can buckle leading to uneven distribution of the filtered material on the membrane filter. Most often we have observed deposition of material around the edges of the membrane filter caused by upward buckling of the support mesh. Care must be taken to ensure that the support mesh is in pristine condition (flat) when filtering the solutions.

Procedure

Liquid Exposure, with or without Washing-induced Wear Simulation:

- Prepare specimens (coupons) of the product under testing.
- Prepare candidate solutions according to ISO or ASTM specifications (if applicable).
- Add 25 ml of the solution into capped Luer lock syringe, then place coupon inside the syringe using tweezers.

- For powder detergents do not subsample from larger stock; instead add corresponding amount of detergent directly into syringe
- In order to simulate washing-induced wear add 5 beads into the syringe.
- Set syringe plunger to 50 ml (50 cc) mark.
- Attach filled syringe to rotating arm assembly with clamps.
- Attach reflective tape on syringe and use tachometer to measure rotating speed. Adjust speed to 40 ± 1 RPM.
- Run rotating arm assembly for a predetermined amount of time, for example 30 minutes.
- After the allotted time, remove syringe from rotating arm assembly and remove coupon from syringe.
- Place coupon in an aluminum pan and dry in a bake module maintained at a constant temperature.
- Store dried coupon for further analysis.
- Subsample 5 ml of the washing solution and store for further analysis. Agitate solution before extraction.

Filtering:

- Assemble in-line stainless steel filter assembly with the gold coated surface of the membrane filter facing the syringe inlet. Wrenches can be used to ensure sufficient tightening of the filter assembly.
- Attach filled syringe to filter assembly, and then to syringe pump.
- Use tube level to check and level filter assembly. Check at least two perpendicular directions to ensure horizontal leveling of the filter assembly.
- Set correct volume and pump rate for the syringe pump. A pump rate of 0.2 mL/minute is recommended, but adjustments can be made depending on the tested material.
- Extract solution remaining inside filter assembly (See Note 3)
- Store filtered solution for further analysis.
- Disassemble filter assembly and remove filter with tweezers.
- Place membrane filter, with gold coated surface facing up, in a disposable aluminum pan, and dry in a bake module maintained at a constant temperature.
- Store dried filter for further analysis.

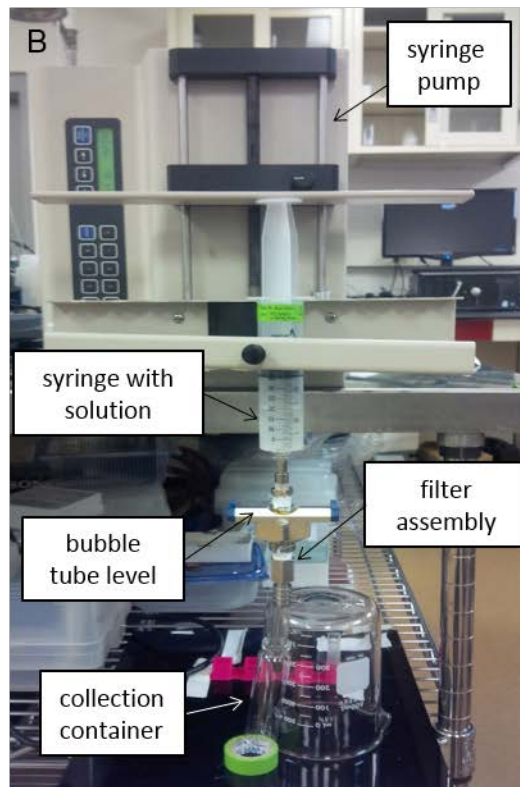
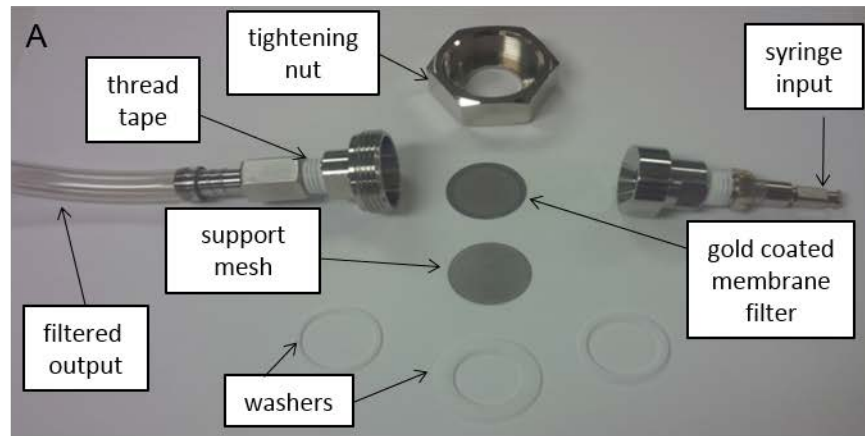


Figure SOP-1. 3. Figure 3. Photographs of the solution filtering process. A. Components of in-line stainless steel filter assembly. B. Filtering apparatus with syringe pump.

Note 3: During the filtering process, when the syringe plunger reaches the end of its travel, a significant amount of unfiltered solution remains inside the filter assembly. For transparent looking unfiltered solutions, which are not likely to deposit a significant amount of material onto the filter, the filter assembly is disconnected from the syringe and connected to a compressed gas (air) line. By blowing air into the filter assembly, filtration of the remaining solution is typically accomplished within 10 minutes. For opaque solutions, which deposit a significant amount of material onto the membrane filter, a gentler approach is used. The syringe is temporarily disconnected from the filter assembly, and the syringe plunger is pulled back to ~25 mL. Filtration resumes at a rate of 0.2 mL/minute. The amount of the filtered solution is periodically monitored

and compared to that of a known standard (for example, 20 mL of DI water in a vial of the same volume and size as the one used to collect the filtered solution). Filtration is deemed complete when the volume of the extracted solution became visually equal to that of the reference; typically within 45 minutes from the start of the second filtration. Alternatively, allow for extra volume (more than 20 mL) to be filtered prior to the initial connection of the syringe to the filter assembly by proper adjustment of the syringe plunger.

Specimen Preparation

Specimen preparation will vary depending on the selected product and desired product condition (pristine, UV-aged, wet weathering, etc.) In addition, specimens should be representative of the product under testing. Specimens with extraneous defects such as surface markings with pen, pencil, permanent marker (dye or metallic) or other type of marker should be discarded. Unless otherwise required or mutually agreed upon, the specimens are required to be 2 inches × 2 inches (50.8 mm × 50.8 mm). All measurements should be ideally performed in triplicate.

Analysis

Liquid exposed coupon, with or without washing-induced wear:

- After the coupon is dried, store it in a labeled container, for further analysis (weighing, SEM, abrasion testing, etc.).

Filtered and unfiltered material, with or without washing-induced wear:

- If the age of solution is an important factor in the post-test analysis, start analysis as soon as the test is completed.
- If solutions are prone to bacterial growth, store in a refrigerator (4 °C) and complete all analyses in a reasonably short amount of time.
- Further analysis could include optical and SEM imaging, UV-VIS spectroscopy, etc.

Membrane Filter:

- After drying the filter should be stored for further analysis
- Further analysis could include optical imaging, SEM imaging, re-suspension for chemical/ particulate analysis, weighing, etc.

Quality Control (QC)

The primary QC requirement is ensuring that all instruments, used during the washing simulation and those used for post-processing analysis, are properly calibrated.

Accelerated UV Aging of Nanomaterials to Study Potential for Release

Scope and Applicability

This SOP applies to the accelerated UV aging of composite materials and products containing nanomaterials through their exposure to conditions such as UV irradiance, moisture, temperature, and chemicals. This practice will serve as a guide for performing an aging test in a laboratory setup and characterize the severity of said aging on the material, through the acquisition of qualitative and quantitative data. The exposure apparatus employs a xenon-arc light source.

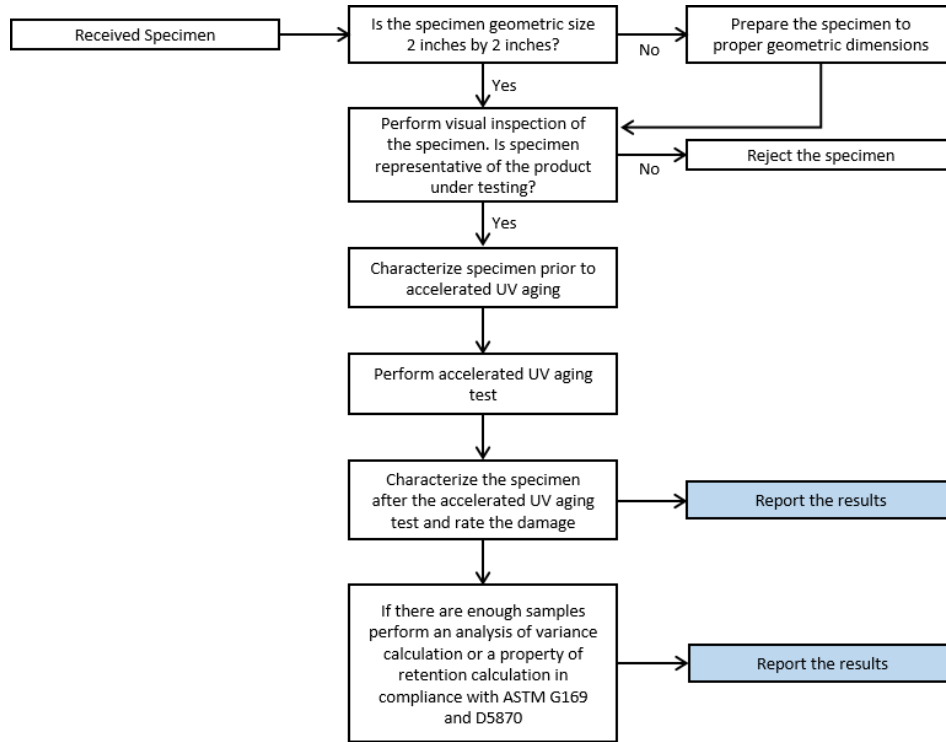


Figure SOP-2. 1. Accelerated UV aging flowchart.

Terminology

Acronyms

ANOVA	Analysis of Variance
ASTM	American Society for Testing and Materials
ISO	International Organization for Standardization
SEM	Scanning Electron Microscopy
SOP	Standard Operating Procedure
STEM	Scanning Transmission Electron Microscopy
TEM	Transmission Electron Microscopy
UV	Ultraviolet
XRD	X-Ray Diffraction
STEM	Scanning Transmission Electron Microscopy

Related Documents

ASTM G151-10 Standard Practice for Exposing Nonmetallic Materials in Accelerated Test Devices that Use Laboratory Light Sources, ASTM International, West Conshohocken, PA, 2010, <http://dx.doi.org/10.1520/G0151-10>

ASTM G156-09 Standard Practice for Selecting and Characterizing Weathering Reference Materials, ASTM International, West Conshohocken, PA, 2009, <http://dx.doi.org/10.1520/G0156-09>

ASTM G113-14 Standard Terminology Relating to Natural and Artificial Weathering Tests of Nonmetallic Materials, ASTM International, West Conshohocken, PA, 2014, <http://dx.doi.org/10.1520/G0113>

ISO 4892-2:2013 -- Plastics -- Methods of exposure to laboratory light sources -- Part 2: Xenon-arc lamps

ASTM G155-13 Standard Practice for Operating Xenon Arc Light Apparatus for Exposure of Non-Metallic Materials, ASTM International, West Conshohocken, PA, 2013, <http://dx.doi.org/10.1520/G0155>

ASTM D6551/D6551M-05(2011) Standard Practice for Accelerated Weathering of Pressure-Sensitive Tapes by Xenon-Arc Exposure Apparatus, ASTM International, West Conshohocken, PA, 2011, http://dx.doi.org/10.1520/D6551_D6551M-05R11

ASTM G169-01(2013) Standard Guide for Application of Basic Statistical Methods to Weathering Tests, ASTM International, West Conshohocken, PA, 2013, <http://dx.doi.org/10.1520/G0169>

ASTM D5870-16 Standard Practice for Calculating Property Retention Index of Plastics, ASTM International, West Conshohocken, PA, 2016, <http://dx.doi.org/10.1520/D5870-16>

ISO/TS 80004-2:2015 - Nanotechnologies -- Vocabulary -- Part 2: Nano-objects, International Organization for Standardization, 2015.

ISO 4892-2:2013 - Plastics -- Methods of exposure to laboratory light sources -- Part 2: Xenon-arc lamps, International Organization for Standardization, 2013.

Definitions

Nanomaterial - object with one, two, or three dimensions in the size range of 1 nm to 100 nm, or produced by nanotechnology.

Nanoparticle - object with all three dimensions smaller than 100 nm.

Nano-scale - size range of approximately 1 nm to 100 nm.

Xenon-arc apparatus - machine based on the use of a special fluorescent bulb that emits a very controlled spectrum of light within the UV spectrum of interest.

Materials and Apparatus

Materials

- Optical microscope for sample characterization
- Scanning electron microscope for sample characterization
- Xenon-arc light apparatus for weathering tests
- Distilled water for wet weathering tests
- Nanocomposite materials for weathering tests

Apparatus

Xenon arc light apparatus - The apparatus required to perform the tests must conform to the specifications in ASTM G155-13 and G151-10 in order to simulate nanomaterials weathering within the acceptable limits to those found when it is exposed to sunlight and moisture. This equipment must be able to run weathering cycles at different conditions of moisture, temperature, and irradiance intensity in a controlled manner to assure reliability and reproducibility of results. It should have a spray system for water, an acidic or alkaline solution. The system must be calibrated according to the manufacturer's instructions.

Procedure

This procedure describes the weathering/aging test of nanomaterials using a Xenon-arc light apparatus; how to execute the test; sample characterization; and report requirements. Specimens from the nanocomposite material are exposed to a weathering/aging cycle based on the desired exposure conditions as specified in ASTM G155-13. After exposure, the surface of the specimens is examined with SEM to rate the severity of the weathering. The specimens can be weighed before and after UV aging to determine mass loss.

Specimen Preparation

Specimen preparation will vary depending on the selected product and desired product condition (pristine, UV-aged, wet weathering, etc.) In addition, specimens should be representative of the product under testing. Specimens with extraneous defects such as surface markings with pen, pencil, permanent marker (dye or metallic) or other type of marker should be discarded. Unless otherwise required or mutually agreed upon, the specimens are required to be 2 inches by 2 inches (50.8 mm by 50.8 mm). All measurements should be ideally performed in triplicate.

Analysis

Specimen Characterization Prior to Accelerated UV Aging

Prepare specimens for scanning electron microscopy (SEM) and scan the surface to take images of the microstructure. Save the images for comparison with the aged samples.

Test Procedure

The specimens are subjected to accelerated UV aging from a xenon-arc apparatus as described in ISO-4892-2:2013.

Note 1: The properties of interest could be color change, cracking, or swelling. If another property is to be studied, refer to the corresponding procedure to assess that property, and compile the relevant information, such as the aging conditions, and include that information in the final report. Remember that variation in results must be expected with changes in test conditions.

Specimen Characterization after Accelerated UV Aging

Prepare specimens for SEM and compare the SEM images visually and rate the damage from 0 (no degradation) to 1 (severe degradation). Perform an ANOVA through the use of statistical software or a property retention calculation as required and report the values according to ASTM G169-01 and D5870-16.

Note 2: The selected SEM magnification must be the same for all the specimens and should be high enough such that the severity of the accelerated UV aging can be observed and rated. The degradation scale is based on the percentage of the area shown in the image that has degraded. Signs of degradation are cracks, dark or white spots, and lines.

Key Results Provided

- Model of the Xenon-Arc light apparatus
- A full description of the specimens and their origin
- Specimen preparation procedure, if different from the one presented here
- Irradiance in W/m^2 nm or radiant exposure in J/m^2
- The exposure times and cycles (if more than one)
- All acquired data and specified in this procedure
- If needed provide the weight of the sample before and after UV aging

Quality Control (QC) Considerations

Repeatability - Repeatability will be quantified through the analysis of the data acquired and comparisons will be made with existing standards as needed or required. The operation should conform to ASTM G155-13 and G151-10.

Bias - the procedure in this test method has no bias, because the value of that property can only be defined in terms of a test method.

6.9. LABORATORY DATA SHEETS (SEE SEPARATE DVD)

6.9.1. SEM MICROGRAPHS – DVD

6.9.2. RAMAN AND TGA RESULTS – DVD

6.10. TERM DEFINITIONS

The definitions list below have been published by the American Society of Testing and Materials (ASTM), the European Commission (EC), the EC-Scientific Committee on Emerging and Newly

Identified Health Risks (SCENIHR), the EC-Scientific Committee on Consumer Products (SCCP), the International Organization for Standardization (ISO), The International Union of Pure and Applied Chemistry (IUPAC), and the U.S. Food and Drug Administration (FDA). Clickable links to pdf versions of each organizational report are also provided where available.

Agglomerate

ASTM: a group of particles held together by relatively weak forces (for example, Van der Waals or capillary), that may break apart into smaller particles upon processing, for example.

EC: a collection of weakly bound particles or aggregates where the resulting external surface area is similar to the sum of the surface areas of the individual components.

SCENIHR: A group of particles held together by weak forces such as Van der Waals forces, some electrostatic forces and/or surface tension. (2008)

SCCP: group of particles held together by relatively weak physical forces, including van der Waals forces, electrostatic forces and surface tension.

ISO: collection of weakly bound particles or aggregates or mixtures of the two where the resulting external surface area is similar to the sum of the surface areas of the individual components.

Aggregate

ASTM: a discrete group of particles in which the various individual components are not easily broken apart, such as in the case of primary particles that are strongly bonded together (for example, fused sintered, or metallically bonded particles).

EC: a particle comprising of strongly bound or fused particles.

SCENIHR: A group of particles held together by strong forces such as those associated with covalent or metallic bonds. (2008)

SCCP: heterogeneous particle in which the various components are not easily broken apart. Secondary particles are formed through agglomeration or aggregation of primary particles (smallest identifiable subdivision in a particulate system). Attention is drawn to the inconsistent definitions in the literature of agglomerate and aggregate, which reflect the uses of these terms according to the industry context. It is recommended that when the term agglomerate is used that it be specified whether the bonding is strong or weak. Aggregate refers to strongly bonded associated particles that cannot easily be re-dispersed by mechanical means.

ISO: particle comprising strongly bonded or fused particles where the resulting external surface area may be significantly smaller than the sum of calculated surface areas of the individual components.

Nanoparticle/Nanomaterial

ASTM: a sub-classification of ultrafine particle with lengths in two or three dimensions greater than 0.001 micrometer (1 nanometer) and smaller than about 0.1 micrometer (100 nanometers) and which may or may not exhibit a size-related intensive property.

EC: a natural, incidental or manufactured material containing particles, in an unbound state or as an aggregate or as an agglomerate and where, for 50% or more of the particles in the number size distribution, one or more external dimensions is in the size range 1 nm-100 nm. In specific cases and where warranted by concerns for the environment,

health, safety or competitiveness, the number size distribution threshold of 50% may be replaced by a threshold between 1 and 50%.

SCENIHR: [Nanoparticle] a discrete entity which has three dimensions on the order of 100 nm or less. (2008) [Nanomaterial] Based on its geometric mean and geometric standard deviation, a material might be considered a nanomaterial when >0.15% of the material, as indicated by the number size distribution, has a size below the designated upper size limit. (2008)

SCCP: particle with one or more dimensions at the nanoscale (at least one dimension <100nm).

ISO: [Nanoparticle] nano-object with all three external dimensions in the nanoscale. [Nanoscale] - Size range from approximately 1 nm to 100 nm. Note 1: Properties that are not extrapolations from a larger size will typically, but not exclusively, be exhibited in this size range. For such properties the size limits are considered approximate. Note 2: The lower limit in this definition (approximately 1 nm) is introduced to avoid single and small groups of atoms from being designated as nano-objects or elements of nanostructures, which might be implied by the absence of a lower limit.

FDA: "When considering whether an FDA-regulated product contains nanomaterials or otherwise involves the application of nanotechnology, FDA will ask: (1) whether an engineered material or end product has at least one dimension in the nanoscale range (approximately 1 nm to 100 nm); or (2) whether an engineered material or end product exhibits properties or phenomena, including physical or chemical properties or biological effects, that are attributable to its dimension(s), even if these dimensions fall outside the nanoscale range, up to one micrometer."

Particle

ASTM: a small object that behaves as a whole unit in terms of its transport and properties.

EC: a minute piece of matter with defined physical boundaries.

ISO: minute piece of matter with defined physical boundaries.

Primary Particle

SCCP: smallest identifiable subdivision in a particulate system.

IUPAC: A primary particle should be defined as the smallest discrete identifiable entity and the method of identification should be mentioned (e.g. transmission electron microscopy, scanning electron microscopy).



Designation: E 2456 – 06

Standard Terminology Relating to Nanotechnology¹

This standard is issued under the fixed designation E 2456; the number immediately following the designation indicates the year of original adoption or, in the case of revision, the year of last revision. A number in parentheses indicates the year of last reapproval. A superscript epsilon (ϵ) indicates an editorial change since the last revision or reapproval.

1. Scope

1.1 Nanotechnology is an emerging field; this standard defines the novel terminology developed for its broad multi- and interdisciplinary activities. As the needs of this area develop, this standard will evolve accordingly. Its content may be referenced and/or adopted, in whole or in part, as demanded by the needs of the individual user.

2. Referenced Documents

2.1 *ASTM Standards:*²

- E 1964 Practice for Compiling and Writing & Terminology
- E 1992 Terminology Relating to Terminology Management

3. Significance and Use

3.1 This standard is intended to facilitate communication among members of the business, research, legal, government, and educational communities.

3.2 Definitions:

3.2.1 Terms and their related standard definitions in Section 4 are intended for use uniformly and consistently in all nanotechnology test methods, specifications, guides, and practices. The purpose of such use is to promote a clear understanding and interpretation of the standards in which they are used.

3.2.2 Definitions of terms are written in the broadest sense possible, consistent with the intended meaning using the following guidance considerations.

3.2.2.1 Terminology E 1992 and Practice E 1964 concepts are considered, especially Sections 6.5, 7, and 8 of Practice E 1964.

3.2.2.2 Terms and nomenclature are based on observed scientific phenomena and are descriptive, distinguishable, and have significant currency in the nanotechnology field as

reflected in peer-reviewed articles and other objective sources. These terms and names should not disrupt accepted usage in other scientific and technological fields, and their preferred usage should follow accepted scientific syntax.

3.2.2.3 When incorporating a term or name from a related field, its underlying meaning is not redefined. Modifications are minimal and are done to elucidate scientific distinctions required by nanotechnology practitioners.

3.2.2.4 When conflicting or overlapping terms and names arise between scientific disciplines, precedence was given to the established term that has behind it a significant body of knowledge.

3.2.2.5 The definition of a term that can have different meanings in different technical fields, especially those fields beyond nanotechnology, is preceded by a limiting phrase, for example, “in nanotechnology.”

3.3 Description of Terms:

3.3.1 Descriptions of Terms are special purpose definitions intended to provide a precise understanding and interpretation of standards in which they are used.

3.3.2 A specific description of a term is applicable to the standard or standards in which the term is described and used.

3.3.3 Each standard in which a term is used in a specially defined manner beyond the definitions in Section 3 should list the term and its description under the subheading, descriptions of terms.

3.3.4 Practice E 1964, Section 13, are used to guide the contents of descriptions.

3.3.5 As nanotechnology is a rapidly developing field, it will be necessary to continually reassess the terms and definitions contained in this standard, for purposes of revision when necessary. The intent of the terms and definitions in this standard is to describe materials containing features between approximately 1 and 100 nm and to differentiate those properties different from properties found in either molecules or the bulk (interior) of larger, micron-sized systems.

3.4 Discussion of Terms:

3.4.1 Discussion sub-paragraphs are non-normative. They are used in this standard to provide explanatory information, to clarify distinctions between the use of terms in this standard as

¹ This terminology is under the jurisdiction of ASTM Committee E56 on Nanotechnology and is the direct responsibility of Subcommittee E56.01 on Terminology & Nomenclature.

Current edition approved Oct. 1, 2006. Published November 2006.

² For referenced ASTM standards, visit the ASTM website, www.astm.org, or contact ASTM Customer Service at service@astm.org. For Annual Book of ASTM Standards volume information, refer to the standard's Document Summary page on the ASTM website.

ERDC SR-16-1

Engineer Research and Development
Center



**US Army Corps
of Engineers**[®]
Engineer Research and
Development Center

ERDC
INNOVATIVE SOLUTIONS
for a safer, better world

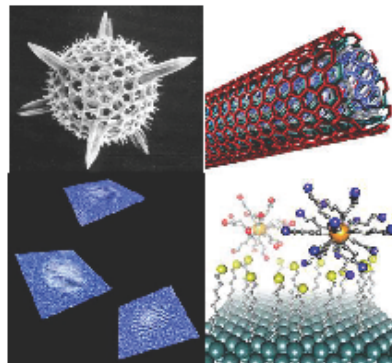
Environmental Consequences of Nanotechnologies

Weathering of Nanomaterials to Study Potential for Release

Scientific Operating Procedure SOP-R-1

Kevin Torres-Cancel, Robert D. Moser, and Aimee R. Poda

February 2016



Approved for public release; distribution is unlimited.